Spring 2022

Primary Cilia in the Pathogenic Mouse Brain & EEG Waveform Analysis of a Mouse Model of Alzheimer's Disease

Ashley Diemand Sterpka
University of New Hampshire, Durham

PRIMARY CILIA IN THE PATHOGENIC MOUSE BRAIN

&

EEG WAVEFORM ANALYSIS OF A MOUSE MODEL OF ALZHEIMER'S DISEASE

BY

ASHLEY DIEMAND STERPKA

M.S. SYRACUSE UNIVERSITY 2015
B.A. SYRACUSE UNIVERSITY 2015

DISSERTATION

Submitted to the University of New Hampshire

In Partial Fulfillment of

The Requirement for the Degree of

Doctor of Philosophy
In

Genetics

May 2022

This dissertation was examined and approved in partial fulfillment of the requirements for the degree of Doctor of Philosophy in Genetics by:

Dissertation Director: Dr. Xuanmao Chen, Associate Professor of Molecular, Cellular, & Biomedical Sciences

Dr. Sherine Elsawa, Associate Professor of Molecular, Cellular, & Biomedical Sciences

Dr. Subhash Minocha, Professor of Biological Sciences

Dr. Paul C. Tsang, Professor of Molecular, Cellular, & Biomedical Sciences

Dr. Don Wojchowski, Professor of Molecular, Cellular, & Biomedical Sciences

On May 9th, 2022

Signatures are on file with the University of New Hampshire Graduate School

DEDICATION

I firstly dedicate this work to Chris,

You have walked with me during each adventure

And stood with me during every challenge.

I love you more than always.

I also dedicate this work to my father.

He taught me the value of knowledge and trusted my instincts.

He was my greatest friend.

ACKNOWLEDGEMENTS & FUNDING

I would like to first and foremost acknowledge my advisor, Dr. Xuanmao (Mao) Chen, who offered me an immense opportunity in working in his lab. When we met, he became a crucial presence during a turning point in my life. Throughout the last five years, he has supported my development as a researcher and a writer. He trained me to excel as a scientist and dared me to test my own limits. I could hardly ask to be trained by a more driven scientist.

I would also like to acknowledge the assistance and support from the rest of my committee members: Dr. Sherine Elsawa, Dr. Subhash Minocha, Dr. Paul Tsang, and Dr. Don Wojchowski. You were all immense assets to me during this work, supporting me with your opinions on my strategies, my pursuits, and always being willing to offer a few words if I stopped by your office or ran into you in the hallway.

I would also like to thank all present and former members of the Chen lab, especially Dr. Liyan Qiu for her extensive procedural knowledge and instruction, Dr. Matt Strobel for his aide with software and positive attitude, Juan Yang for her knowledge of techniques and readiness to talk, and Yuxin Zhou for being a reliable and ultimately indispensable fixture during my time as a graduate student. I would also like to offer special thanks to Tori Denovellis, an undergraduate in the Chen lab, for her time and efforts in EEG analysis.

I would lastly like to extend appreciation to Dr. Linnea Morley and Dr. Dean Elder for their aide with animal care and Dr. Mark Townley for his help with microscopy training.

This research was supported by University of New Hampshire Teaching Assistantships, Summer TA Fellowship Awards, Center for Integrated Biomedical and Bioengineering Research (CIBBRE) Grant, and NIH Grants (R21MH105746, K01AG054729, P20GM113131, R15MH126317, and R15MH125305).

All vertebrate animal research was conducted under the supervision and approval of the University of New Hampshire Institutional Animal Care and Use Committee (IACUC). Copies of IACUC research approval letters can be found in the relevant Appendix.

LIST OF TABLES

LIST OF FIGURES

TABLE 1: LIST OF ABBREVIATIONS

AC3:	ADENYLYL CYCLASE 3
AD:	ALZHEIMER'S DISEASE
APP:	AMYLOID PRECURSOR PROTEIN
APP MICE:	APP23 STRAIN (AD MOUSE MODEL)
ARL MICE:	ARL13B-MCHERRY; CENTRIN2-GFP STRAIN
ARL13B:	ADP-RIBOSYLATION FACTOR-LIKE 13B
BSD:	BURST SUPPRESSION DENSITY
CA1-3:	CORNU AMMONIS Region 1-3
cAMP:	CYCLIC ADENOSINE MONOPHOSPHATE
CSF:	CEREBROSPINAL FLUID
DG:	DENTATE GYRUS
EEG:	ELECTROENCEPHALOGRAM
EMG:	ELECTROMYOGRAM
GAP:	GTPASE ACTIVATING PROTEIN
GEF:	GUANINE NUCLEOTIDE EXCHANGE FACTOR
GFAP:	GLIAL FIBRILLARY ACIDIC PROTEIN
GOF:	GAIN OF FUNCTION
GTP:	GUANINE TRIPHOSPHATE
IFT88:	INTRAFLAGELLAR TRANSPORT 88
IHC:	IMMUNOHISTOCHEMISTRY
INPP5E:	INOSITOL POLYPHOSPHATE 5-PHOSPHATASE
KO:	KNOCKOUT
LOF:	LOSS OF FUNCTION
NREM:	NON-RAPID EYE MOVEMENT
PAC:	PHASE AMPLITUDE COUPLING
PBS:	PHOSPHATE BUFFER SALINE
PET:	POSITRON EMISSION TOPOGRAPHY

PFA: PARAFORMALDHYDE

PSD: POWER SPECTRAL DENSITY

REM: RAPID EYE MOVEMENT

SHH: SONIC HEDGEHOG

CONTENTS

ABSTRACT

In the last two decades, primary cilia have become recognized as tiny sensory organelles with considerable physiological function including regulation of cell division and modulation of transduction pathways. Scientists build on former discoveries, identifying new connections and accentuating the value of primary cilia in disease and intercellular signaling. Astrocytes, the most numerous cell type within the brain, act in support of neurons and maintain neurological health by providing neurotrophic factors and removing synaptic debris. These cells are particularly significant in reparations following neural injury and diseases, altering shape and function to protect healthy tissue. Astrocytes display primary cilia, yet little is understood about the function of this organelle within these cells.

My dissertation research sought to determine the morphological changes of astrocytic primary cilia under neuropathological conditions, such as brain injury and epilepsy, and explore electroencephalogram activity under anesthesia in a mouse model of Alzheimer's disease (AD). This research comprised of three major projects: (1) identifying morphological and condition-based differences between neuronal and astrocytic primary cilia, (2) evaluating the implications of Arl13B during cortical injury, and (3) quantifying EEG waveform pattern in an AD mouse model for distinctions indicative of the presence of the disease prior to the phenotypic onset.

Immunohistochemistry was used to explore morphological differences and alterations in primary cilia associated with cell-type and the development of astrocytic reactivity. Cortical injury procedures were used to form a localized astrocytic response in Arl13B loss-of-function and gain-of-function strains, as well as an IFT88 knockout

strain to compare the role of Arl13B in glial scarring. Electroencephalogram/electromyogram (EEG/EMG) recordings were furthermore used to substantiate seizure activity in a strain of mice prone to epileptic behavior.

Finally, the APP23 mouse, a murine model of AD, was exposed to isoflurane anesthesia while EEG waveform was recorded. These recordings were filtered and processed via Brainstorm, a MATLAB graphical interface, and analyzed for Power Spectral Density, Burst Suppression Density, and Phase Amplitude Coupling.

Results of morphological changes in cilia were consistent with the hypothesis that similarly to neuronal primary cilia, astrocytic cilia are implicated under reactive conditions assessed by morphological changes. Immunohistochemical analysis also revealed regional and strain differences of primary cilia. However, comparison of Loss-of-Function and Gain-of-Function studies did not collectively support the hypothesis that the ciliary protein Arl13B is a functionally relevant component of GFAP-based neurological repair one week following injury, although injured tissue did consistently show heightened Arl13B close to cortical lesion.

Finally, EEG waveform analysis of a mouse model of AD during exposure to anesthesia revealed 3-4-month-old mice show a statistically significant difference in levels of Burst Suppression Density during anesthesia and Power Spectral Densities of Delta, Theta, and Alpha. These results support the potential foundation of waveform analysis during anesthesia as a prudent diagnostic tool to allow for early diagnosis of the disease.

This research elucidates (1) the role of astrocytic primary cilia in the pathogenic brain, (2) relevance of Arl13B in brain injury, and (3) provides a possible basis for quantifiable hallmarks of AD in EEG waveform under isoflurane-induced anesthesia.

Chapter 1

INTRODUCTION & BACKGROUND

Within the brain, astrocytes function in the regulation of neuronal functioning by providing neurons with essential substrates, modeling synapses, and demarcating healthy and necrotic tissue [1]. They are primary responders to pathogenic conditions, including brain injury, epilepsy, multiple sclerosis, and numerous other diseases [1]. Under these conditions, astrocytes change morphology, alter function, and sometimes proliferate in the development of “reactivity” [2-4]. The type and extent of pathology affect the degree of response of astrocytes, which additionally varies between organisms [5].

Astrocytes display a singular primary cilium, a minute structure that has signaling and sensory capacities [6-8]. Primary cilia are known to be essential to the entry of mitosis in most vertebrate cells [9]. Thus, astrocyte reactivity marked by signal-induced morphological alterations requires functional primary cilia to ensure effective proliferation of new cells. Furthermore, Arl13B, a ciliary protein highly expressed in mature astrocytic cilia, is reportedly unique in its GTPase activity, but remains unclear in its range of functionality. It is known to regulate the Sonic Hedgehog pathway [10], a pathway upregulated in brain injury [11], and has been reported to display increased intensity proximal to cortical injury [6], but its role in neurological homeostasis is unclear.

AD is the most common form of dementia in the United States, accounting for over half of reported cases [12]. Although its etiology is not fully understood, many

advancements in understanding the development of AD have occurred through current research. There is no cure of AD to fully reverse the clinical symptoms, and early intervention allows for the best management of its physiological effects and associated changes in behavior. Yet, there is limited diagnostic capacity while the patient suspected of AD is living [13]. This presents the clinical need to identify new methods to evaluate the incidence of AD, preferably in a non-invasive and cost-effective technique.

i. Primary Cilia

Primary cilia are tiny, microtubule-based structures that protrude from the surface of most vertebrate cells. They were first named by Sergei Sorokin in 1968, after determination of the foundational dynamics of ciliogenesis in fetal lung cells [14]. Decades of research have yielded findings underscoring ciliary importance in cellular function and physiological homeostasis including initiation of mitosis [9] and regulation of brain development [15]. Furthermore, primary cilia are involved in modulation of the sonic hedgehog pathway, a pathway that regulates development [10, 16], as well as cellular mechanoreception [7, 9, 17, 18]. Additionally, scientific findings have demonstrated the importance of primary cilia in many diseases, termed “ciliopathies”, wherein ciliary dysfunction can elicit physiological defects [19].

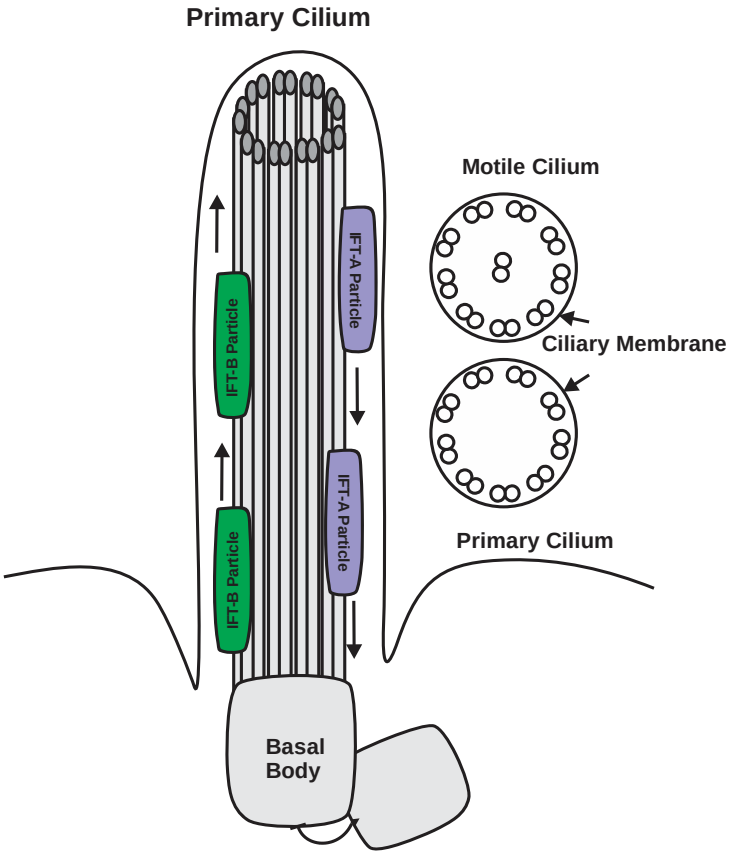

Figure 1: Primary Cilia Axoneme Structure and Intraflagellar Transport. The primary cilia axoneme is composed of nine outer doublets without the inner doublet found within motile cilia. IFT-A particles traffic elements in a retrograde direction towards the basal body, while IFT-B particles carry cargo towards the ciliary tip in an anterograde direction.

Primary cilia differ from motile cilia in structure and function. The cytoskeletal organization that forms the internal design of primary and motile cilia is called the "axoneme" [20, 21]. This microtubule-based axoneme is comprised of nine outer doublets and either two or zero inner doublets [20, 21] (**Figure 1**). The presence of two inner doublets supports the mobile functionality of motile cilia, while the absence of an inner doublet prevents movement of the primary cilium [20].

Within the axoneme, intraflagellar transport (IFT) is vital to the extension of primary cilia that must occur during ciliogenesis, as well as the trafficking of proteins through the cilium [20, 22]. As primary cilia lack the machinery necessary for protein

synthesis, proteins must first be synthesized in the Golgi apparatus and then transported to the base of the cilium [20]. Two complexes comprised of small particles and motor proteins, IFT-A and IFT-B, propel cargo in retrograde and anterograde directions, respectively [20, 23]. The transition zone, a specialized region located at the base of the primary cilium, controls the translocation of proteins into and out of the cilia [20, 24]. **Figure 1** shows a detailed representation of the structure and transport proteins of primary cilia.

Dismantling of primary cilia is reported to function in the initiation of mitosis in ciliated cells [9]. They arise from the mother centriole, termed the “basal body”, and maintain their form as a cell surface projection during interphase [9, 17]. Prior to the entrance of mitosis, the primary cilium must first undergo translocation of ciliary proteins, thereby causing structure decapitation, and then retraction into the cell [9, 17]. This resorption allows the mother and daughter centrioles to duplicate and migrate to different poles of the cell to produce spindle fibers needed during metaphase and anaphase [9, 17]. Only by this resorption and translocation can effective mitosis occur within a ciliated cell.

Consequently, defects in the resorption or projection of primary cilia can result in abrogated or heightened cell proliferation, thus impacting the development of certain forms of cancer. Some of these include: medulloblastomas [25, 26], glioblastomas [27-29], and pancreatic cancer [30, 31]. Additionally, the involvement of primary cilia in modulation of certain cell signaling pathways, including Sonic Hedgehog [10, 32], Wnt [32], and ERK/MAPK [32] is also known to contribute to the development of certain types of cancer by means of altered ciliary signaling pathways.

Primary cilia are recognized to play an essential role in a range of diseases. Pathologies that are directly attributed to the malfunction of primary cilia belong to a spectrum called “ciliopathies” [19], which include diseases such as: polycystic kidney disease resulting from impaired mechanoreception of urine in the kidney [33, 34]; Joubert Syndrome, a disease resulting from an impaired ciliary protein and defective cilia [35]; Bardet-Beidl Syndrome, a condition caused by impaired basal bodies and correlated ciliary defects (BBS) [35]; amongst numerous others. These conditions are respectively characterized by cysts within the kidneys [33], polydactyly and cognitive delay [36, 37], and obesity along with cognitive delay and renal malformations [38].

Primary cilia also function in detection of extracellular signals. They are thought to act as mechanoreceptors that instigate Ca^{2+} signaling [39] and act to sense fluid flow within the kidney [34]. Neuronal primary cilia are known to maintain regulatory enzymes, such as Adenylyl Cyclase III, Melanin-concentrating hormone receptor type 1, Somatostatin receptor type 3, and serotonin receptor type 6, signifying further involvement in sensory input [40, 41]. Additionally, BBS, a ciliopathy resulting from malfunctioning basal bodies and primary cilia, is characterized by anosmia and retinal degeneration, likewise supporting primary cilia as having sensory roles [18, 42, 43].

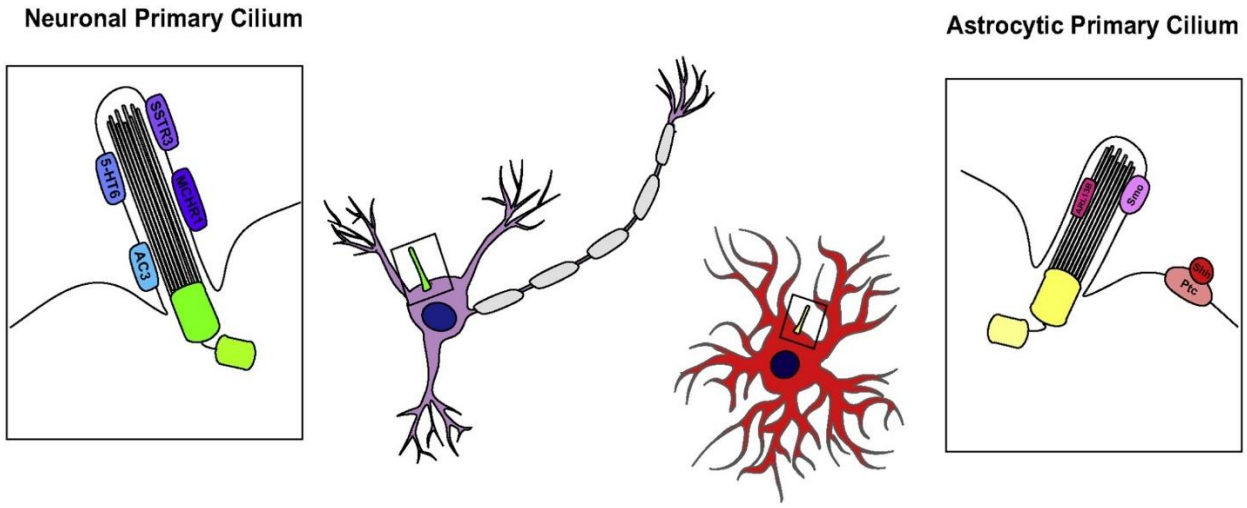

Figure 2: Neuronal and Astrocytic Primary Cilia in the Mature Brain. *Figure sourced from Sterpka and Chen, 2018 [7].* Mature neurons and astrocytes exhibit primary cilia, arising from the mother centriole. Neuronal cilia are known to exhibit membrane proteins, including 5-HT6, AC3, SSTR3, and MCHR1 [7]. Astrocytic cilia are known to exhibits Arl13B in their membrane and shuttle Sonic Hedgehog components Smoothened and Patched1 pendant on ligand binding [7].

Within the mature brain, astrocytes and neurons are known to maintain primary cilia (**Figure 2**) [6, 7]. Studies have shown that cells display variance in existence of these organelles, and that function and morphology are not conserved [6, 7, 16, 44-47]. Cellular function likely results in the diversity of ciliary morphology and functionality. Neurons are reported to maintain longer cilia than those of astrocytes [6, 7, 48]. The non-mitotic nature of neurons compared to the proliferative capacity of astrocytes may explicate why the cilia show a marked difference in length. **Table 2** outlines the differences between neuronal and astrocytic primary cilia. Immature oligodendrocyte precursors are reported to exhibit primary cilia, although in maturity no ciliary appendage can be distinguished [49]. It is possible that the lack of distinguishable primary cilia in oligodendrocytes may be due to ineffective antibodies or a differential functioning at maturity. Furthermore, microglia, similar to other immune cells within the body, do not exhibit cilia, regardless of their continued modulation of Shh components

[7, 48]. This variation suggests ciliary diversity may be due to the functional differences of the cell type.

Due to their minute size, primary cilia present investigative challenges. There are limited antibodies known to effectively stain ciliary proteins, and there is no ubiquitous marker that can identify all primary cilia. This is especially true with *in vivo* research, which poses more opportunity for background with non-specific binding. Ciliary knockout mice are one of the more commonly used experimental tools for loss-of-function study. IFT88 mice crossed with a tamoxifen inducible Cre strain synthesize a hybrid strain that can conditionally knockout ubiquitous or cell-specific primary cilia [50, 51]. Furthermore, lines of transgenic mice have been procured that contain fluorescent proteins linked to ciliary protein, such as the Arl13B-mCherry;Centrin2-GFP mouse, which allow for more efficient visualization of primary cilia [52].

Table 2. Neuronal and Astrocytic Primary Cilia in the Mature Brain

Features	**Neurons**	**Astrocytes**
Origination	Ectoderm [53] Neuroepithelial Cells and Radial Glial Cells [54]	Ectoderm [53] Neuroepithelial Cells and Radial Glial Cells[54]
Excitability	Excitable	Non-excitable
Differentiation	Terminally differentiated [55]	Regional differentiation & become reactive in response to insults
Proliferative Capacity	Lose mitotic ability in maturation [55]	Maintain proliferative capacity throughout life [4]
Cilia Markers	AC3, SSTR3, 5-HT6 & MCHR1 [48]	ARL13B [48]
AC3	Highly expressed in neuronal primary cilia [8]	few in astrocyte cilia in adult brain [8]
ARL13B	not well expressed in primary cilia of mature neurons [8]	Highly expressed in astrocytic primary cilia in the mature brain [8]
Cilia Length (Hippocampus)	5.0–5.9 μm (AC3-positive) [48]	2.8–3.2 μm (ARL13B-positive) [48]
Shh signaling Components	Expression in primary cilia of mature neurons not shown	Smoothened and Patched1 detected in primary cilia of astrocytes in the postnatal brain [25]
Structural Dynamics	Relatively stable	Subject to dynamic change during astrocyte proliferation
Ciliogenesis	*De novo* ciliogenesis not reported	Maintains ciliogenesis [28, 56]
Nanoscale Structure[#]	Without ciliary pocket	Have ciliary pocket

Ciliary Disease Implications	Obesity, cognitive impairment & mental disorders [57]	Astrocytoma/glioblastoma [28, 56]
*Epileptic Insults**	Neuronal primary cilia in CA1 and CA3 become shorter	ARL13B-positive astrocyte cilia become shorter
*Brain Injury Insults**	Neuronal primary cilia become shorter near injured tissue	Arl13B-positive cilia undetectable, Arl13B protein expression increases and trans-locates to the cell body
This table is modified from Sterpka and Chen 2018. * Data from this dissertation research; [#] *Presented by Ott CM from Janelia Research Campus.*		

Table 2: Comparison of Neuronal and Astrocytic Primary Cilia in the Mature Brain. *Table modified from [7, 58].* Within the mature brain, astrocytes and neurons display marked morphological and functional differences. Their primary cilia also show differences in structure, labeling antibodies, and pathogenic response.

ii. Astrocytes

Astrocytes are the most prevalent cell type within the brain [4, 59, 60]. They are markedly diverse in form and function and are essential to the survival and health of neurons [61]. Astrocytes develop from the same progenitors as neurons [61], although during development, astrocytes localize to the brain only after primary neurogenesis and neural migration [62]. Relatedly, synapses only appear following the production of astrocytes [61], and termination of astrocytes results in the inability of neuronal survival [61].

Astrocytes participate in a wide range of functions, including the maintenance of synapses and structure of the tripartite synapse [61-63], provision of neurotropic factors such as lactate to neurons [64], and recycling excess neurotransmitters [65]. Importantly, astrocytes protect healthy tissue against neurological insults by altering phenotype to become “reactive” and encompassing potentially harmful debris from viable tissue [1, 4, 66-68].

Due to the high level of diversity in astrocytes, there is not a ubiquitous marker. It is possible that the absence of developmental finality in astrocytes restricts the

identification of a singular effective identifier, but presently glial fibrillary acidic protein (GFAP) is accepted in the scientific community as the most appropriate protein which labels the majority of astroglia and reflects the development of reactivity by heightened expression [43]. It is an intermediate filament protein expressed in most astrocytes [68]. There are 10 known isoforms of GFAP, and their specific functions remain unclear, apart from $GFAP_{\delta}$ [69]. $GFAP_{\delta}$ is reported to adjust the elements of astrocytic intermediate filaments and be heightened in astrocytic reactivity [69].

S100B is a calcium-binding protein involved in synaptic plasticity [70]. It is another known marker of astrocytes, but is also displayed in other cell-types, thereby limiting its capacity to specifically mark astrocytes in immunohistological analysis [71]. Assessment of cell-type specificity of S100B revealed its expression in a high percentage of oligodendrocytes, especially in the white matter of the brain [72]. Additionally, it was shown to be expressed in ependymal cells, lymphocytes, vascular endothelial cells, amongst other cells in the brain [72], thus supporting the selection of GFAP as the most effective astrocytic marker in the following studies.

Fundamentally, astrocytes have been grouped into two categories of morphology: protoplasmic and fibrous [73]. Protoplasmic astrocytes display long branches terminating with fine processes and are found in the grey matter of the brain [73, 74]. Fibrous astrocytes, which display a bushier morphology with a larger number of fine processes, primarily localize in the white matter of the brain [73, 74]. There have been reports that protoplasmic astrocytes express S100B more heavily, while fibrous astrocytes are reported to ordinarily express GFAP, but GFAP is recognized as the most applicable marker for general astrocytic identification [68, 73, 74]. Although both

types of astrocytes are reported to contact blood vessels [4], they are known to have diversity in their functionality. Protoplasmic astrocytes are reported to play a role in synaptic maintenance and formation of the blood brain barrier [73, 74]. Less is known about the functional breadth of fibrous astrocytes, although it has been suggested that they function in myelination via contact with Nodes of Ranvier [4, 73].

Astrocytes have proven to be vital to synapsing between neurons. They are known to regulate the formation and stability of synapses [75]. Remarkably, synapses only appear after astrocytes have differentiated [61]. By the 3rd postnatal week in mice, astrocytes are morphologically distinguished to their locale and connect with neurons [61]. Astrocytes release factors that alter both pre- and post-synapses, thereby inhibiting or stimulating synaptic formation [61]. *In vitro* studies have shown that neurons will die without the presence of astrocytes and also fail to synapse with one another, thereby making them essential to neurological functioning [61].

iii. Reactive Gliosis

Astrocytes are major proponents in maintenance of neurological homeostasis [61, 63]. Under pathogenic conditions, in which neurological balance is disturbed such as brain injury or epilepsy, astrocytes can become “reactive” [2, 59, 76]. Reactive astrocytes are altered to one of two types: (1) protective of the survival of remaining viable neurons or (2) debilitating to damaged cells [1]. Under these conditions, astrocytes change morphology, hypertrophy, and heighten GFAP expression [1, 43, 60]. These changes are often accompanied by proliferation to support glial scarring and can

be easily identified by additional processes and increased protein expression [77]. As a result of this altered phenotype, tissue within the brain can be demarcated for death or survival [1, 4]. Regardless of the functional diversity of astrocytes, all types maintain this ability to become reactive in response to neurological disease [4].

Traumatic brain injury can elicit a range of responses based on the severity of the event and the health profile of the afflicted individual. The injury can produce either focal or diffuse tissue damage, which often hybridize [68]. These types of injuries can trigger astrocytes to become reactive and proliferate to form a glial scar, although the degree of response is region and severity dependent [4, 68, 78]. The glial scar is a combination of reactive astrocytes, extracellular matrix proteins, and activated microglia formed around the lesion area [79]. This assortment of protective materials appears as a dense region of interwoven tissue. The alterations that ensue in astrocytes after the initiation of reactivity support the protection of viable neurons from excitotoxic substances and also support repair of the blood brain barrier [1].

The occurrence of seizures can correspond with traumatic brain injury or occur independently, often accompanying another form of neurological condition, such as epilepsy [68]. Epilepsy, characterized by the abnormal firing of neurons and convulsive behaviors, is one of the most common neurological disorders [76]. Seizure activity is accompanied by the development of astrocyte reactivity [3]. Questions regarding the role of astrocytes in seizure activity remain, with special interest in whether the alterations from reactivity propagate or oppose epileptic activity. Reactive astrocytes show variation in glutamate receptors and responsiveness, possibly perpetuating seizure activity, while also releasing factors that can promote tissue health [76, 80]. An

understanding of astrocytic function in seizures is unclear and somewhat debated, but it is recognized and accepted that reactive astrocytes undisputedly exist in a brain displaying seizure activity.

iv. ADP-ribosylation factor-like 13B (Arl13B)

Arl13B is a small GTPase belonging to the ARF family, a subset of the Ras super family of GTPases [81-85]. It is a ciliary membrane protein, commonly used in immunostaining of immotile primary cilia [8, 48]. It has been reported to have an assortment of roles in the regulation of cellular function, including ciliary trafficking [86] and migratory prompting [87, 88]. Reported to have functional diversity around the ciliary domain, Arl13B has profound implications in physiology, morphology, and function. Defects in this protein can elicit abnormal structure, altered capabilities, and morbidity. The full range of functioning of Arl13B is unclear.

The Ras family of GTPases is a large group of G-proteins, divided into multiple families [82-85, 89, 90] (**Figure 3**). These include Ras, Rho, Ran, Rab, Rheb, and Arf families [83]. Grouped together due to homologous structure [82, 83], they all function in cellular homeostasis and are divided by commonality in role [82, 83]. These include activities in protein trafficking, cytoskeletal remodeling, and proliferation, among other functions [82, 83]. Identified as “molecular switches [82, 83],” GTPases are activated by Guanine-Exchange-Factors (GEFs) and deactivated by GTPase- Activating-Proteins (GAPs), which mediate function based on effector binding [10, 68, 83-85, 89-91].

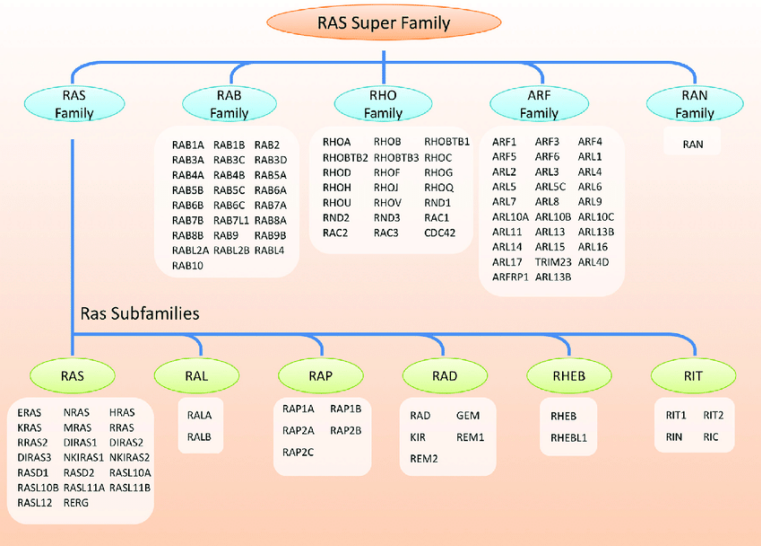

Figure 3: Ras Super Family of GTPases. Figure sourced from Liu et al, 2018 [92]. The Ras Super Family of GTPases is divided into multiple families of structurally and/or functionally similar proteins. ADP-ribosylation factors (ARFs) are a subgroup of GTP-binding proteins which maintain similar function in membrane cargo trafficking [84]. ADP-ribosylation-factor-like proteins (Arls) are structurally similar to ARFs, although their functionality ranges [90].

The Adenosine-diphosphate-Ribosylation Factor or “Arf” family is reported to participate in cellular proliferation [93], selection and trafficking of cargo [83, 84, 93, 94], and employment of enzymes [84, 94]. Arf-Like-Proteins, or Arls, are classified owing to their structural similarity to Arfs, although they lack consistency in their functional range [90]. Particularly unique to this group is Arl13B, which maintains a larger structure than other Arls [82] and a distinctive range in functioning [82, 83, 95]. It is structurally unlike other Arls due to a unique coil in its c-terminal [96] and a proline rich region in the g-domain [96]. Its full range of functioning is still unclear, but the structural variation suggests the possibility of distinctiveness in function of Arl13B.

The ortholog Arl13 is understood by the scientific community to be lost early during evolution in unciliated cells [97]. It is reported to only exist within ciliated cells [95], although it is reported to function outside of the primary cilium [98, 99]. There are

two known paralogs, Arl13A and Arl13B [100]. Arl13A is effectively underdetermined in function, although it has been reported to be expressed in craniofacial structures during early development of the zebrafish [100]. During early zebrafish development, Arl13A is reported to be expressed alongside Arl13B in mitotic and ciliated cells and binds tubulin accordingly [100]. Located on chromosome 3, specifically at 3q11.1-q11.2 [101], Arl13B is well-studied as an atypical GTPase [102], although its full range of functioning is unclear.

The implication of Arl13B is well established in Joubert Syndrome (JS). JS is identified as a “ciliopathy” or disease resulting from abnormalities in ciliary function [7, 103]. 3 missense mutations in Arl13B are known to result in this autosomal recessive disease [37] [102]. JS is characterized by a range of morphological and cognitive abnormalities [37, 103, 104]. These include anatomical defects of the cerebellum and brain stem known as the “molar tooth sign” [101], These neurological defects are accompanied by cognitive delays and developmental impedances [101]. Additionally, those afflicted with JS display renal problems such as cystic kidneys, liver abnormalities such as hepatic fibrosis, and visual disturbances such as oculomotor apraxia [36, 37, 101, 103-105]. JS is also often accompanied by polydactyly, a morphological condition yielding 6 digits that is shared with several other ciliopathies [101, 106].

Arl13B has been distinguished as a primary cilia marker in mature astrocytes [6-8, 48]. Within the adult brain, Arl13B lacks cohesive expression in other primary cilia and is consequently the most suitable marker for labeling mature astrocytic primary cilia. This protein can also be weakly expressed in immature neuronal cilia, but this

expression is variable and becomes weak during cellular maturation [8]. Thus, Arl13B can be effectively used as an astrocytic primary cilia marker [6, 7].

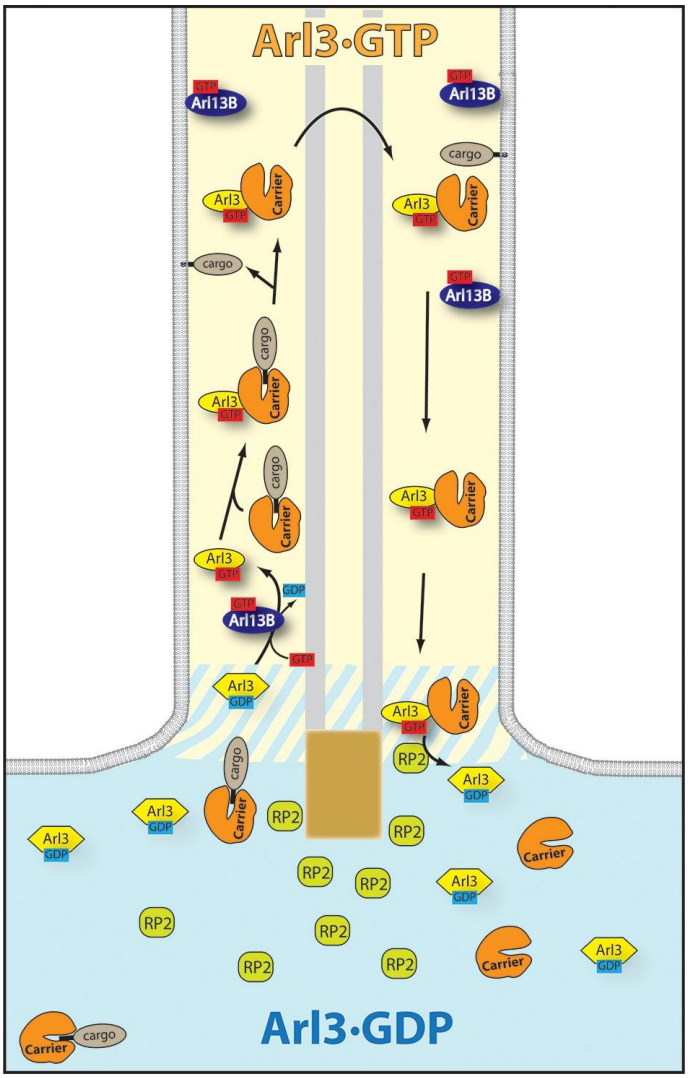

Figure 4: Arl13B is the GEF of Arl3. *Figure sourced from Gotthardt et al., 2015 [96].* Although GTPases are rarely activators or deactivators of other GTPases, Arl13B has been reported to have guanine-nucleotide-exchange factor (GEF) activity for ARL3, and thus stimulates its ability to carry ciliary cargo [96].

Although GTPases rarely act as GEFs, Arl13B is reported to maintain GEF activity of another ciliary protein, Arl3 [82, 96, 102]. It is well established that Arl13b is required to activate Arl3 (**Figure 4**) and induce its functioning. Arl3 is reported to assist

with the translocation of ciliary cargo, such as phosphatidylinositol 4,5-bisphosphate 5-phosphatase (Inpp5e) [82, 104, 107]. Conversely, it has been reported that Arl13B, not Arl3, modulates the translocation of Inpp5e [82, 108]. Regardless of the conflict in conclusions, it can be surmised that Arl13B regulates Inpp5e cargo in the primary cilium, either directly or indirectly. As translocation of Inpp5e is integral to resorption of primary cilia required for mitosis or ciliated cells [9], Arl13B can thus be concluded as an essential component of cellular proliferation.

The role of Arl13B in Sonic hedgehog (Shh) is well established. Shh is a signaling pathway necessary for cellular proliferation, survival, and embryonic patterning [10, 66, 109]. It is well studied and now established to be propagated by Arl13B [97]. Shh pathway requires a number of components which are known to be transduced by the primary cilium [97]. Ablation of Arl13B has been reported to weaken and reduce Shh activity [10]. Interestingly, the function of Arl13B with respect to control of Shh signaling was uncoupled from the primary cilium in a study by Gigante et al. [97]. In this investigation, researchers observed the effects of a mutant form of Arl13B that was expressed outside of the primary cilia and determined that although it elicited structural and protein defects in the cilium itself, its presence in the cell was sufficient to regulate Shh activity [97]. It has been reported that GPR161 (inhibitor of Shh signaling) cannot exit the cilium in Arl13B mutants, thereby preventing activation of Shh pathway [110].

The protein Arl13B participates in the regulation of different cells within the brain, as well as cellular migration. In 2012, Barral et al. identified a previously unknown interaction between Arl13B and cytoskeletal actin [86], suggesting a role in cytoskeletal remodeling and cellular movement. *In vivo* and *in vitro* studies completed by Casalou et

al. in 2019 demonstrate that Arl13B acts to control breast cancer cell migration via regulation of focal adhesion size and ß3-Integrin levels [87], likely a result of Arl13B's role in cytoskeleton alterations.

Arl13B was reported to regulate the ability of radial glia to control the proliferation and migration of cells in the cerebral cortex [111]. Embryonic division of radial glial creates a neurological framework which directs the orientation and generation of neurons [111]. Higginbotham et al. revealed that time specific deletion of Arl13B resulted in abnormal cortical development [111], thus solidifying the crucial role that Arl13B has in neurophysiological development. Furthermore, by rendering Arl13B inactive, Ferent et al. demonstrated that Arl13B is essential to the appropriate commissure axon management [98]. In this study, Arl13B was targeted to manipulate Shh, thereby affecting neuronal development [98].

Due to its implicit role in Shh activity, Arl13B has been investigated as a therapeutic tool. In 2018, Bay et al. targeted Arl13B as a potential treatment for Shh-dependent medulloblastomas (MB) [10]. To weaken and abrogate Shh function, Bay et al. selectively deleted Arl13B. In this study, researchers effectively deleted Arl13B in MB cell lines, as well as in an inducible Cre line of mice carrying the MB phenotype. This effectively reduced Shh signaling and MB growths *in vitro* and *in vivo* conditions. This study provides a foundation of Arl13B manipulation as a potential treatment of pathologies resulting from abnormal Shh activity but did elicit a range of abnormal anatomical and physiological problems.

Furthermore, immunohistological investigations of Arl13B-positive primary cilia surrounding cortical injury found a dramatic reduction of ciliary presence near the lesion

site, as well as an increased expression of Arl13B [6]. Cells proximal to the cortical injury displayed heightened Arl13B in their soma and processes [6]. Investigation of Arl13B-mCherry; Centrin2-GFP mice, which carry fluorescent proteins fused to Arl13B and do not require use of an Arl13B primary antibody, displayed the same increase of protein intensity near the injury site [6]. Although the full function of Arl13B is not yet understood in the conditions of brain, the consistent results of increased Arl13B suggest a previously unknown role in certain types of neurological damage.

Ablation of Arl13B is known to be embryonic lethal [112, 113]. Its deletion can result in anatomical abnormalities [97]. *In vivo* ablation of Arl13B has resulted in the presence of kidney cysts [10]. Arl13b deletion affects Shh signaling, a pathway necessary for morphological patterning. Due to its regulation of Shh signaling, research investigated the knockout of Arl13B to treat Shh-based cancers, such as medulloblastomas [10].

Although the entirety of the range of functioning of Arl13B is still unclear, scientific research has demonstrated its value in a variety of processes. It has been proven to be integral to primary cilia by means of regulation of intraflagellar trafficking and ciliogenesis. Relatedly, its function in vesicular transport, although not fully understood, is undebatable. Its modulation of the Shh pathway is well recognized, and now accepted to extend past ciliary control. It atypically maintains GEF activity of another GTPase and modulates the migration of certain cells. Its activities pertaining to cytoskeletal remodeling and brain injury reparations are still unclear, but Arl13B's implication in disease and morphological disturbances is distinct. Although categorized

with other small GTPases, Arl13B stands out with functional diversity and unique behavior.

v. Adenylyl Cyclase 3 (AC3)

Adenylyl Cyclases (ACs) are a class of regulatory enzymes known to synthesize the second messenger cyclic adenosine monophosphate (cAMP) from adenosine triphosphate (ATP) [57, 114]. There are nine known isoforms of AC with similar structures that span the plasma membrane twelve times and a single, more recently discovered soluble type that varies in formation [57, 114, 115]. Their ability to form different homodimers and heterodimers produces differing physiological effects by way of cAMP production [114, 115]. cAMP aids in a regulatory purpose as a second messenger, binding to various effector proteins to induce homeostatic changes [114]. It is essential to the initiation of various developmental processes throughout the body and in the Central Nervous System [115].

ACs are regulated by G Proteins [116]**.** The guanosine triphosphate (GTP)-bound α-subunit of Gs is reported to prompt activity in different isoforms of AC [116]. Furthermore, the subunits Gi, Go, and Gz are known to halt AC activity, based on the isoform type [116]. βy subunits are known to have initiating or abrogating effects on ACs, also pendant on the isoform [116]. Ultimately, G-Coupled-Protein Receptors maintain the ability to regulate the activity of ACs, and thus the synthesis of cAMP.

AC3 is an isoform of ACs reported to localize in various tissues within the body, including, but not limited to the liver, pancreas, lungs, heart, and brain [117]. Within

the brain, AC3 localizes on the ciliary membrane of mature neurons, and is an effective and accepted neuronal primary cilia marker [8, 41]. It is also reportedly expressed in primary cilia of mesenchymal descent, such as osteocytes, endothelial cells, and fibroblasts [41].

Loss-of-function experiments have been utilized to explore the range of functioning of AC3. Defects in AC3 are reported to elicit physiological and cognitive impairments [57]. These include diseases such as depressive behaviors [118], obesity [119], and impairments in olfaction (anosmia) [116]. Moreover, conditional ablation of AC3 has been reported to elicit defects in learning and memory [120]. Collectively, the effects produced by the elimination of AC3 support the importance of this enzyme in homeostatic functioning of different physiological systems.

vi. Alzheimer's Disease

Alzheimer's Disease (AD) is the most common cause of dementia affecting a growing number of adults in the world's population. Commonly afflicting those aged sixty and older, this pathology is associated with seven stages ranging from mild to severe symptoms; the onset commonly starting with forgetting small tasks and its progression marked with a loss of additional faculties, including cognitive impairment and damaged motor control [13]. It is a devastating disease, and much is still unclear about its etiology and development. It is known that early detection of AD has proven valuable in managing symptoms and promoting quality of life, but diagnostic tools are still limited.

The true etiology of AD is incompletely understood, and there are two main theories of its cause: the cholinergic theory and the amyloid beta theory [121]. The premise of the cholinergic theory of AD is that there is a deficit of cholinergic neurons in brains afflicted with AD [121]. It is reported that choline acetyltransferase is impaired, resulting in a reduction of overall acetylcholine in the brain [121]. This diminution would impede cognitive function by attenuating neuronal excitability [122]. It is also reported that acetylcholinesterase is impacted by Amyloid Beta [121]. Presently, the Amyloid Beta hypothesis is better understood and studied in AD [121], thus the current thesis will focus on that hypothesis and its relevance to the design of this study.

Within the brain, Amyloid precursor protein (APP) is known to support neuronal growth and repair [123]. Interestingly, deletion of this protein is not reported to elicit significant phenotypic changes [124]. Secretases cleave APP into smaller peptides, including beta-amyloid [12]. High levels of beta-amyloid, especially beta-amyloid-42, can lead to plaques within the brain, a hallmark of AD [12]. It is still debated whether the accumulation of amyloid-beta plaques is direct cause of AD, as plaques can be found in both demented and healthy aged brains [124], but it is reported that the levels of beta-amyloid-42 in cerebrospinal fluid decrease with the progression of AD, while increasing in the brain itself, indicating a reduction of expulsion of the peptide [123, 124].

The protein tau is also associated with the development of Alzheimer's disease [125]. Tau stabilizes microtubules within the brain and neurons to aid in intracellular transport and stability [125]. This results in maintenance and regulation of the microtubules. It is reported that amyloid-beta plays an important role in the development of hyperphosphorylated tau [125], although it is not fully understood. In AD and other "tauopathies," tau is hyperphosphorylated, thus

destabilizing from microtubules and binding to itself [124, 125]. This deterioration results in neurofibrillary tangles, and cell death [124, 125].

Conclusive diagnosis of AD necessitates postmortem analysis, although clinical evaluation and examination of the presence of specific biomarkers can aide in detection in living patients [126]. Currently, diagnosis of AD is based on a combination of factors, including progressive cognitive decline, imaging Positron Emission Topography (PET), and Cerebrospinal Fluid (CSF) markers [127]. Although early detection cannot eliminate the course of AD, it can allow for proactive administration of treatments that can enhance the well-being of afflicted individuals [126]. Electroencephalography (EEG) analysis has proven to be a noninvasive tool in evaluation of AD, differentiating it from other dementias by showing variances in the data waveform [128, 129]. EEG is now used when AD is suspected, but introduction of this monitoring during routine appointments as proactive screening has not yet been explored, including its use with anesthetized patients.

vii. Statement of Research Questions & Aims

This dissertation was divided into three major projects and sought to answer the following three questions:

1. **Is there a distinction between neuronal and astrocytic primary cilia in the healthy and pathogenic mouse brain?**

The first goal of my dissertation research was to investigate the morphological dynamics of astrocytic primary cilia, when compared to neuronal primary cilia [7]. This was completed in the healthy and reactive brain to identify a previously unknown function.

My first aim was to compare astrocytic and neuronal primary cilia under reactive conditions. Astrocytes and neurons embody a dichotomy of functioning in the brain. This split suggests contrasting ciliary function in activities and behaviors. I hypothesized that astrocytic primary cilia are implicated in reactivity and detectable by morphological change, and used two models, a localized cortical injury model and a spontaneously occurring audiogenic seizure model to investigate morphological alterations in cilia.

My results show that astrocytes maintain significantly longer primary cilia than those of neurons in the healthy brain, with apparent differences in length between regions of the hippocampus. Furthermore, these findings indicate that similar to hippocampal neurons, astrocytes within the dentate gyrus are affected in mice exhibiting seizure activity. I was unable to find astrocytic primary cilia with Arl13B staining in our cortical injury model. IFT88 staining was also unable to indicate the presence of primary cilia. We furthermore found an increased expression of Arl13B in injured tissue, with the highest intensity proximal to the cortical wound. I determined that the ciliary shortening may have been attributed to proliferation, but the alterations in Arl13B expression suggested an unknown and possibly important role of this protein in tissue regeneration.

2. **Does Arl13B regulate the development of reactive astrogliosis during cortical lesion?**

Next, I sought to detect the contribution of Arl13B in brain injury and glial scarring. Heightened understanding of the activity of astrocytic primary cilia and Arl13B under reactive conditions establishes their importance in neuropathology and elucidates potential therapeutic targets.

My second aim, founded on the data gathered from my first aim, was to determine the role of Arl13B in cortical injury. Arl13B is known to direct neuronal migration embryonically and additionally is implicated in Joubert's syndrome [88, 110]. I hypothesized that Arl13B is involved in the reparations following brain injury, including ciliary destabilization and expression in the cell body. Specifically, we postulated that the signaling mechanisms of Arl13B require absorption of the primary cilium to allow for translocation of the protein into the cell body. Furthermore, we proposed that signaling differences initiate cytoskeletal reorganization required for the morphological alterations in reactive astrocytes.

My results showed that in four strains of mice, C57BL/6 Control, Arl13B-mCherry; Centrin2-GFP (Gain-of-Function), Arl13B Loss-Of-Function, and Conditional IFT88-UBC-Cre/ert2 Knockout, Arl13B expression levels were heightened near the cortical lesion seven days post injury. GFAP expression levels were mixed between the strains and did not reveal significant trends in heightened or decreased gliosis seven days post injury. Our findings suggest that although Arl13B shows a clear pattern of heightened expression proximal to the injury site, GFAP-positive astrocyte expression is not clearly impacted. Although these findings do not negate the possible implication of Arl13B in brain injury, they do not support its relevance in astrogliosis.

3. Can EEG waveform analysis be used as a non-invasive means of early diagnosis of AD prior to the onset of symptoms?

Lastly, I sought to determine if waveform analysis of electroencephalogram (EEG) could be used to identify early hallmarks of Alzheimer's Disease prior to the onset of symptoms, subsequently providing the foundation for early diagnosis and proactive therapeutic intervention.

My third aim was to investigate the electroencephalogram (EEG) patterns of a mouse model of Alzheimer's disease (AD) to determine if EEG recordings can be used to determine the presence of the disease prior to the onset of symptoms. I hypothesized that power spectral density and burst suppression density quantification could yield relevant characteristics indicative of the dormancy and potential of AD while the subject was anesthetized with isoflurane. Specifically, I postulated that examination of differences in frequency bins associated with drowsiness and sleep (Alpha, Theta, and Delta) and the percentage of suppressed epochs would differ in young (three-month-old) mice if carrying the mutation indicative of the future onset of the disease.

Our findings reveal that at 3 months of age, the time at which APP23 mice may begin to develop the AD phenotype, APP mice display a lower relative percent of Delta power spectral density than that of control mice during isoflurane exposure. Both Theta and Alpha were shown to be higher in APP mice at this age. Burst Suppression Density increased in all age ranges tested as the length of isoflurane exposure increased, and it was significantly higher in young (3-4-month-old) APP23 mice when compared to controls. These findings substantiate our hypotheses that there are statistically significant differences detectable in the anesthetized EEG of a mouse model of AD.

viii. Rationale & Significance

A multitude of research focuses on the implication of primary cilia in disease. They are known to be involved in obesity [57, 130], polycystic kidney disease [34, 68], cognitive impairment [46], Joubert's syndrome [103], and certain forms of cancer [92]. Current neuroscience research focused on primary cilia target neurons, determining their transduction pathways and signaling dynamics. Yet, there is limited research conducted on astrocytic primary cilia.

Astrocytes, which become more recognized every passing year for their importance in neurological homeostasis and repair, possess primary cilia, yet research pertaining to this subject is extremely limited. While several studies show that astrocytic primary cilia are involved in the development of glioblastomas, there is incomplete understanding of their function and role within the mature brain. During the progression of reactive gliosis and development of conditions resulting in altered and potentially impaired brain function, the role of astrocytic primary cilia is unknown. Comprehensive understanding of the development and proliferation of reactive astrocytes requires explication of the participation of astrocytic primary cilia under reactive conditions. Clarification of the roles of astrocytic primary cilia could illuminate potential therapies and enhance understanding by the scientific community.

Furthermore, the functionality of Arl13B, the accepted astrocytic primary cilia marker, is poorly understood. This unique GTPase is known to promote ciliogenesis [131], maintain GEF activity of Arl3 [102], and regulate Sonic Hedgehog Signaling [113]. However, its full range of functioning is unknown. Our initial investigations revealed

alterations in protein expression of Arl13B proximal to cortical injury, indicated an unexpected and previously unreported role of Arl13B in the regulation of brain injury.

Lastly and of great importance with consideration of the pathogenic brain, is the need to determine early and non-invasive methods of diagnosis for Alzheimer's disease. AD accounts for more than half of case of dementia in the United States [12], but there is currently no method of reversal of the disease. Once the disease has progressed, it is reported to show abnormalities in EEG patterns and power spectral density [132], but this research is limited. Additionally, it is not reported whether burst suppression can be used as a diagnostic tool for this disease, especially prior to presentation of disease symptoms. EEG analysis while under anesthesia is a cost-effective and minimally intrusive means to examine brain activity. Power spectral density and burst suppression density can be quantified algorithmically and visually from a patient's EEG recordings, allowing for different methods of analysis provide early diagnosis, thereby supporting early intervention.

Chapter 2

METHODS

i. Transcardial Perfusions & Tissue Fixation

For transcardial perfusions, mice were first sedated with ketamine administration or euthanized with carbon dioxide. Most 4-8-month-old adult mice were deeply anesthetized by an intraperitoneal injection of ketamine (Ved Co, KetaVed, NDC 50989–161-06,)/xylazine (AKORN, NDC 59399–111-50) and monitored for non-responsiveness. Lack of response was measured via absence of pedal reflex from a toe pinch and absence of vertebral response via tail squeeze. After complete lack of response was verified, specimen was stabilized with pins and the thoracic cavity was exposed.

Several mice used for experiments were instead euthanized by carbon dioxide administration, prior to immediate transcardial perfusion. After being individually placed in an empty, clean cage, carbon dioxide administration would begin at a rate of 10-30% of the chamber volume per minute. Twenty seconds following last breath, (roughly 3-4 minutes of exposure), the mice were removed for immediate perfusion and secured to dissection pad.

Once secured and the thoracic cavity exposed, the right atrium was punctured with surgical scissors and a catheter was inserted into the left ventricle. Ice cold Phosphate Buffer Saline (PBS) was infused at a rate of 20 mL/min for approximately 5 minutes.

This cleansed tissue from blood and prepared it for fixation. At least 20 mL of 4% paraformaldehyde (PFA) (Sigma-Aldrich, 252,549-1 L) was then infused for preliminary fixation.

Whole brains were extracted and placed in 4% PFA overnight, while rocking at a slow rate at 4˚C. The following day, tissue was washed in and then placed in 30% sucrose in PBS for dehydration purposes. Dehydration is an essential step of the fixation process, which removes fixative and tissue fluid in preparation for staining. Tissue remained rocking at 4˚C for approximately 48 hours or until tissue sank completely. Following this fixation and dehydration process, tissue was then flash frozen on dry ice and stored at -80˚C until sectioned.

ii. Cryostat Sectioning

Prior to staining, flash frozen tissue was sectioned on a Leica CM3050 S cryostat to 30–35-micron sections at −18 °C. Tissue-tek optimal cutting temperature compound (OCT) was used to mount tissue within the cryostat. Once fully secure, brain tissue was sectioned from anterior to posterior, with attention to the location of injured cortex or hippocampal regions. Desired regions were distributed into Eppendorf tubes filled with cryoprotectant (3:3:4, glycerol: ethylene glycol: PBS) and maintained at -20˚C until use for immunohistochemistry.

iii. Immunohistochemistry

To remove cryoprotect and residual OCT, thawed and sectioned tissue was first washed 3 times at 10 minutes each in PBS at room temperature (RT) on an orbital shaker. Large tissue pieces were transferred using baskets in a 12 well plate, while small and fragile tissue pieces, like those from cortical injury studies, was transferred by use of a Pasteur pipette in a 48 well plate. Tissue was then permeabilized in 0.5% Triton in PBS (PBST) 3 times at 10 minutes each at RT to reduce background and enhance the accessibility of cellular epitopes. Tissue was then blocked at RT in blocking buffer: 10% donkey serum (Sigma, D9663–10 ML), 2% bovine serum albumin (Sigma-Aldrich, A7906-100G), and 0.1 M glycine (Apex, 18–109) in 0.5% PBST for 1.5 to 2 hours.

Following this staining preparation, tissue was then stained with a selection of the primary antibodies listed in **Table 1** while gently rocking overnight at 4˚C. The following day, tissue was washed 3 times at 10 minutes each in 0.5% PBST and then incubated with Alexa Fluor secondary antibodies 488, 546, and 647 at 1:500 dilution for 1.5 hours. Stained tissue was then washed 1 time in 0.5% PBST and 2 times in PBS for 10 minutes each. Floating sections were then mounted to gelatin coated slides with DAPI nuclear stain, and coverslips were secured with clear nail polish. Slides were stored at -20˚C until imaging with confocal microscopy.

iv. *Seizure Phenotyping*

To phenotype mice displaying spontaneous audiogenic seizures, Arl13B-mCherry; Centrin2-GFP transgenic mice (Arl mice) were monitored for seizure-like behavior graded with a modified Racine scale (Table 2). The Arl mice have a hybrid FVB; BALB; C57BL/6 background. Strains of FVB mice are known to show predispositions to audiogenic seizures [133-135]. This suggests that the seizure activity found in our population of Arl mice may have been a of the partial FVB background.

Mice were observed individually 10 times over 2 weeks. To determine presence of seizure activity, mice were individually removed from their home cage and placed in a clean, empty cage for 30-60 seconds. This activity was usually enough to initiate seizure activity. Afflicted animals were marked with an animal marker and then returned to littermates in their home cage. Following the 2-week initial period of observations, mice were checked weekly throughout the duration of the experiment to determine phenotypic changes and re-mark as necessary.

v. EEG/EMG Recording

To verify that the epileptic-like behavior being observed was in fact seizure activity, mice underwent EEG/EMG surgeries and recordings. Equivalent numbers of seizure and non-seizure 4-8-month-old mice were further divided into equally sexed groups. This age range was used to provide the opportunity for the onset of seizure activity, which was not displayed in younger mice. Mice were individually anesthetized with 1.5–3% isoflurane (Henry Schein, NDC 11695–6776-2). Once fully sedated, mice were stabilized in a stereotaxic frame (Kopf instruments) by non-rupture ear bars. Once

secured, isoflurane anesthesia was maintained and mice were prepared for surgery by hair removal and skin sterilization with alcohol and 4% chlorhexidine (Phoenix, NDC 57319–612-09). Ophthalmic ointment (Solutions, Alta lube Ointment, X0020S6KF) was applied to prevent corneal drying. An injection of 1 mg/kg lidocaine (Phoenix, NDC 57319–533-05) was administered to the scalp and 5 mg/kg carprofen (Putney, NDC 26637–521-02) was injected subcutaneously in the dorsal region.

A single incision was made along the sagittal suture and skin was pulled laterally. The surface of the cranium was dried with sterile cotton swabs. The EEG/EMG head-mount (Pinnacle Technology Inc., Cat # 8201) was then fixed to the cranium with VetBond (3 M VetBond, 1469SB) and 3 holes were drilled into the skull with a sterile 24-gauge needle. Micro-screws (Pinnacle Technology Inc., Cat # 8209) were used to further secure the head mount with Resin (Resin lab, SEC 12334GR) positioned between the screws and head-mount prior to tightening.

Two probes attached to the back of the head-mount were inserted into the spinotrapezius of the cervical region of the mouse. Skin was then sutured around the base of the implant as needed. Following this, the head-mount and screws were secured with dental cement. Recovering mice were allowed to rest on a heating pad until fully active. Mice were given 5 mg/kg carprofen injections (Putney, NDC 26637–521-02) or meloxicam tablets in cage (Meloxicam (233634, BioServe, MD275-0125) as analgesia for 2-3 days following surgery and monitored for weight or health fluctuations.

After a recovery period not exceeding 1 week, mice were secured with EEG/EMG Pinnacle Technology recording equipment and monitored for 48 hours. During this time, mice were housed in individual enclosures and allowed food and water ad libitum.

Recording equipment did not interfere with the free movement of animals. Mice were sacrificed via transcardial perfusion within 24 hours of the completion of their recording.

vi. Isoflurane Administration

Approximately one week following EEG/EMG head-mount surgery, mice were secured with Pinnacle EEG/EMG recording equipment. Mice were allowed to move freely for at least five minutes and then placed [singularly] into a chamber filled with 3% isoflurane gas. Mice remained in the isoflurane chamber for 15 minutes before being removed and allowed to rouse. Times were recorded and added to parallel virtual file system (pvfs) files to support accurate waveform analysis. All mice were monitored until they fully righted and showed normal activity.

vii. Sirenia Software Analysis

Sirenia Seizure Pro software (Pinnacle Technology Inc. Version 1.8.3) was used to identify seizure activity. Automated software was used to identify seizure-like electrical activity greater than 5 seconds. All artifacts were confirmed visually and then compared for sexual bias, time of day, length of event, EEG and EMG amplitude. Seizure behavior was characterized by frequent and chaotic EEG peaks displaying high power. This activity was often correlated with heightened EMG activity.

Sirenia Sleep Pro scoring software (v. 2.1.0) was used to examine EEG/EMG recordings of four Arl mice for the first twenty-four hours of recording. Mice were gender

balanced, with two having been phenotyped as displaying seizure activity and two without prior knowledge of this behavior. To maintain consistency with analytics from Sirenia, power was set to Sleep Pro defaults as follows: Alpha 8-13; Beta 13-30; Gamma 35-44; Delta 0.5-4; and Theta 4.5-8.5. Activity was first scored into Wake and NREM via cluster scoring of EEG2 Delta against EMG 50-150. Activity was then visually confirmed and scored by the following criteria: Wake was associated with moderate to high EMG activity; NREM maintained low EMG activity and high EEG power; REM displayed low EMG activity, but low power and high frequency.

viii. Confocal Imaging & ImageJ Analysis

Tissue stained via immunohistochemistry was imaged with a Nikon A1R HD25 microscope. Tiled and non-tiled Z-stacks were collected while imaging hippocampal regions and/or cortical injury of different murine strains. Variation in tissue quality and antibody binding required small variations in visualizing controls to enhance picture quality. 2-4 Z-stacks were acquired of each cornu ammonis 1 (CA1), cornu ammonis 3 (CA3), and dentate gyrus (DG) regions of the hippocampus (**Figure 5**). 2-4 images of the ipsilateral and contralateral hemispheres were acquired in support of injury analysis.

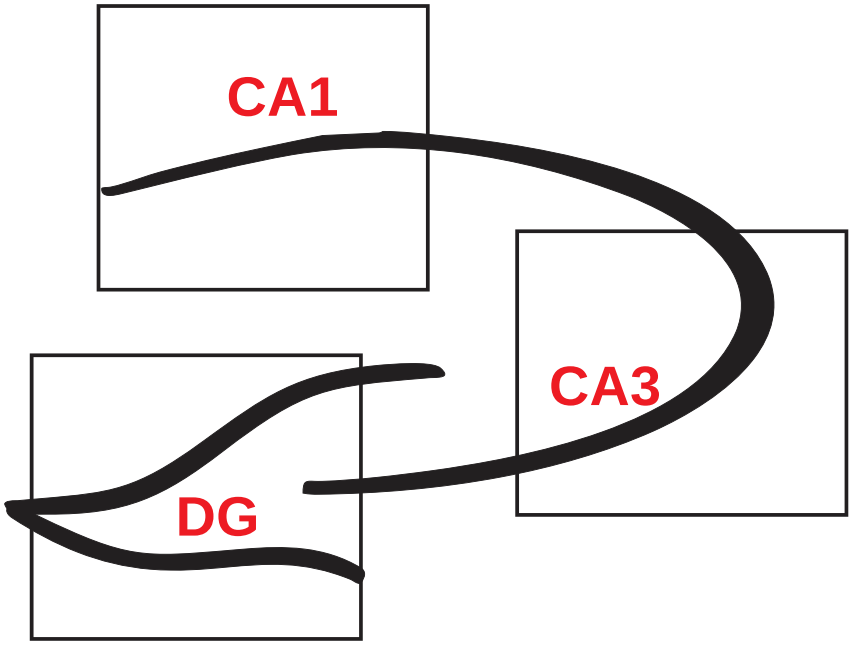

Figure 5: Architecture of the Hippocampus. Astrocytic and neuronal primary cilia were measured in the CA1, CA3, and DG regions of the hippocampus. Squares represent locations in which cilia were measured. Distinguishable astrocytic cilia were measured within the white regions of the squares. Neuronal primary cilia were measured within the black, cellular localizations within the squares.

Collected images were then quantified with Fiji ImageJ Analysis (ImageJ 1.52f, Java 1.8.0_172 (64-bit). Analysis consisted of ciliary measurements and protein intensity analysis. To verify that only Arl13B-positive astrocytic cilia were measured, distinguishable cilia in the tissue surrounding to the cellular localizations of CA1, CA3, and DG were used only (**Figure 5**). Distinguishable AC3-positive neuronal cilia were measured directly within the gathering of cells in hippocampal regions. Due to the limited number of Arl13B-positive cilia in CA1 and CA3, all fully identifiable astrocytic cilia were measured and used for analysis in these regions. For Arl13B-positive cilia in the DG and cortex, and all AC3-positive cilia, there were significantly more distinct cilia. Thus, approximately 50 cilia were measured per image in these regions.

Astrocytic reactivity was identified via somatic differences of astrocytes within the hippocampus or cortex. GFAP expression was elevated in these cells, as measured with GFAP intensity, and reactive astrocytes encompassed a larger region, extending processes into the territory of neighboring astrocytes. GFAP and Arl13B protein intensity was quantified with a plot profile of ImageJ pixel intensity analysis of 3-4 500-micron lengths per region of the brain and then averaged per site.

ix. Cortical Injury Model

Experimental mice were individually sedated with 1.5–3% isoflurane (Henry Schein, NDC 11695–6776-2). Once unresponsive, mice were secured in a stereotaxic device (Kopf instruments) by non-rupture ear bars. While under anesthesia, mice were prepared for surgery by hair removal and skin sterilization with alcohol and 4% chlorhexidine (Phoenix, NDC 57319–612-09). Corneal drying was prevented by the administration of ophthalmic ointment (Solutions, Alta lube Ointment, X0020S6KF). 1 mg/kg of lidocaine (Phoenix, NDC 57319–533-05) was injected into the scalp and 5 mg/kg carprofen (Putney, NDC 26637–521-02) subcutaneously administered posterior to the thoracic cavity.

A small sagittal suture was made to expose bregma and lambda, the intersections of the sagittal suture and coronal and occipital suture respectively . Cranial bones were dried and cleansed with sterile cotton swabs or gauze. A single hole was drilled 1-3 mm lateral to the sagittal suture and approximately 3 mm anterior to lambda. A sterile needle was then secured to the stereotaxic frame and lowered to the meninges. The

needle was then inserted 3 mm deep into the brain by the stereotaxic arm. This insertion was repeated in triplicate to ensure effective cortical injury. The incision was then sutured, and mice were allowed to recover on a heating pad. They were monitored until fully active and given meloxicam (233634, BioServe, MD275-0125) as analgesia for 3 days following surgery. Mice were sacrificed via transcardial perfusion within one week following surgery.

x. Brainstorm Analysis

Power spectral density and Phase Amplitude Coupling were quantified using Brainstorm software (version 3.220115) [35] via the MATLAB platform (version R2021b_9.11.0.1809720). Brainstorm is a graphical user interface (GUI) created for analysis of EEG waveform [35]. EEG recordings of APP23 mice undergoing exposure to isoflurane anesthesia were extracted by Sirenia sleep pro software and converted to EDFs. EDF files were uploaded into brainstorm to be filtered and processed.

Filtering

All EEG recordings incorporated into Brainstorm underwent three forms of processing. First, DC offset was removed to reduce offset from digitization [136]. A band pass filter [136-138] was then applied between 0.5 and 199 Hz (Butterworth filter, low pass order 4, high pass order 3). Lastly, a notch filter [136, 139] was applied at 60 and 120 Hz with a bandpass of 1, to remove power line noise and its harmonics.

Power Spectral Density

Brainstorm was then used to apply Welch's Power Spectral Density algorithm [140, 141] to the filtered EEG files to quantify the density of the power frequencies. Powers were identified based on the following parameters: Delta: 0.5-4; Theta: 4-8; Alpha: 8-13; Beta: 13-30; Gamma: 30-200 [142]. Relative percentages of frequencies of PSDs averaged across bins per strain with respect to age and compared based on length of isoflurane exposure. Statistical significance was set as a P value of less than 0.05 via the Mann Whitney Test.

Phase Amplitude Coupling

Phase Amplitude Coupling (PAC) was calculated via the Brainstorm plugin of MATLAB. A high bandwidth of 50-120 Hertz was used as a nesting frequency against a low bandwidth of 3-10 Hertz, to compare Gamma and Theta, respectively [143, 144]. Statistical significance of maximum PAC was set as a P value of less than 0.05 via the Mann Whitney Test.

xi. Burst Suppression Density

Sirenia sleep pro software (version 1.0.3) was used to visually score eeg1 and eeg2 for periods of suppression by manually scoring epochs. First, time of isoflurane exposure was logged onto EEG recordings. After being sectioned into five-second

epochs, time intervals of one minute were compared and contained epochs were scored as suppressed or nor suppressed (**Figure 6**). Identification of suppressed epochs was quantified by five-second periods with little or no electrical activity as compared to epochs containing bursts of activity, indicative of neuronal firing. Total number of suppressed epochs were divided by the total number of epochs per minute (12) and multiplied by 100 to give the density of suppression [145]. All scored epochs were confirmed by a second scorer.

$$BSD = \frac{epochs_{suppressed}}{epochs_{total}} x\ 100$$

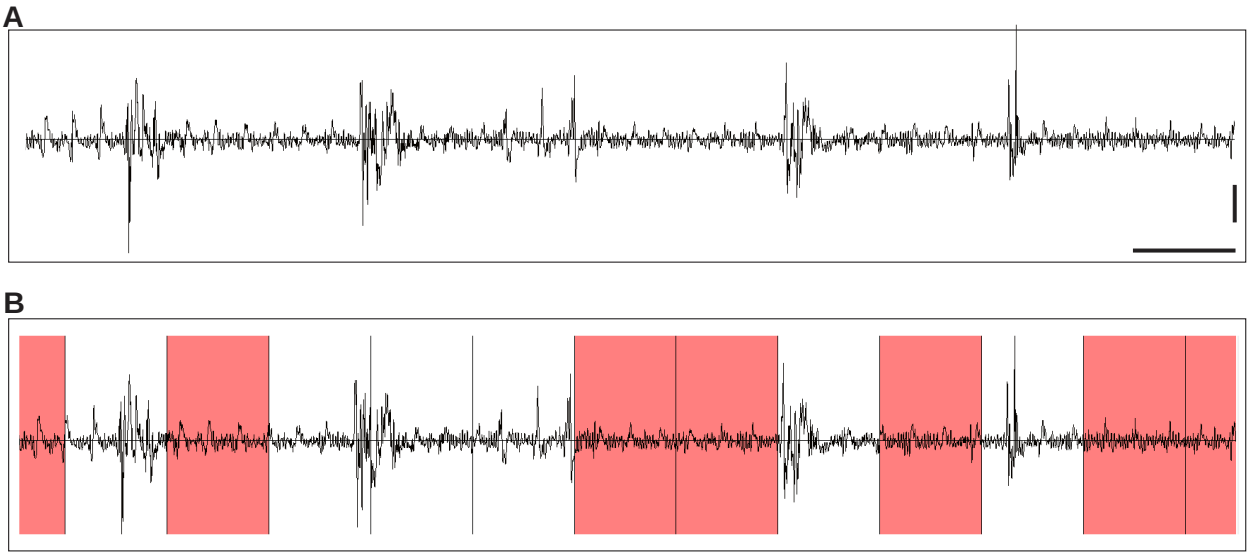

Figure 6: Identification of Suppressed Epochs. Sample of 60 seconds of raw EEG2 recording showing burst suppression pattern (A) sectioned into 5 second epochs (B) scored with red to indicate suppression (B). Y Scale bar: 50 µV.; X time scale: 5 seconds.

xii. Mouse Strains

FVB/N

The Friendly Virus B mouse (FVB) strain acquired from Jackson laboratories (Stock number: 001800) is widely used in scientific research. Known for fecundity and delivery of large litters, this strain has proven useful in genetic manipulation and analysis [146]. Predisposition to spontaneous audiogenic seizure activity has been reported in this strain [133-135]. This activity is usually initiated by mild to moderate stimuli, such as tail tattooing, clipping, and loud noises [133]. FVB mice were used as a control for ciliary length comparisons in these studies.

C57BL/6J

The C57BL/6J (Jackson lab stock number 000664) murine strain is one of the most commonly used strains in research [147]. This strain is generated to support a variety of studies, especially transgenic and knockout studies, and is the foundation of many investigations [148]. The C57BL/6J strain was used as a control for ciliary length comparisons and cortical injury studies.

Arl-mCherry; Centrin2-GFP

The Arl-mCherry; Centrin2-GFP strain (Arl mouse) can also be attained from Jackson Laboratories (stock number 027967). This is a hybrid strain with a mixed

background of FVB, BALB/c, and C57BL/6 strains (Jackson Laboratory). This strain was first generated by Bangs et al. in 2015 to investigate the expression of primary cilia during development [52]. In the following studies, the Arl strain was used to study ciliary length, overexpression of Arl13B, spontaneous seizure activity, and cortical injury.

UBC-Cre-ER2

UBC-Cre-ER2 mice (stock number 007001) acquired from Jackson Laboratories can be crossed with mice containing loxP sites to produce a tamoxifen inducible knockout of the floxed gene. This strain was crossed with IFT88 floxed and Arl13B floxed mice to produce a hybrid that could allow for selective gene knockout.

IFT88$^{flox/flox}$

IFT88^{flox} mice (stock number 022409) were acquired from Jackson laboratories and crossed with UBC-Cre-ER2 mice to produce IFT88; UBC hybrid strain. IFT88^{floxed} mice contain loxP sites around exons 4-6 of the IFT88 gene essential for intraflagellar transport and structure of the cilium (Jackson Laboratory). The hybrid cross of IFT88; UBC knocks out IFT88, resulting in ubiquitous ablation of primary cilia [50].

Arl13B$^{fox/flox}$

Arl13B^{floxed} mice (stock number 031077) were acquired from Jackson laboratories and crossed with UBC-Cre-ER2 mice to produce Arl13B; UBC hybrid strain. Arl13B^{floxed} mice contain loxP sites around exons 2 of the Arl13B gene (Jackson

Laboratory). The hybrid cross of Arl13B; UBC knocks out Arl13B, resulting in ablation of this GTPase in primary cilia and the surrounding tissue [149].

APP23

APP23 mice (stock number 030504) were acquired from Jackson laboratories. Both non-carriers and mutants hemizygous for Thy-1 APP were used as controls and AD models, respectively. These mice were transgenically modified to display an overexpression of the human amyloid precursor protein, which allows for the manifestation of AD-like symptoms starting at 3-months of age and progressively worsening [150].

xiii. Data Analysis

All data quantified with ImageJ were analyzed and graphed with GraphPad Prism (9.3.1) and JMP statistical analysis software. Analyses were completed with unpaired Student's T-Test with Welch's correction, one-way ANOVA with Bonferroni correction, density analysis, Kolmogorov-Smirnov test, and Mann-Whitney test [151]. Significance was denoted as follows: a *p* value less than 0.05 (*), less than 0.01 (**), and less than 0.001 (***). Data was presented as mean ± standard error of the mean.

CHAPTER 3

PRIMARY CILIA LENGTH VARIANCE

i. ASTROCYTIC VERSUS NEURONAL PRIMARY CILIA

Astrocytes and neurons present a functional diversity in the brain [6]. Astrocytes are supportive cells, which participate in a wide range of functioning and maintain proliferative capacity throughout maturity [4]. They are highly heterogenous and maintain versatility in pathogenic conditions. Neurons are electrically excitable cells primarily acting in signal transduction, which lose mitotic ability after differentiation [152]. Neurons rely on astrocytes to synapse with one another and succumb easily to damage [1, 61, 62, 70, 153].

Although both astrocytes and neurons exhibit primary cilia, their functional differences manifest in contrasting roles for this organelle. Morphologically, neuronal primary cilia are significantly longer than astrocytic cilia in the hippocampus; approximately 5.5 microns compared to roughly 3.0 microns respectively [7]. In order for ciliated vertebrate cells to mitose, the primary cilium must first retract into the cell to free the centrioles for translocation and spindle fiber production needed in anaphase [9]. The proliferative capacity of astrocytes indicates the potential requirement of ciliary

retraction, while the role of neurons as predominant signal transducers in the brain without mitotic capability suggest the structural logic in their ciliary length.

Astrocytic and neuronal primary cilia require different ciliary markers for effective antibody labeling. Astrocytes are known to express Arl13B in their ciliary membrane at maturity [8, 48]. Alternative antibodies that effectively stain astrocytic cilia in both *in vitro* and *in vitro* conditions are unknown. Neuronal cilia are known to express several ciliary proteins and thus have multiple ciliary markers that are effective under different conditions. These include AC3, SSTR3, 5-HT6, and MCHR1 [48].

It has been reported that astrocytes and neurons display differential ciliary protein levels at immaturity. In 2014, Kashara et al. reported that although colocalization of Arl13B and AC3 can appear in cilia of P10 mice, astrocytes at P56 predominantly express Arl13B and neurons express high levels of AC3 [8]. The distinction between ciliary protein expression indicates functional variations between these cell types.

We hypothesized that the functional differences between astrocytes and neurons manifest in morphological differences in their primary cilia. We thus used immunohistochemistry, confocal microscopy, Arl13B antibody and AC3 antibody to visualize cilia. We focused on regions within the hippocampus to support quantitative imaging with regional consistency. We compared 3 strains of mice: C57BL/6, FVB, and Arl13B-mCherry; Centrin2-GFP (Arl mice).

Results

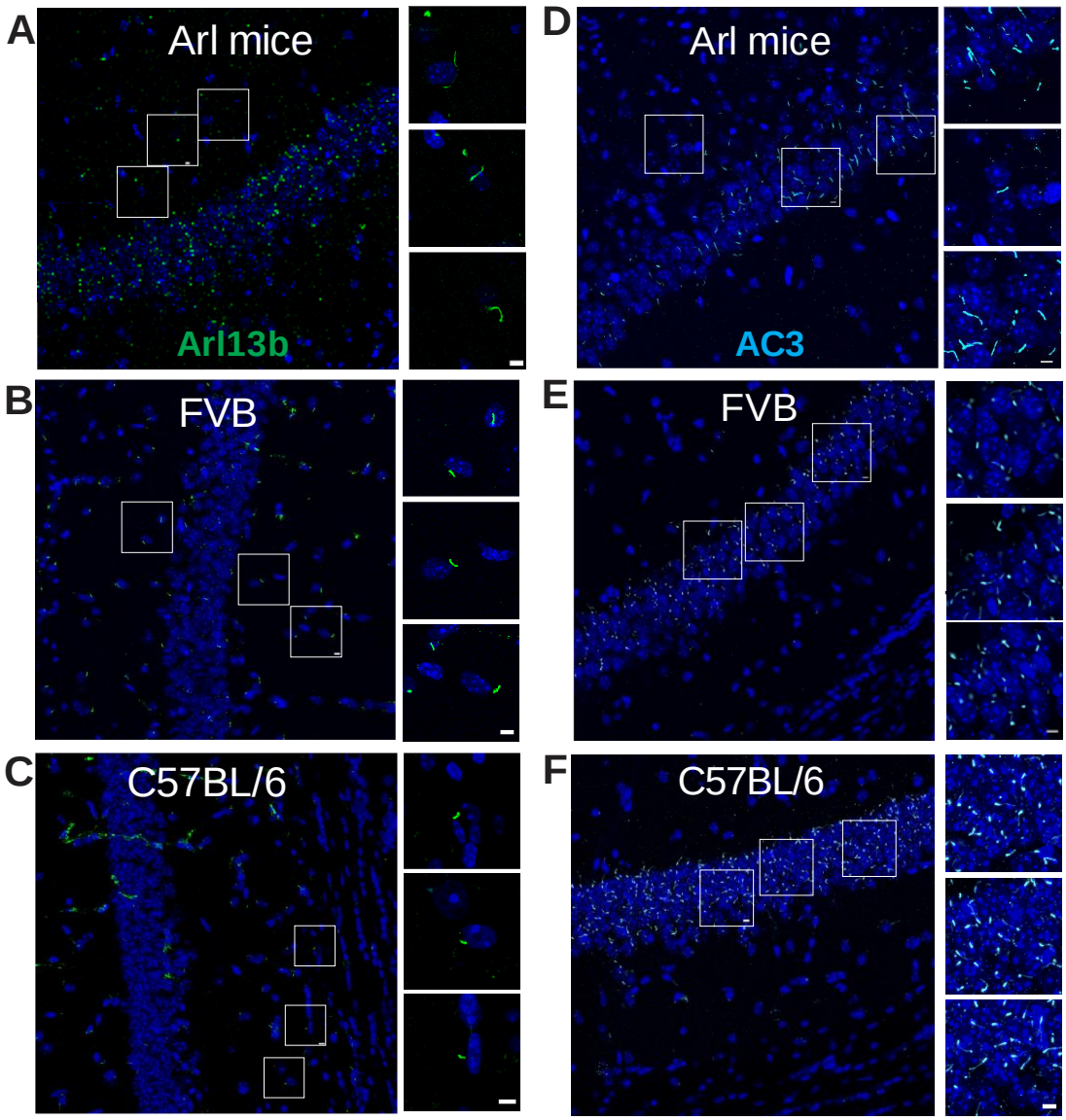

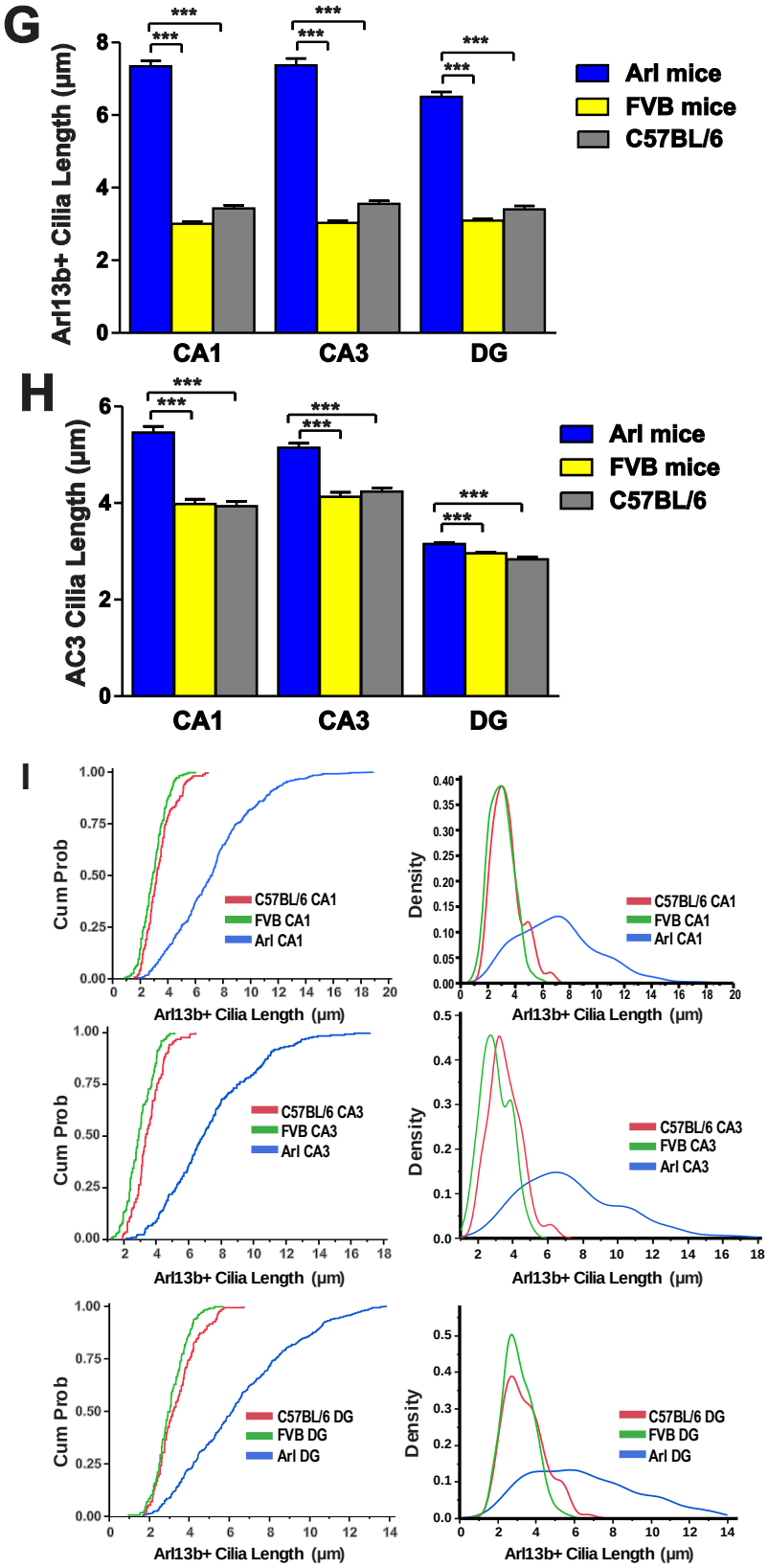
G
Arl13b+ Cilia Length (µm)
Arl mice
FVB mice
C57BL/6
CA1
CA3
DG
H
AC3 Cilia Length (µm)
I
Cum Prob
Density
C57BL/6 CA1
FVB CA1
Arl CA1
C57BL/6 CA3
FVB CA3
Arl CA3
C57BL/6 DG
FVB DG
Arl DG
Arl13b+ Cilia Length (µm)

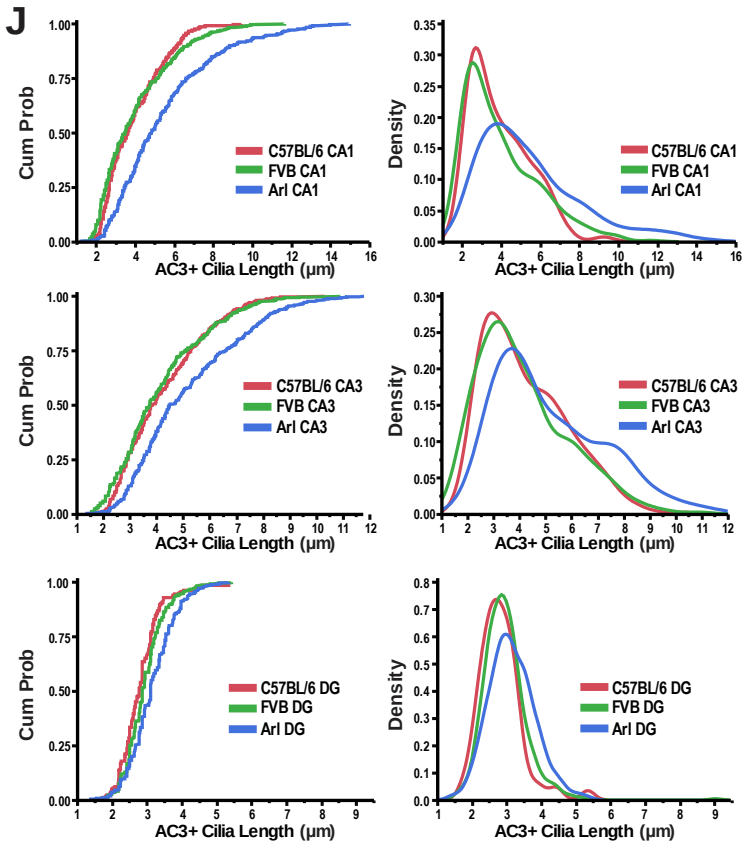

Figure 7: Regional Variance of Primary Cilia Length in the Hippocampus. *Figure sourced from Sterpka et al., 2020* [6]. Arl13b-positive and AC3-positive primary cilia of Arl mice are longer than those of FVB/N and C57BL/6 wildtype mice. **a-c, g** Arl mice had longer Arl13b-positive primary cilia than control mice in the hippocampal CA1, CA3, and DG regions. **a** Arl mice, **b** FVB/N controls, **c** C57BL/6 controls. Representative images were taken from the CA1 region. Scale bar, 5 µm. **g** Comparison of Arl13b + cilia length in the hippocampal CA1, CA3, and DG of three mouse strains. Arl mice, $N = 8$; FVB/N mice, $N = 5$; C57BL/6, $N = 4$. Cilia number: Arl mice: 399, 230, and 435; FVB/N: 213, 146, and 254; C57BL/6: 144, 118, and 116. Data were compared with one-way ANOVA test with post hoc Tukey test. CA1: $F(2, 753) = 307$, $p < 0.001$; CA3: $F(2, 491) = 251$, $p < 0.001$; DG: $F(2, 802) = 241$, $p < 0.001$. (**d**-**f**, **h**) Arl mice had longer AC3-positive primary cilia in three subregions in the hippocampus. **d** Arl mice, **e** FVB/N controls, **f** C57BL/6 controls. Scale bar, 5 µm. **h** Comparison of AC3+ primary cilia length in hippocampal CA1, CA3, and DG regions. Arl mice, $N = 4$; FVB/N, $N = 5$; C57BL/6, $N = 3$. Cilia number: Arl mice, 403, 471, and 527; FVB/N mice: 386, 343, and 555; C57BL/6: 202, 422, and 180. Data were analyzed with one-way ANOVA test with post hoc Tukey test. CA1: $F(2, 988) = 58$, $p < 0.001$; CA3: $F(2, 1233) = 40$, $p < 0.001$; DG: $(2, 1259) = 21$, $p < 0.001$. **i** CDFs and histogram density of cilia length show the distribution differences of Arl13b-positive cilia length in different hippocampal regions of the three mouse strains. **j** CDFs and histogram density of cilia length demonstrate the distribution differences of AC3-positive cilia length in different regions of three mouse strains. *Legends sourced from Sterpka et al, 2020 [6].*

Confocal imagery revealed length differences between Arl13B-positive and AC3-positive primary cilia, regional variations of length within the hippocampus, and even strain variance *(***Figure 7: A-F**). Measurements revealed that Arl13B-positive cilia were significantly shorter than AC3-positive cilia in all regions of the hippocampus for C57BL/6 and FVB mice **(Figure 7: G-H**). Arl mice displayed significantly longer astrocytic and neuronal cilia in all regions than both other strains, suggesting an overexpression of Arl13B **(Figure 7: G-H)**. Density comparison analysis and cumulative distribution functions were used to verify significance **(Figure 7: I-J).**

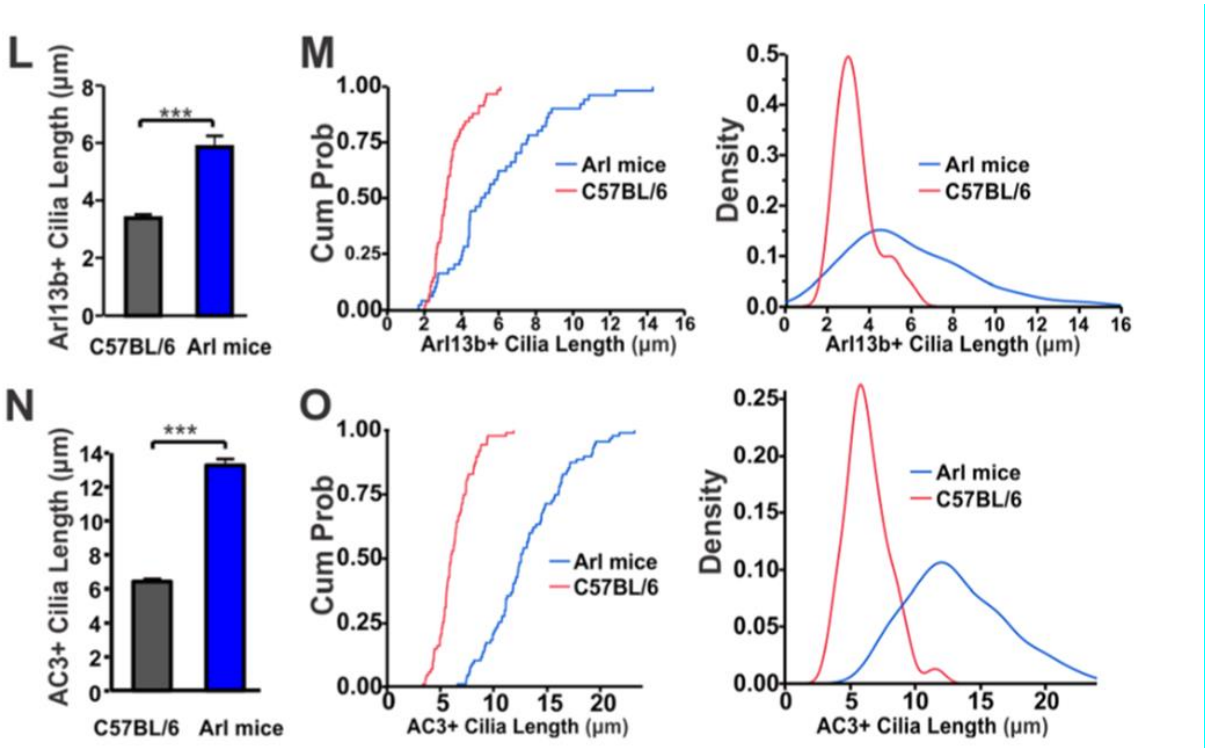

Figure 8: Arl13b Elongates Cilia length in Primary Cultures. *Figure sourced from Sterpka et al, 2020 [6].* **l** Arl13b-positive cilia in primarily cultured astrocytes were significantly longer than those derived from C57BL/6 mice (***, $p < 0.001$, unpaired Student's t-test). Data were collected from 6 Arl cultures, 5 C57BL/6 cultures. Cilia number: Arl mice, 50; C57BL/6 mice, 57. **m** CDFs and density comparisons demonstrate the differences in Arl13b-positive cilia length between Arl mice and C57BL/6 mice. **n** AC3-positive cilia in primarily cultured cortical neurons (~ 10 days in vitro) were significantly longer than those derived from C57BL/6 mice (***, $p < 0.001$, unpaired Student's t-test). Data were collected from 6 Arl cultures, 6 C57BL/6 cultures. Cilia number: Arl mice, 87; C57BL/6 mice, 87. **o** CDFs and density

comparisons demonstrate the differences in AC3-positive cilia length between Arl mice and C57BL/6 mice [6]. *Legends sourced from Sterpka et al, 2020 [6].*

To substantiate morphological variances between Arl and C57BL/6 mice, primary cultures of astrocytes and neurons were harvested to investigate variations in Arl13B-positive primary cilia and AC3-positive primary cilia respectively. Cortical tissue from day old pups was used to create pure cultures. Immunocytochemistry uncovered significant length differences in primary cilia, with Arl mice exhibiting significantly longer astrocytic and neuronal cilia lengths (**Figure 8: L-O**).

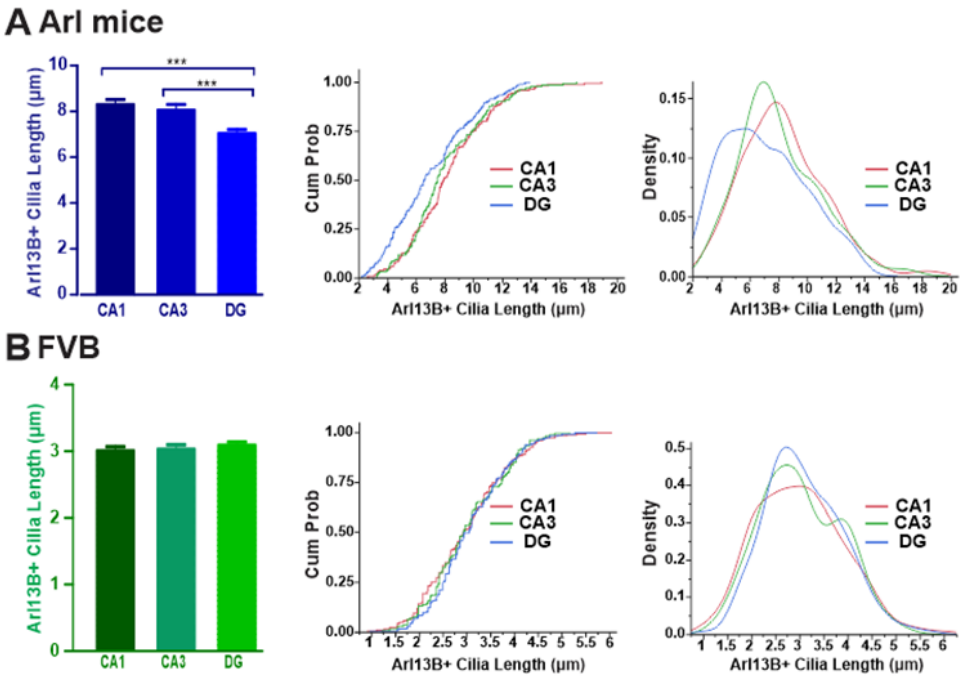

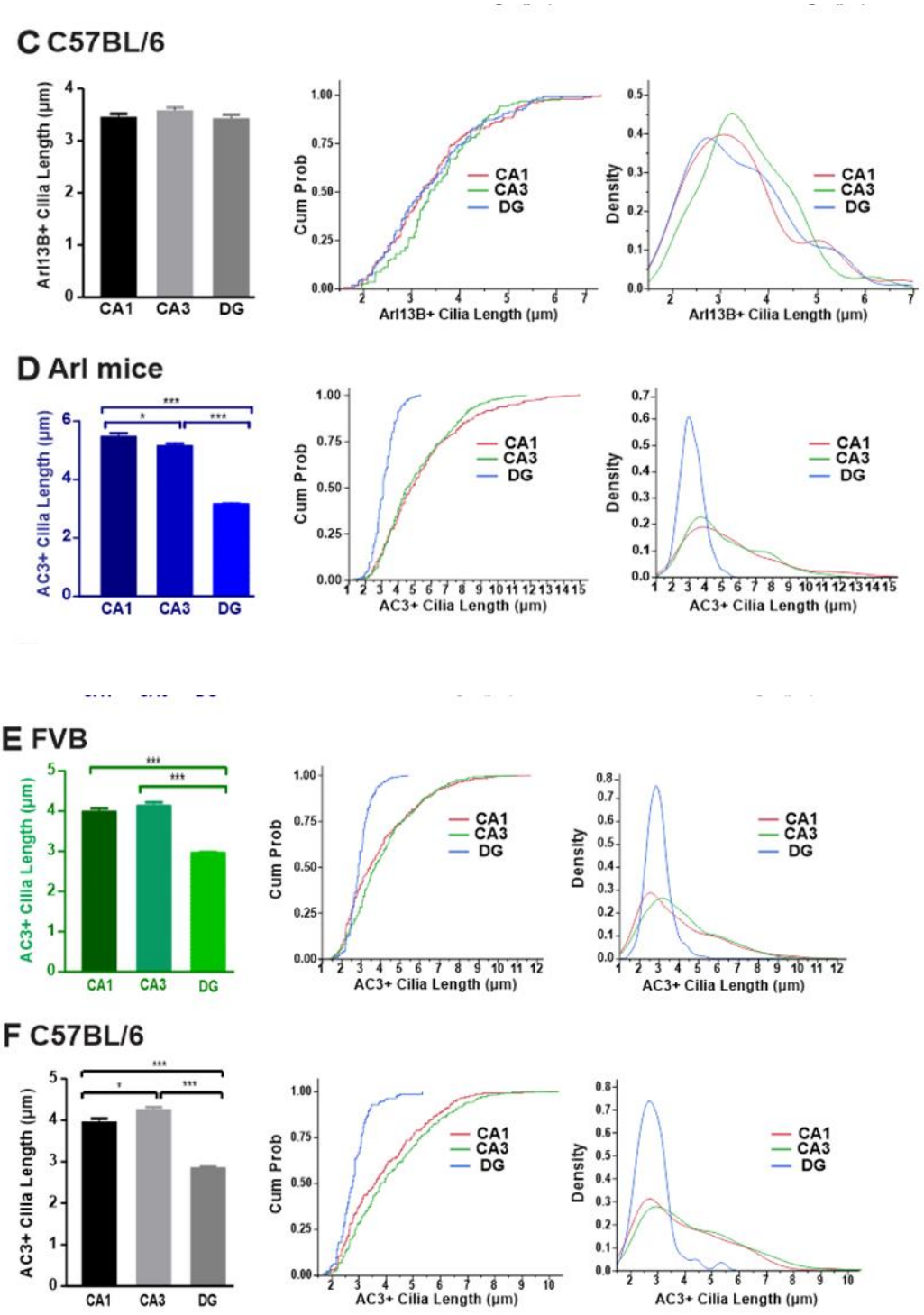

Figure 9: Primary Cilia Length in Different Strains of Mice. *Figure sourced from Sterpka et al, 2020 [6].* Regional cilia length variations in the hippocampal CA1, CA3 and DG in Arl mice, FVB/N and C57BL/6 mice. **a** Arl13b-positive cilia in hippocampal regions of Arl mice were significantly shorter cilia in the DG than in CA1 or CA3 (***, $p < 0.001$, unpaired Student's t-test). $N = 8$ mice. Cilia number: 399, 230, and 435. **b** Arl13b-positive cilia of FVB/N mice had no significant differences in length among hippocampal CA1, CA3, and DG regions. $N = 5$ mice. Cilia number: 213, 146, and 254. **c** Arl13b-positive

cilia of C57BL/6 mice had no significant differences in length among the hippocampal CA1, CA3, and DG regions. $N = 4$ mice. Cilia number: 144, 118, and 116. **d** AC3-positive cilia in the hippocampal DG region of Arl mice were significantly (***, $p < 0.001$) shorter than in the CA1 and CA3 regions, and significantly shorter in the CA3 than in the CA1 (*, $p < 0.05$). $N = 4$ mice. Cilia number: 403, 471, and 527. **e** AC3-positive cilia in hippocampal DG regions of FVB/N control mice were significantly (***, $p < 0.001$) shorter than in the CA1 and CA3 regions. $N = 5$ mice. Cilia number: 386, 343, and 555. **f** AC3-positive cilia in hippocampal DG regions of C57BL/6 mice were significantly (***, $p < 0.001$) shorter than in the CA1 and CA3 regions. $N = 4$. Cilia number: 202, 422, and 180. Data were analyzed with one-way ANOVA with post hoc Tukey test. Arl13b: Arl strain: $F(2, 1061) = 11.05$, $p < 0.001$; FVB: $F(2, 610) = 0.5850$, $p = 0.4632$; C57BL/6: $F(F(2, 3775) = 0.7700$, $p = 0.4632$; AC3: Arl Strain: $F(2, 1398) = 213.6$, $p < 0.001$; FVB: $F(2, 1281) = 93.82$, $p < 0.001$; C57BL/6: $F(2, 801) = 62.96$, $p < 0.001$

Remarkably, FVB and C57BL/6 mice did not display any regional differences in Arl13B-positive ciliary length (**Figure 9*).*** Arl mice showed a marked decrease in length of cilia residing in the dentate gyrus. AC3-positive cilia displayed shortened lengths in the dentate gyrus of all 3 strains, and a moderate shortening in CA3.

Clear morphological differences exist between Arl13B- and AC3-positive cilia, supporting the hypothesis of functional diversity. The maintained heterogeneity of astrocytes warrants the need for shortened cilia to accompany proliferation and cellular migration. The extended and stable cilia of neurons support the signaling nature of neurons. Regional variations in the hippocampus manifesting in a variance of ciliary length may indicate locale-based functional variance. The variation in ciliary length based on murine strain was likely due to an overexpression in the Arl mouse based on the CAGG promoter location of fusion protein. There were no obvious differences between the two control strains.

ii. EFFECT OF SEIZURES ON PRIMARY CILIA

Reactive astrocytes are reported to develop during seizure activity, although their complete role in countering or propagating seizures remains unclear [3, 154-156]. The

reactivity of astrocytes is a hallmark of the epileptic brain, but it is unknown whether reactive astrocytes are simply a homeostatic response to aggravated conditions or perpetuators of seizure activity. The basic elements of the development of reactive gliosis indicate toxicity present in the brain requiring demarcation of healthy tissue or altered astrocytic function, correlative with variations in morphology [1, 153]. Contrasting views suggest that the altered expression and function of astrocytes yield seizure activity by reduction of synaptic maintenance, and subsequent excess of neurotransmitters [3, 154, 156].

Scientific investigations have reported that seizures induced with piloporcaine and kainic acid disrupt neuronal primary cilia lengths [157, 158], but these studies are limited in their investigation of different types of primary cilia in the brain, as well as the type of seizure induction. One study generalized glial cilia with use of Arl13B and GFAP antibodies and analyzed their lengths after seizure induction, but no differences were reported [157]. This study showed that neonatal seizure activity was enough to disrupt neuronal ciliary lengths in the developing mouse [157]. Nonetheless, there are presently no scientific studies investigating the response of astrocytic primary cilia to seizure activity.

We hypothesized that astrocytic primary cilia were implicated under epileptic conditions. Under the assumption that glial cells were overlooked in past research based on the generalized focus on neuronal cilia, we postulated that the importance of astrocytic function, signaling, and proliferation under reactive conditions would result in ciliary morphological alterations. Specifically, we expected a shortening of cilia in astrocytes to support the need of ciliary resorption

A percentage of FVB/N strain of mice is reported to display spontaneous, audiogenic seizure activity [133-135]. This epileptic activity is initiated by mild manipulation of the mouse, including cage changes and loud noises [133-135]. Research has shown that mice exhibiting convulsive behavior suffer an array of physiological disturbances, including: lower weights [135], decreased motor neuron function [135], lower neuronal densities [134], astrocyte hypertrophy [133], and necrotic neuronal tissue [133].

The Arl13B-mCherry; Centrin2-GFP strain we acquired from Jackson Laboratory is a hybrid cross, including FVB/N in its background. Cage changing revealed that a high portion of our population of Arl mice displayed seizure activity. This occurrence of epileptic activity presented a unique opportunity for us to investigate the effect of repetitive, spontaneously occurring seizures on primary cilia. We thus pursued verification and immunohistochemical analysis of these mice.

To first determine the percentage of mice displaying a seizure phenotype, all animals were individually observed on a daily and then intermittent basis. I found that 42% of our population displayed seizure activity (**Figure 10**)**.** To substantiate that the convulsive behaviors were in fact seizures, we next performed EEG/EMG probe implants and 48-hour recordings on cohorts of control and seizure Arl mice. Recordings were analyzed with Sirenia Seizure Pro Software (Pinnacle Technology), which verified that chaotic electrical activity corelated with seizure events (**Figure 10**).

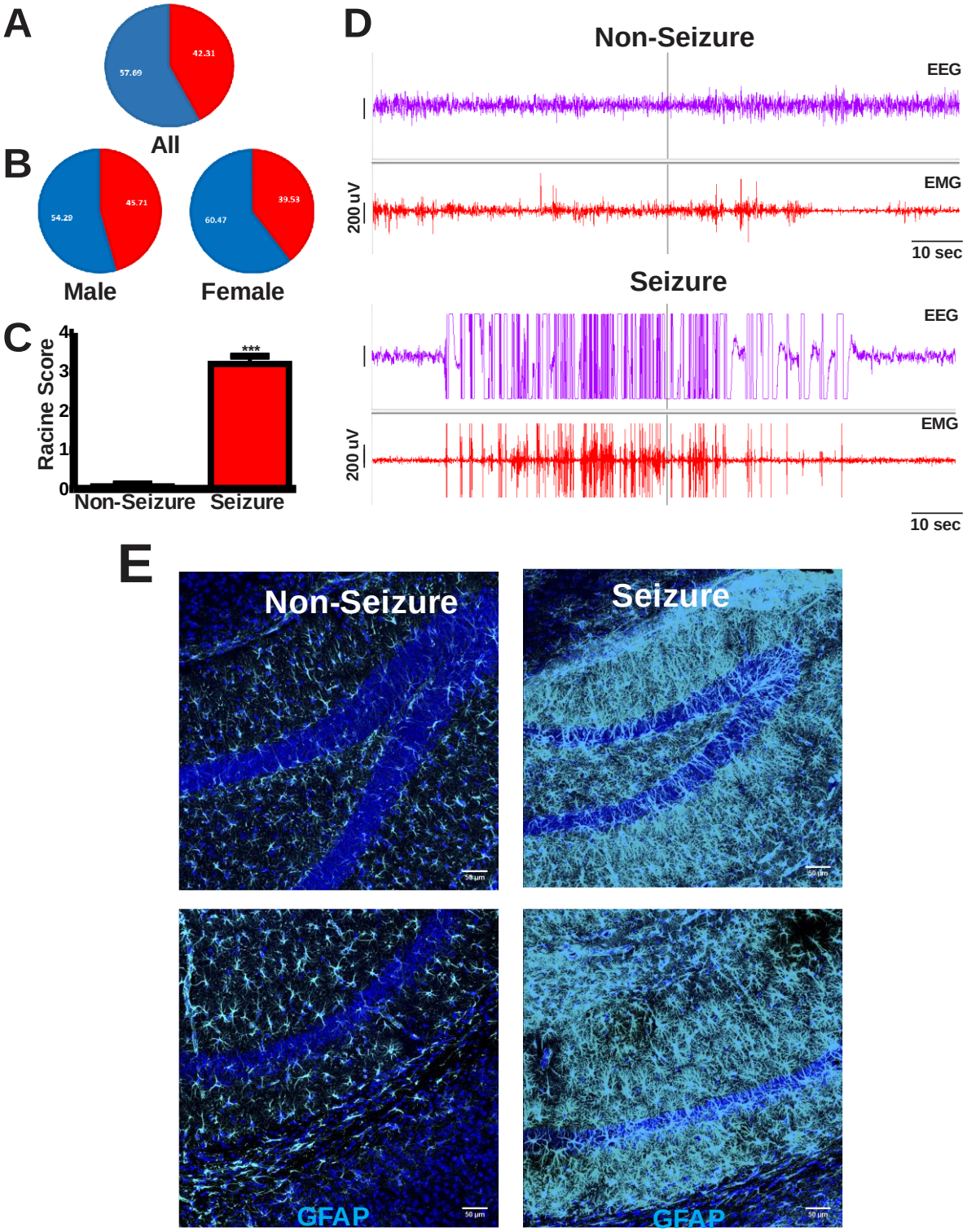

Figure 10: Arl13B-mCherry; Centrin2-GFP Mice Exhibit Spontaneous Seizure Activity. *Figure sourced from Sterpka et al., 2020 [6].* Arl mice exhibit a high incidence of spontaneous seizure

activity. **a** Naturally occurring seizures occur in a large proportion of Arl mice. Blue: non-seizure; red: seizure. *N* = 78. **b** Both male and female Arl mice had seizure activity. Males had 16 mice out of 33 total exhibiting seizures. Females had 17 seizure mice out of 43 total. **c** Arl seizure mice exhibit a high Racine score on average. 15 non-seizure mice were compared with 10 seizure mice. ***, $p < 0.001$, unpaired Student's t-test. **d** EEG/EMG recordings confirmed the occurrence of seizures among Arl mice. Epileptic waveform of EEG/EMG recording verified seizure activity in a mouse grading high on Racine score (bottom), compared to non-seizure Arl mice which lacked high-amplitude EEG/EMG waves (top). **e** Immunofluorescence staining of non-seizure and seizure brain tissue shows drastically elevated GFAP expression in tissues from seizure mice, indicative of astrocyte reactivity. Top, DG; bottom, CA1 region. Scale bar, 50 μm

Immunohistochemistry using Arl13B and AC3 antibodies revealed a shortening effect of seizure activity on primary cilia (**Figure 11**). AC3-positive primary displayed a shortening in all regions of the hippocampus. Remarkably, Arl13B-positive primary cilia showed the strongest shortening in the Dentate Gyrus, with limited effects in CA1 and CA3.

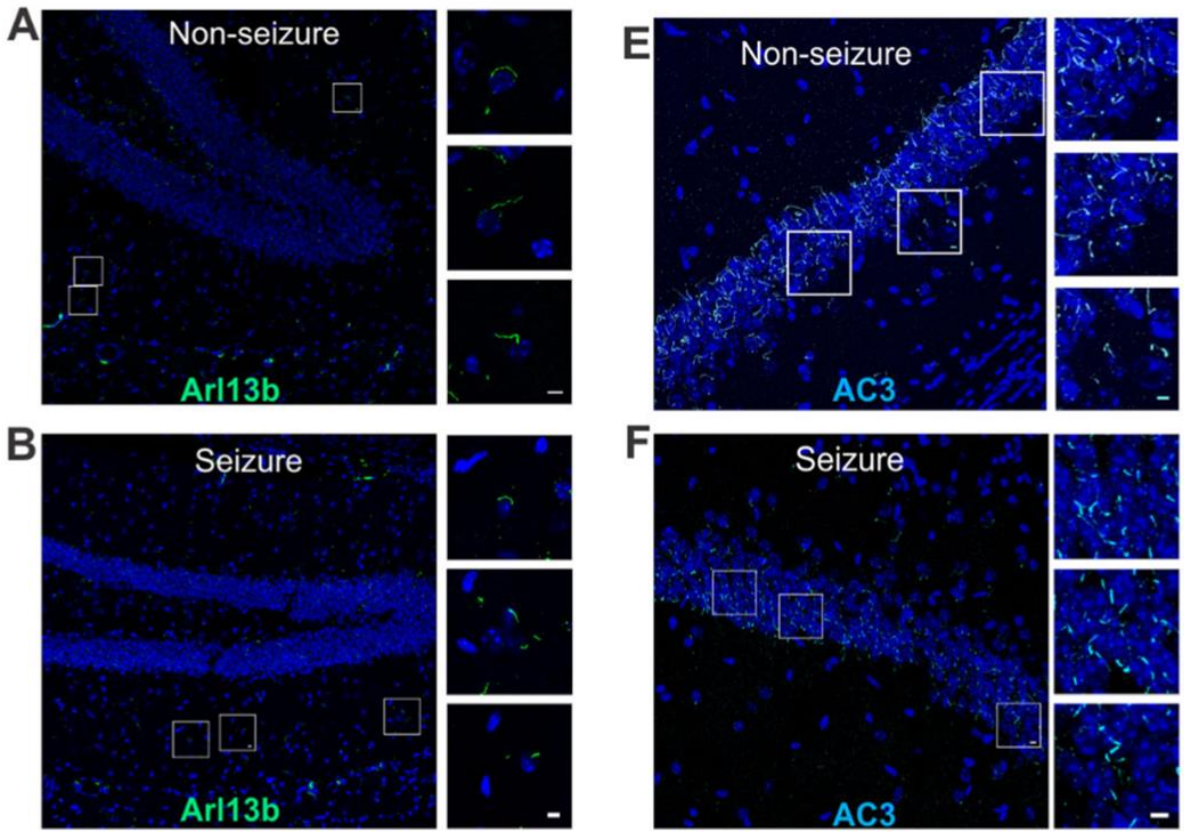

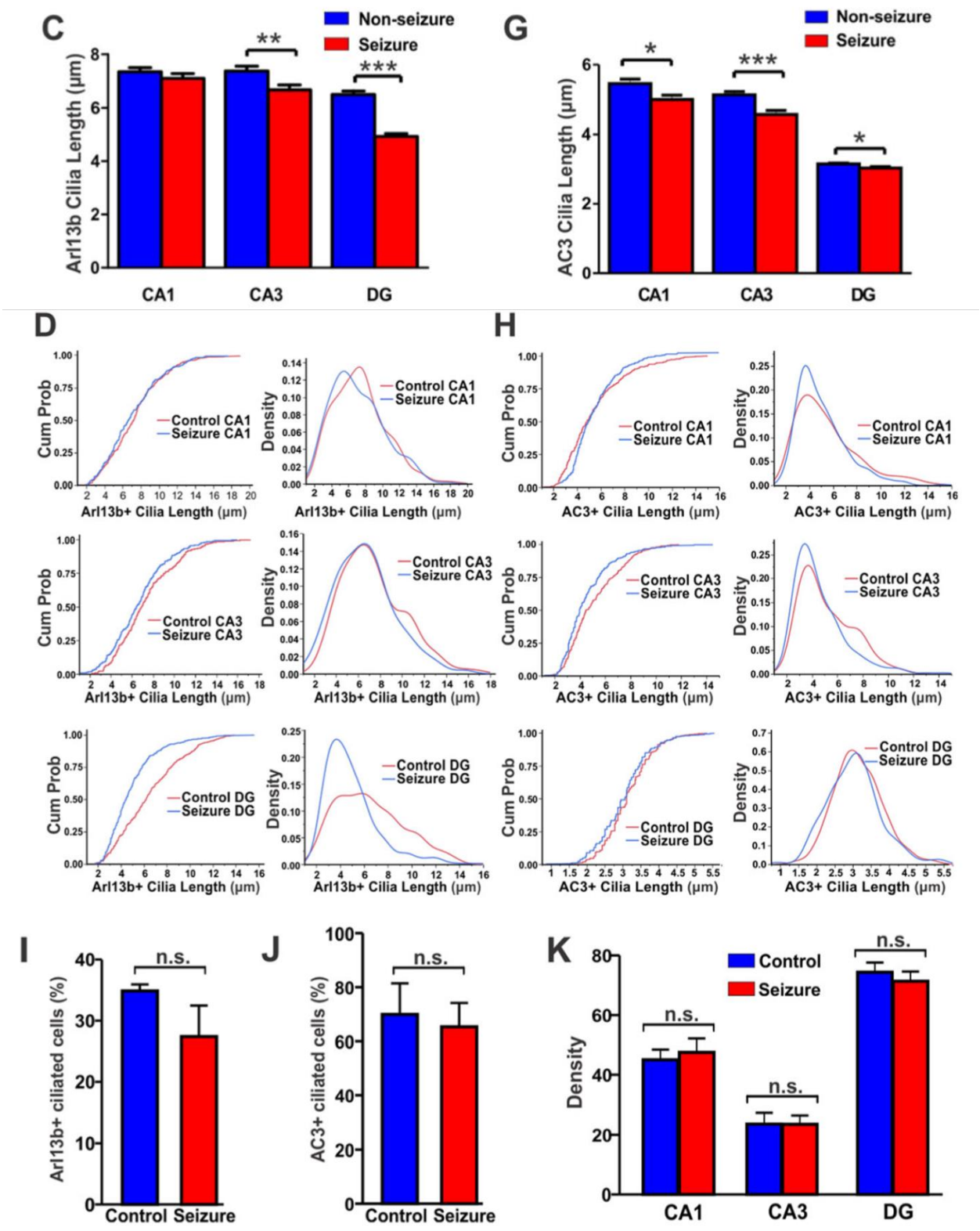

Figure 11: Spontaneous Seizure Activity Shortens Primary Cilia in the Hippocampus. F*igure sourced from Sterpka et al., 2020 [6].* Naturally occurring seizures reduce the length of AC3-positive and Arl13b-positive primary cilia in the hippocampus. **a-b** Arl13b-positive cilia in the hippocampal CA1 and DG regions of Arl seizure mice (**b**) were shorter than those of non-seizure Arl control mice (**a**). Scale bar:

5 µm. **c** the length of Arl13b-positive cilia in the CA1 and DG regions, but not in the CA3 region, was significantly shorter in Arl seizure mice than in Arl non-seizure mice (***, $p < 0.001$, unpaired Student's t-test). Arl non-seizure controls, $N = 4$; Arl seizure mice, $N = 5$. Cilia number: non-seizure mice: 160, 130, and 253; Seizure mice: 180, 131, and 183. **d** CDFs and histogram density comparison present the length of Arl13b-positive cilia in the CA1, CA3, and DG regions. **e-f** AC3-positive cilia in the CA3 region of Arl non-seizure control mice (**e**) and Arl seizure mice (**f**). Scale: 5 µm. **g** Cilia length comparison revealed the shortening of AC3-positive cilia in three hippocampal regions of seizure mice (CA1: *, $p < 0.05$, CA3: ***, $p < 0.001$, DG: *, $p < 0.05$, unpaired Student's t-test). Non-seizure controls, $N = 4$; seizure mice, $N = 5$ animals. Cilia number: non-seizure mice: 403, 471, and 527; seizure mice: 374, 294, and 375. **h** CDFs and histogram density show AC3-positive cilia length in the hippocampal CA1, CA3, and DG regions. **i** Seizure does not significantly affect the percent of Arl13b-positive cilia in the DG. Data collected from 3 non-seizure and 3 seizure Arl mice. Cell number: control: 185; seizure: 196. Cilia number: control: 64; seizure: 51. n.s. not significant, with unpaired Student's t-test. **j** Seizure does not significantly affect the percent of AC3-positive cilia in the DG. Data collected from 3 non-seizure and 3 seizure Arl mice. Cell number: control: 292; seizure: 414. Cilia number: control: 221; seizure: 282. n.s. not significant, with unpaired Student's t-test. **k** Centrin2-GFP expression in hippocampal regions in Arl seizure mice had no significant difference with that in Arl non-seizure mice. Centrin2 imaging density over 50 μm^2 regions per mouse was calculated. Data were collected from 3 non-seizure and 3 seizure Arl mice. $p = 0.6$, 0.9, and 0.5 respectively with unpaired Student's t-test

The shortening of astrocytic primary cilia in this study may differ from a singular, previous report of no change [45] due to the form of seizure induction. For methods of control and consistency, many researchers use piloporcaine or kainic acid to initiate seizure activity [157, 158]. The murine model we used displayed spontaneous and repetitive seizure activity without any occurrences of death or disruptions to fecundity. The sustained and repetitive seizure may be the basis of the ciliary shortening observed in astrocytes. The duration of time during which consistent seizure activity occurred could also be linked to heightened reactivity and thus a more observable effect in astrocytes.

It is surprising that seizure activity affected astrocytic primary cilia more drastically in the DG than any other region of the hippocampus (**Figure 11**). It is possibly due to the functional difference of this region compared to the other parts of the hippocampus. It has been reported that piloporcaine induced epilepsy can result in astrocyte degeneration specifically in the DG, which indicates a conditional difference of astrocytes within this region [159]. Adversely, astrocytes in the DG are reportedly of a

similar group and number as in CA3 [160], which further emphasizes the distinctiveness in this result. Different means were used to verify the accuracy of this result, and it was repeatedly substantiated. This surprising result suggests a functional difference of astrocytic primary cilia in the DG.

iii. EFFECT OF CORTICAL INJURY ON PRIMARY CILIA

Astrocytes are crucial responders to traumatic and toxic events in the brain. They assist with recovery of the injured Brain Blood Barrier [161], maintain the health and integrity of neuronal synapses upon damaged conditions [1, 2, 4, 153], and manage the creation of the glial scar around lesioned tissue [79, 162]. Glial scarring is a reparative event restricted to the central nervous system that is a hallmark of brain injury [163]. Wounded and toxic tissue is surrounded by a mass of astroglia, microglia, and cellular matrix to impede migration of harmful debris and toxic substances, thereby protecting certain functionality in healthy tissue [162].

The inherent role of astrocytes in neurological pathology supported the development of our hypothesis that astrocytic primary cilia must also function in and be implicated in the development of astrogliosis. Ciliary research has demonstrated that primary cilia are integral to signaling in physiological health and certain pathologies [164]. We thus hypothesized that astrocytes must (1) shorten and withdraw their primary cilia in order to proliferate and (2) use their primary cilia in signaling towards producing reparations guided by alterations in astrocytic morphology. Similarly, neurons, being vulnerable in their morphological rigidity, are particularly sensitive to injury. They lack

proliferative capacity and easily succumb to a toxic environment. We hypothesized that their primary cilia, acting primarily as signaling centers, would also be implicated during the development of reactivity and potential destruction of neurons.

Results

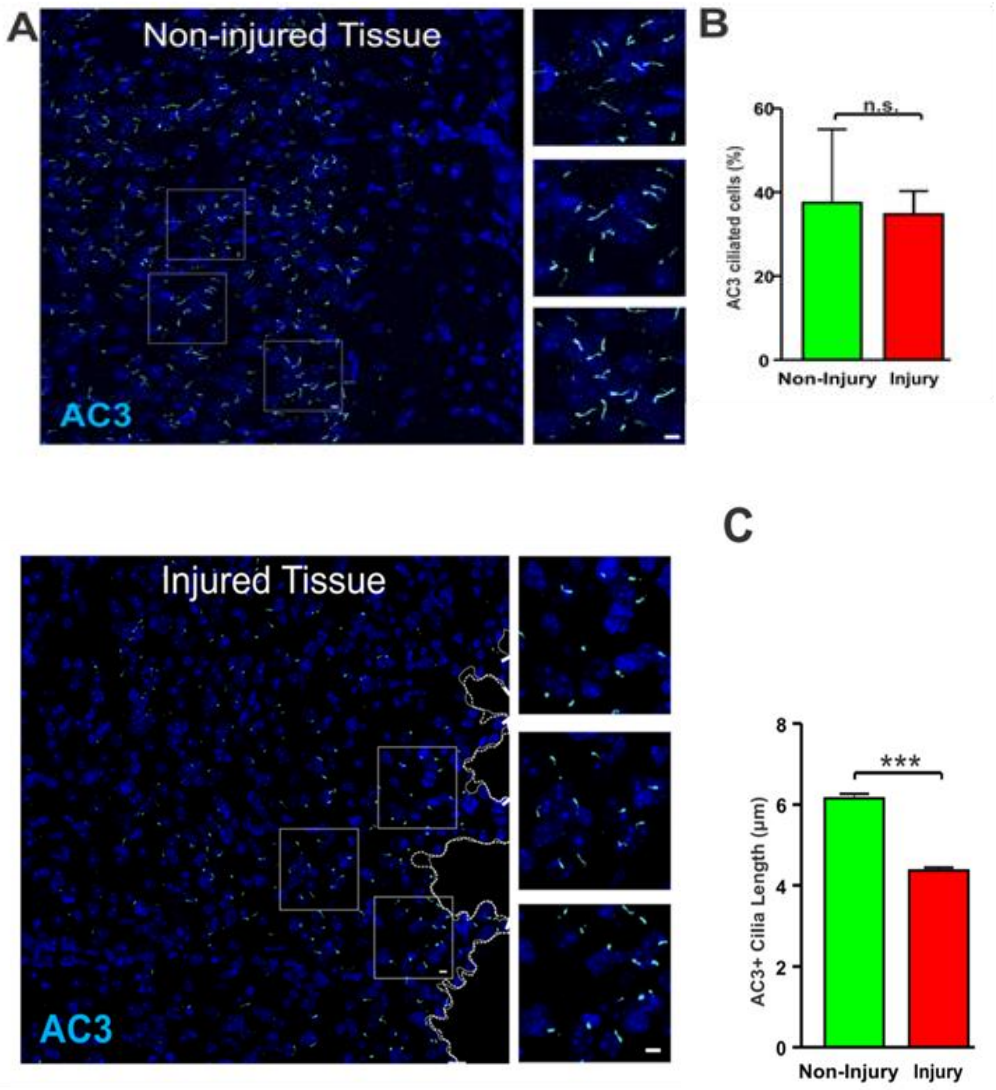

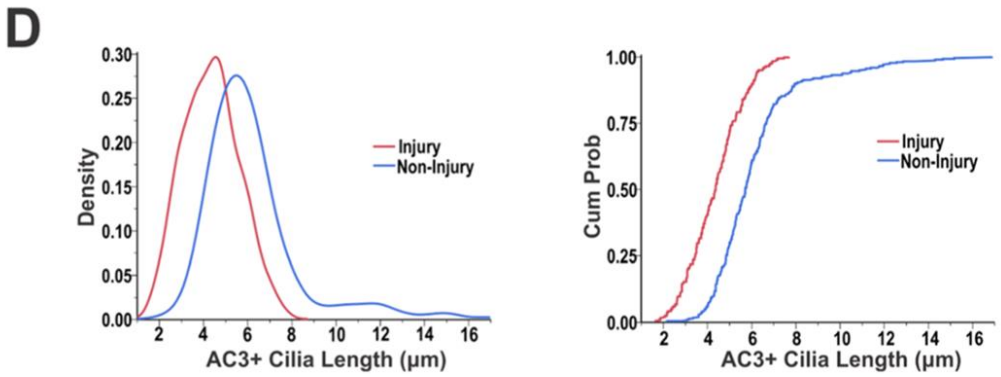

Figure 12: Cortical Injury Shortens Neuronal Primary Cilia. *Figure sourced from Sterpka et al., 2020 [6].* Tissue injury decreases the length of AC3-positive primary cilia. **a** AC3-positive cilia were shortened close to injured tissues. Scale bar: 5 µm. Top, non-injured tissues; bottom, injured tissues. **b** the frequency of AC3-positive cilia was not changed between injured and non-injured tissues (n.s. not significant, unpaired Student's t-test). **c** Comparison of AC3-postive cilia lengths reveals significant decrease in cilia length proximal to injury sites compared to injured tissues (*** $p < 0.001$, unpaired Student's t-test). $N = 5$, C57BL/6 mice. Non-injured sites were from opposite hemisphere of the injury site of the same animals. Cilia number: non-injured sites: 271; injured sites: 326. **d** CDFs and density comparison indicate the shortening of AC3-positive cilia length near to injury sites

We found that neuronal primary cilia displayed a significant shortening proximal to injured cortical tissue (**Figure 12**). This aligned with a heightened expression of GFAP shown by reactive astrocytes close to the injury (**Figure 13**). Curiously, I found that astrocytic primary cilia became indistinguishable near injured tissue, while Arl13B expression increased dramatically (**Figure 13**). We interpreted this result as likely resorption of cilia allowing for proliferation or morphological alterations accompanying astrocytic reactivity. To support our conclusion of ciliary ablation, we used IFT88, an additional ciliary antibody, known for staining a protein involved with ciliary trafficking, to determine presence of astrocytic cilia, but the stain proved unsuccessful. Due to the absence of an additional astrocytic cilia marker proven to be effective *in vivo*, we cannot

conclusively state that astrocytic primary cilia are fully eliminated near injured tissue, but the absence of primary cilia would effectively indicate the proliferation of astrocytes needed in formation of a glial scar around the injured cortex.

The translocation of Arl13B away from primary cilia and upregulation near the injured cortex was unexpected but uncovered a potentially important role for this GTPase in brain injury. To ensure that the upregulation of Arl13B was not due to non-specific binding of the antibody, we used immunohistochemistry of Arl mice, void of the requirement of antibody staining of Arl13B. Injured specimens displayed the same increase in Arl13B expression, thereby removing the possibility of the intensity being the result of an antibody issue and confirming the Arl13B is in fact upregulated in traumatic brain injury induced astrocytic reactivity.

CHAPTER 4

ARL13B IN BRAIN INJURY

i. ELEVATED EXPRESSION NEAR CORTICAL LESION

The increase of Arl13B expression proximal to the injury site in our original studies was ultimately surprising. We hypothesized that astrocytic cilia would be reduced or ablated due to the requirement of ciliary resorption prior to mitosis [9]. Arl13B presence in primary cilia was drastically limited (**Figure 13**) but we cannot definitively state that astrocytic cilia were completely removed due to the absence of an additional and effective antibody.

Using our initial results as a foundation, I postulated that Arl13B upregulation would align with the heightened expression of GFAP, a hallmark of astrogliosis. We assumed that Arl13B would translocate into the cell body, allowing for alterations in cellular function and/or signaling. I continued to use immunohistochemistry and ImageJ analysis to identify Arl13B and GFAP intensity in brains which underwent a cortical stab wound injury.

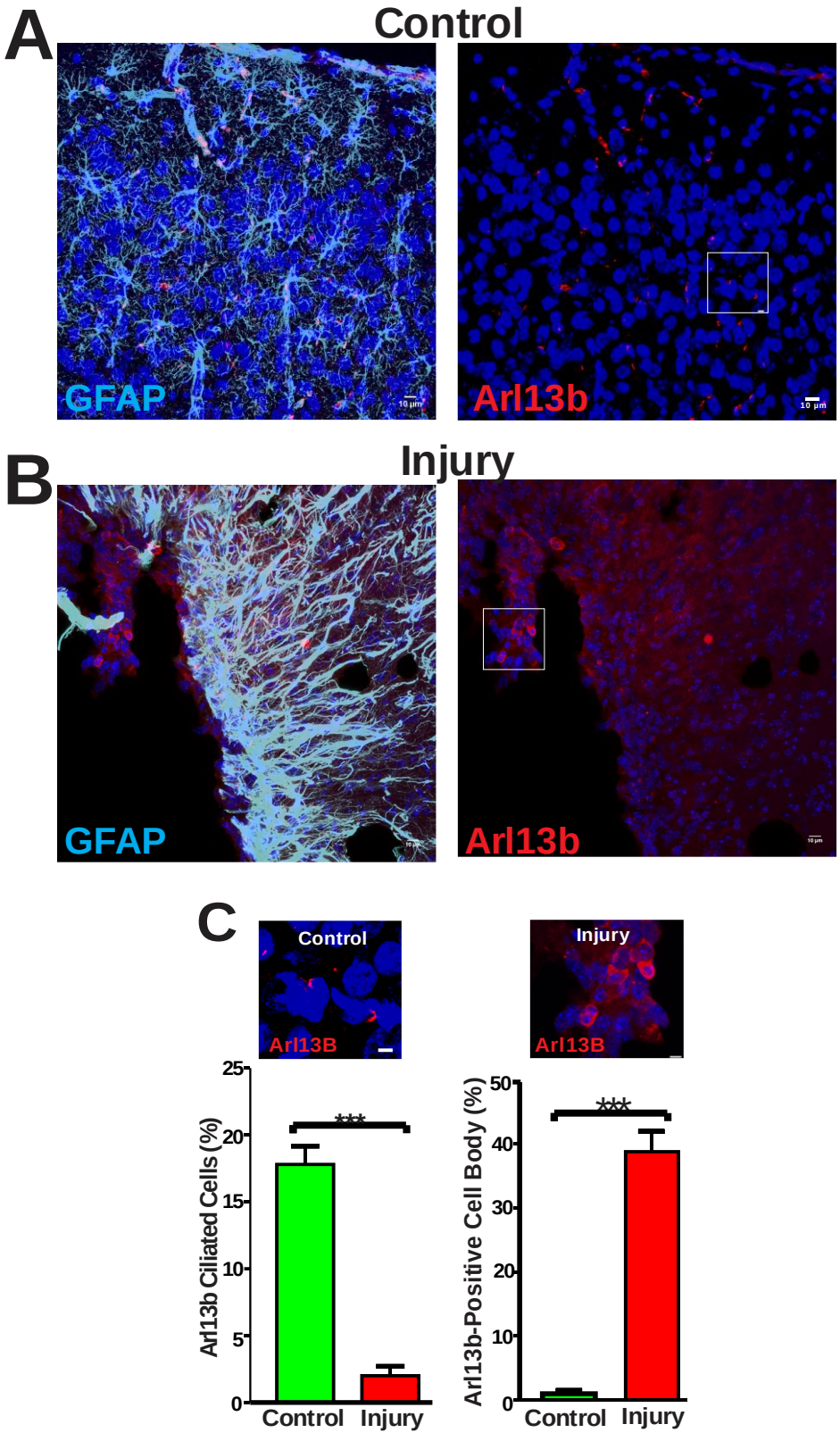
A
Control
GFAP
Arl13b
B
Injury
GFAP
Arl13b
C
Control
Arl13B
Injury
Arl13B
Arl13b Ciliated Cells (%)
25
20
15
10
5
0
***
Control
Injury
Arl13b-Positive Cell Body (%)
50
40
30
20
10
0
***
Control
Injury

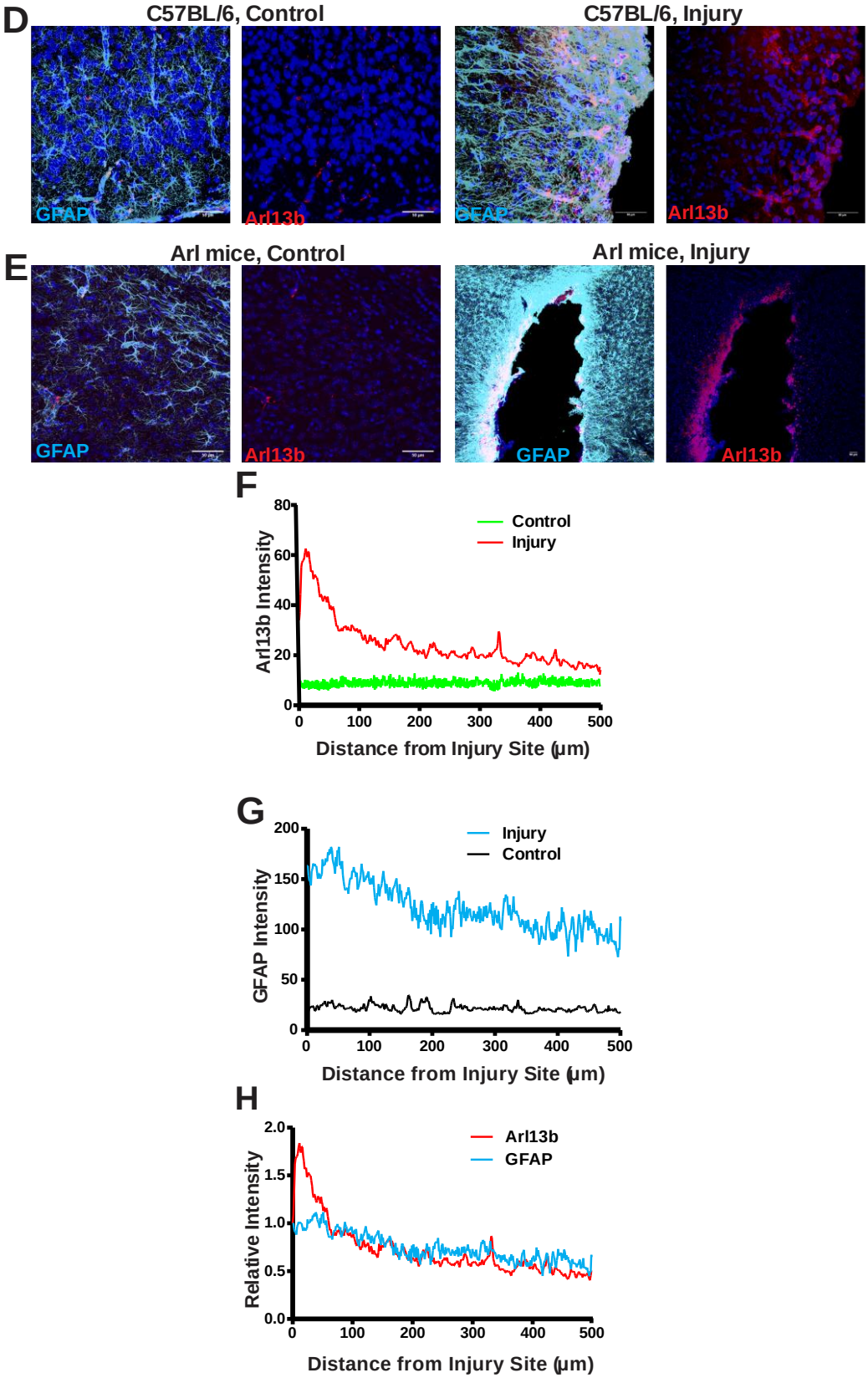
D
C57BL/6, Control
C57BL/6, Injury
GFAP
Arl13b
GFAP
Arl13b
E
Arl mice, Control
Arl mice, Injury
GFAP
Arl13b
GFAP
Arl13b
F
Control
Injury
Arl13b Intensity
0
20
40
60
80
0
100
200
300
400
500
Distance from Injury Site (µm)
G
Injury
Control
GFAP Intensity
0
50
100
150
200
0
100
200
300
400
500
Distance from Injury Site (µm)
H
Arl13b
GFAP
Relative Intensity
0.0
0.5
1.0
1.5
2.0
0
100
200
300
400
500
Distance from Injury Site (µm)

Figure 13: Cortical Injury Promotes Arl13B Expression. *Figure sourced from Sterpka et al., 2020 [6].* Absence of Arl13b-positive astrocytic primary cilia but robust Arl13b expression in tissues proximal to injured sites. **a-b** Increased Arl13b expression proximal to an injury site (**b**) compared to a non-injury site (A). Scale: 5 μm. Note that Arl13b-positive primary cilia were detected in non-injured tissues (**a**), but undetectable in injured tissues (**b**). **c** the percentage of ciliated cells near injury sites decreased dramatically compared to control tissues (left). ***, $p < 0.001$, unpaired student's t-test. Injured tissues: total cell number: 665, ciliated cell N: 13; non-injured tissues: total cell number: 265, ciliated cell number: 47. Injured tissues had significantly increased percentage of Arl13b-positive cells compared to that of non-injury tissues (right). ***, $p < 0.001$, unpaired Student's t-test, $N = 3$. Injury site cell $N = 806$; non-injury site cell number 600. Two Arl13b images from injured and non-injured sites are shown in the left. Non-injury sites were from the opposite hemisphere of the injury site of same mouse. **d** Increased Arl13b expression near injured sites in the cortex of C57BL/6 mice. GFAP (cyan) and Arl13b (red) were stained with their antibodies, respectively. Left, non-injured site; right, injured site. **e** Increased Arl13b expression near injured sites in Arl mice. Red: Arl13b-mCherry; Cyan: immunofluorescence staining using anti-GFAP antibody. **f** Distinct Arl13b expression density in injured and non-injured tissues. Arl13b had the highest expression near to the injury site. $N = 5$. **g** GFAP expression was strongly increased near to injured tissues compared to non-injured tissues. **h** Correlation of relative expression density of GFAP and Arl13b over a range of 500 μm distance from the injured site. ***, $p < 0.001$ by correlation analysis

Approximately two weeks after cortical injury, the heightened amplitude of Arl13B aligned with the increase of GFAP expression characteristic of astrocyte reactivity (**Figure 13**)**.** The increase in intensity of Arl13B indicates that this accepted ciliary protein must translocate out of the primary cilium into the soma or processes in order to reach full functional potential. Its GEF activity of Arl3 and role in trafficking of INPP5E indicate that this shift may be required for proliferation [103, 165]. Furthermore, it is possible that Arl13B, in being a unique GTPase, may have other unknown roles, particularly in the case of brain injury and the reparations that follow. The increase of Arl13B appeared around cell bodies and aligned with the heightened expression of GFAP, thereby aligning with reactivity and suggesting a previously undefined role.

ii. STRAIN-DEPENDENT FUNCTION OF ARL13B IN BRAIN INJURY

The atypical GTPase, Arl13B, is known to function in ciliary trafficking of vesicles [131], GEF activation of ARL3 [102], and cancer cell migration [87]. Furthermore, Arl13B

is known to function in the translocation of INPP5E, a ciliary protein known to function in proliferation [103, 110], as well as modulate Shh components [49, 113, 166].

Our initial study built a foundation implicating the function of Arl13B in brain injury. Its function in trafficking signaling proteins, role in proliferative elements, migratory capacity, and transduction of Shh all support its relevance in astrocytic reparatory functioning. We accordingly hypothesized that Arl13B would work to support astrocytic reactivity and impact glial scarring. To explore this, I used strains of mice to act as a loss-of-function, control, and gain-of-function of Arl13B. These strains included Arl13B$^{flox/flox}$; UBC treated with tamoxifen to ablate Arl13B, Arl13B$^{flox/flox}$; UBC treated with a vehicle as a control, and Arl13B-mCherry; Centrin2-GFP showing an overexpression of Arl13B.

Results:

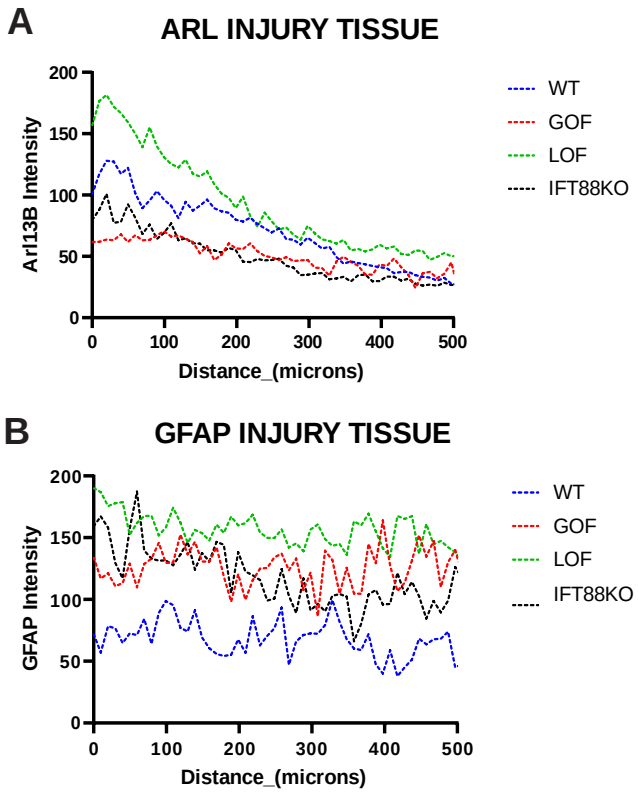

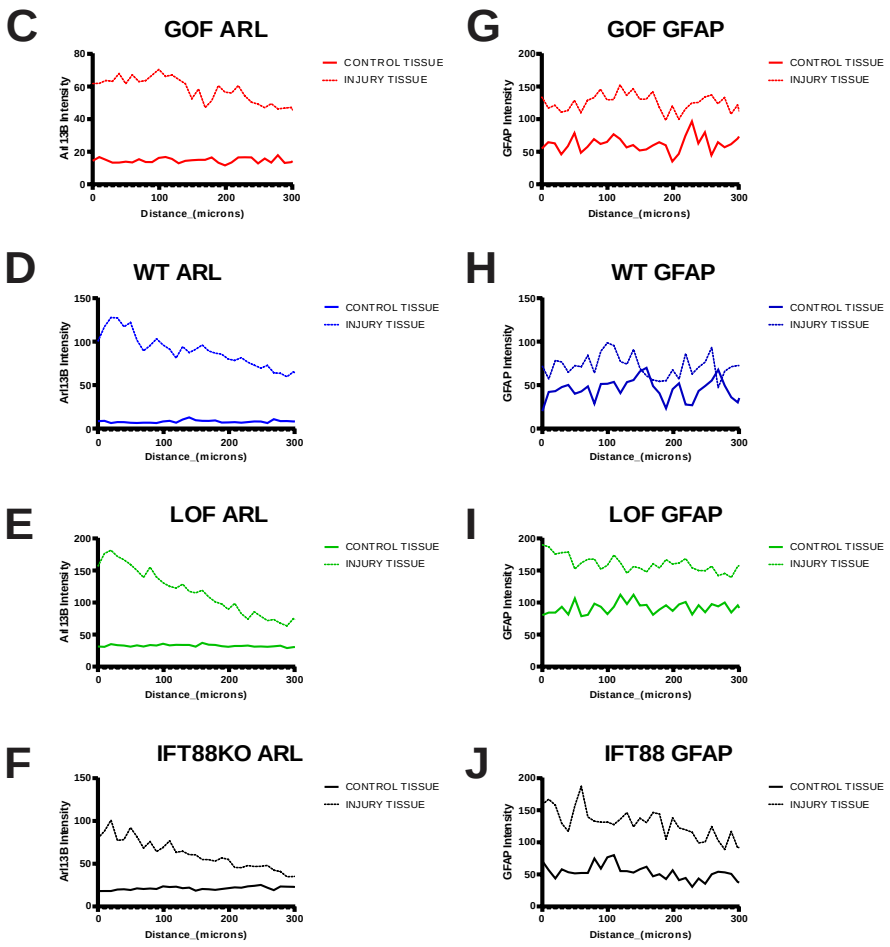

Figure 14: Effect of Arl13B Expression on GFAP Expression. Arl13B and GFAP immunostaining results seven days following injury of wildtype (blue), Arl13B Gain-of-Function (red), Arl13B Loss-of-Function (green), and Ift88-Knockout (black). All mice show a heightened intensity of Arl13B close to lesion site (0 on x-axis) with a higher expression of Arl13B in control tissue. Heightened GFAP expression, indicative of glial scarring and neural repair, is not consistently enhanced or decreased with regard to Arl13B or ciliary expression in mice.

Seven days following cortical lesion, vehicle treated Arl13B$^{flox/flox}$; UBC mice (control mice), Arl13B$^{flox/flox}$; UBC mice treated with tamoxifen (LOF mice), Arl13B-mCherry; Centrin2-GFP mice (GOF), and IFT88$^{flox/flox}$;UBC mice treated with tamoxifen (KO) were sacrificed. All mice displayed a heightened expression of Arl13B in injured tissue compared to control tissue distal from the injury site, consistent with previously

published data [6] (**Figure 14: A, C-F**). This pattern of heightened Arl13B expression suggests the continued involvement of this protein in brain injury across strains.

The increased display of Arl13B in the Arl13B floxed mice indicates that its knockout may not be ubiquitous in this strain and that it maintains a role in the reparations following brain injury, regardless of reductions in expression. The heightened level of Arl13B in the injury tissue of IFT88 Knockout mice supports reports that Arl13B does not require localization on the primary cilia in order to be functionally relevant [97].

GFAP expression was heightened in the injury tissue of all four strains, indicative of the development of reactive gliosis. GFAP expression did not show significant trends between strains, although visibly lowest in the WT strain and highest in the *Arl13B^{floxed}* LOF mice (**Figure 14B**). With the high levels of GFAP expression also observable in the results of cortical lesions in IFT88 KO and GOF mice (**Figure 14B**), there is no direct evidence of effect of Arl13B expression with the development of GFAP-based glial scarring at 7 days following cortical lesion.

iii. SLEEP ANALYSIS OF ARL13B-MCHERRY; CENTRIN2-GFP MICE

To examine sleep patterns of Arl mice, Electroencephalogram/Electromyogram (EEG/EMG) recordings were used to score cortical and muscular activity patterns into Wake, NREM, and REM. Wake activity represents cognitive alertness and muscular activity of most mammals [167]. Sleep can be divided into Non-Rapid-Eye-Movement (NREM) and Rapid-Eye-Movement (REM) activity [168, 169]. NREM comprises the

majority of sleep activity, it can be split into three stages and is characterized by high Delta activity [170]. REM sleep exhibits an extremely high amplitude and can occur in microbursts or in slightly longer periods during NREM [40]. It is characterized by brain activity similar to the waves seen during wakefulness, along with reduced EMG activity and quick eye movements [171]. REM sleep is accompanied by high Theta activity [172]. Examination of these EEG/EMG patterns can yield trends and disruptions in activity based on genotype and phenotype.

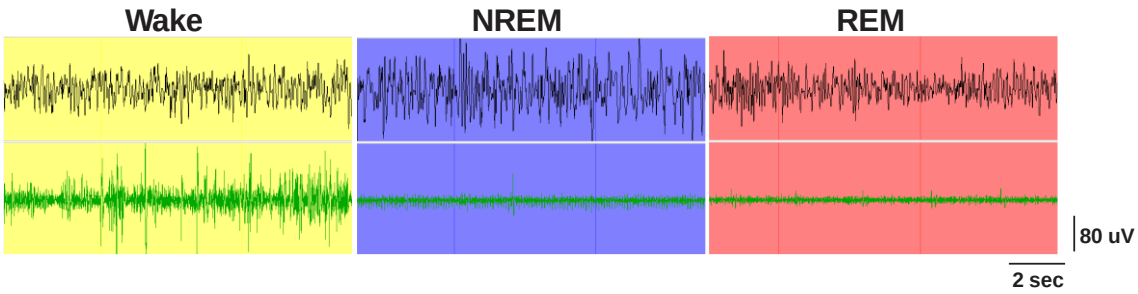

Figure 15: Sleep Stages of Arl Mice. EEG/EMG activity was staged into Wake, NREM, and REM in Arl mice. Wake displayed high EMG activity, while both NREM and REM showed far less EMG activity. EEG recordings showed a high power in NREM, but a lower power and higher frequency in REM activity. EEG activity shown in upper row, EMG activity shown on lower row.

In four mice used for seizure verification, the first twenty-four hours was scored with Sirenia Sleep Pro scoring software (v. 2.1.0). To maintain consistency with analytics from Sirenia, power was set to Sleep Pro defaults as listed in Methods. Activity was first scored into Wake and NREM via cluster scoring of EEG2 Delta against EMG 50-150. Activity was then visually confirmed and scored by the following criteria: Wake was associated with moderate to high EMG activity; NREM maintained low EMG activity and high EEG power; REM displayed low EMG activity, but low power and high frequency (**Figure 15)**.

Results

Analysis of seizure activity in Arl mice showed the occasional presence of artifacts and possible seizures in mice phenotyped as controls. Thus, equal sexes of two “control” and two “seizure” mice were pooled together for this analysis to account for the abnormal cortical activity present in this strain and inability to fully account for a singular or rare seizure occurrence. This combination supports a more accurate analysis of the Arl strain.

Arl mice displayed increased wake activity during night, and increased NREM during the day (**Figure 16**). REM activity was observed to be highest just prior to the onset of lights out (**Figure 16**). The first twenty-four hours following recording revealed 53.26% of averaged wake time, 40.39% NREM, and 3.40% REM. Sleep was separated into 92.25% NREM activity and 7.75% REM (**Figure 17**). Wake and NREM durations are comparable to those reported in other experiments, although REM activity in Arl mice quantified in this study is less than that of percentile reports of other strains [118, 173].

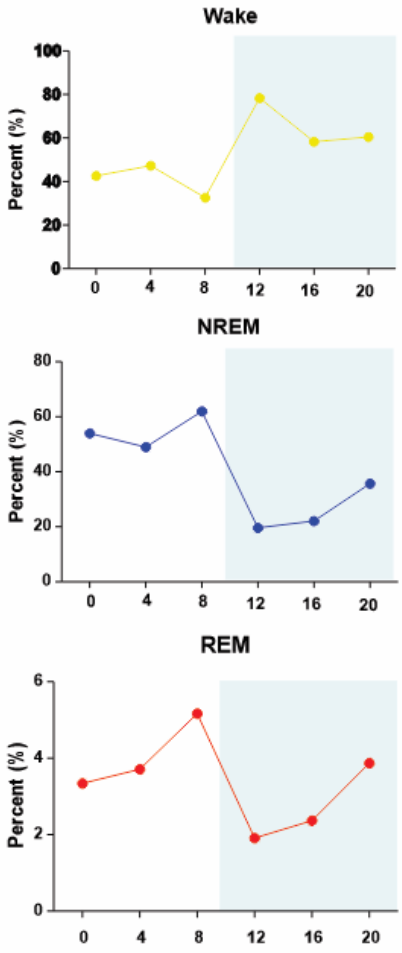

Figure 16: Sleep Score throughout Day. Arl mice exhibited higher levels of wake activity in the absence of light and higher levels or NREM and REM during the presence of light. REM activity spikes prior to the removal of lights. X-axis shows four-hour increments of time.

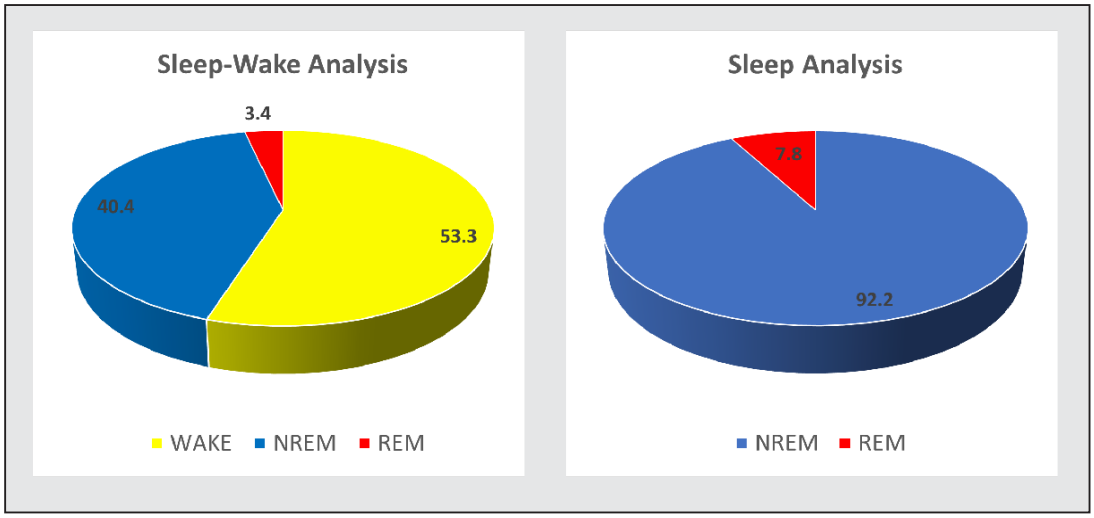

Figure 17: Sleep Analysis Arl Mice. Arl mice revealed just over half of the first day of EEG/EMG recording in wake, with the remaining time primarily spent in NREM. Only 3.39% of this 24-hour recording was spent in REM activity. Analysis of time spent asleep revealed that REM activity comprised 7.75% of the duration of sleep, with the remaining time spent in NREM.

Percentages of REM activity reported of old and young C57BL/6 recorded over twenty-four hours mice and interpreted by Wimmer et al. [173] are both higher than that of the Arl mice examined in this data collection. Additionally, REM activity of AC3 +/+ mice reported in a sleep analysis examining the role of AC3 in Major Depressive Disorder by Chen et al. [118] is comparable, although higher than that of the Arl mice examined in this experiment. This reduction of REM activity in Arl mice could be a result of the disruption of normal environment by connection to Pinnacle recording software and immediate recording, or due to the spontaneous seizure activity reported in this strain.

Seizure occurrence is distinctly reduced during REM stages [174] and is reported to have an inverse correlation with the length of REM activity during sleep [174]. It has been reported that epilepsy and seizure activity reduce REM duration [175, 176], and approximately only 1% seizures occur during REM sleep [175]. Theta activity, associated with REM sleep, is reported to have an overall inhibitory effect on seizure

activity [177]. Increased seizure activity has been correlated with deficiencies in REM stages in cats [178], although there are limitations in scientific investigations to the direct effect of seizure activity on REM sleep in mice. Thus, it is likely that the reduced REM activity extracted from the EEG/EMG recordings of these Arl mice (**Figure 17**) is a result of epileptic behavior and the presence of seizures in this strain.

CHAPTER 5

EEG WAVEFORM ANALYSIS OF MOUSE MODEL OF ALZHEIMER'S DISEASE UNDER ISOFLURANE-INDUCED ANESTHESIA

The following experiments sought out to determine if EEG waveform analysis of a mouse model of AD contains hallmarks unique to the disease prior to manifestation of cognitive defects. Burst Suppression Density (BSD), Power Spectral Density (PSD), and Phase Amplitude (PAC) were investigated in EEG2 recordings of subjects exposed to 15 minutes of isoflurane anesthesia. This sedation was intended to reduce the noise from peripheral neuronal firing seen during wake, thereby allowing for a controlled and uninterrupted waveform, reminiscent of sleep and repeatable in all subjects.

i. BURST SUPPRESSION OF APP23 MICE

APP23 mice are transgenically engineered to display the Alzheimer's phenotype starting at approximately 3 months of age [150]. This strain carries a double mutation [human] expressed in the neocortex and hippocampus [150] and is specific for neuronal expression [179]. This mutation is enacted by the Thy1 promotor [179], and this strain exhibits amyloid-beta and tau levels in its cerebrospinal fluid indicative of the development of AD starting as a mature adult [150]. The phenotypic changes that progressively worsen with age include deficiencies in completing the Water Morris maze [180], inadequacies in contextual fear conditioning [181], and disturbances in sleep [182].

Isoflurane anesthesia is reported to be associated with BSD [145, 183]. Burst suppression is a pattern of EEG activity that shows suppressed activity of neurons

indicated by a flat (isoelectric) or near-flat EEG followed by short bursts of high activity [145]. This is commonly associated with anoxia, hypothermia, coma, and other pathologies that implicate the brain [145]. This electrical behavior is caused by the depletion of intracellular calcium inhibiting synaptic signaling, thereby causing the reduced activity [184]. This is followed by neuronal pumps restoring calcium and allowing for heightened neuronal signaling in the form of a burst [145, 184]. The natural (without intervention) incidence of burst suppression is associated with a poor prognosis, with longer periods of isoelectric activity being insidious [145, 184].

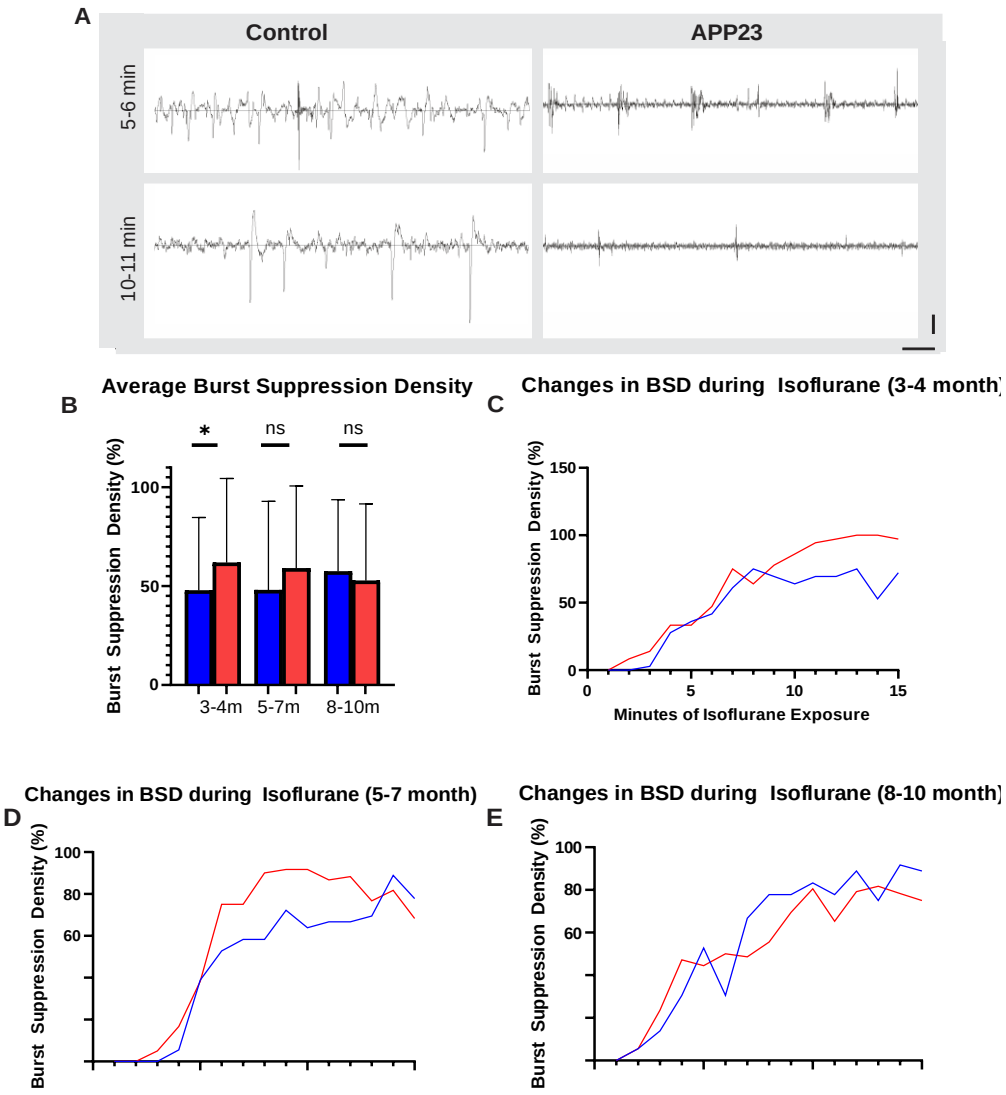

Figure 18: Burst Suppression Density of APP23 Mice. A. EEG2 recordings of 3–4-month-old Control (left) and APP23 mice (right) show visual differences in patterning minutes 5-6 and 10-11 of isoflurane exposure. X Scale: 50uV; Y Scale 5 seconds. B. 3–4-month-old age range show a significantly (p,0.05) higher density of suppressed epochs than Control mice of the same age range. C-E. Changes of BSD shown over the 15 minutes of isoflurane exposure. Control: blue; APP23: red) Significance calculated with the Mann-Whitney test.

Isoflurane exposure is reported to elicit Burst Suppression patterning [145]. Thus, our findings of this activity in anesthetized mice were not unexpected. We explored young (3-4 months), middle-aged (5-7 months) and old (8-10 months) mice and found

that all ages showed an increase in BSD from the beginning until end of 15 minutes of isoflurane exposure (**Figure 18 C-E**). The percentage of suppressed epochs increases with the length of isoflurane exposure in all age groups but remains higher in 3-4- and 5-7-month-old APP23 mice (**Figure 18 C-D**). The percentage of suppressed epochs increases with the length of isoflurane exposure but shows mixed density between 8-10-month-old APP23 mice and Controls.

Note the high levels of electrical activity on the left side of the panel of both Controls and the near Isoelectric activity on the two mice on the right panel (**Figure 18 A**). I found that the youngest age group showed statistical relevance. These findings show that while under isoflurane exposure, 3–4-month-old APP23 mice exhibit a statistically significant difference in level of BSD than controls of the same age group (**Figure 18 B**). No statistically significant differences were found in BSD of 5-7- and 8-10-month-old APP23 and Controls.

The absence of statistical difference of the older age groups is not completely surprising, as the aged brain can exhibit various forms of compromise. This includes affected BSD [185]. Our findings that BSD is statistically different in young mice is promising in identifying a characteristic unique for the age group at the onset or prior to the manifestation of the phenotype, thus supporting our hypothesis and development of the foundation of a new method of AD evaluation.

ii. POWER SPECTRAL DENSITY ANALYSIS OF APP23 ELECTROENCEPAHLOGRAM

PSD is a common and well-established analytical method used to compare EEG activity [132, 186, 187]. It analyzes the distribution of EEG waveform power, composing oscillations into quantifiable frequency bins [132]. The respective frequency reflects cortical cell activity with respect to amplitude and the average power over time. Each frequency, or brain wave, is associated with a degree of consciousness [188].

The frequencies evaluated with PSD include Gamma, Beta, Alpha, Delta, and Theta [188]. They are associated with the following types of consciousness and brain activity: Gamma is associated with intra-brain communication, voluntary movement, learning, and memory processing [188, 189]; Beta is dominant during periods of wake and characteristic of an actively engaged mind [188, 190]; Alpha relates to a drowsy and relaxed state [188, 190]; Theta occurs normally with REM sleep and dreaming [172, 188, 190]; and Delta brain waves are seen in slow wave sleep and NREM sleep [188, 190]. As isoflurane sedation was used to mimic sleep-like behavior in oscillations of the brain, the following experimental design targets data collected from Alpha, Theta, and Delta.

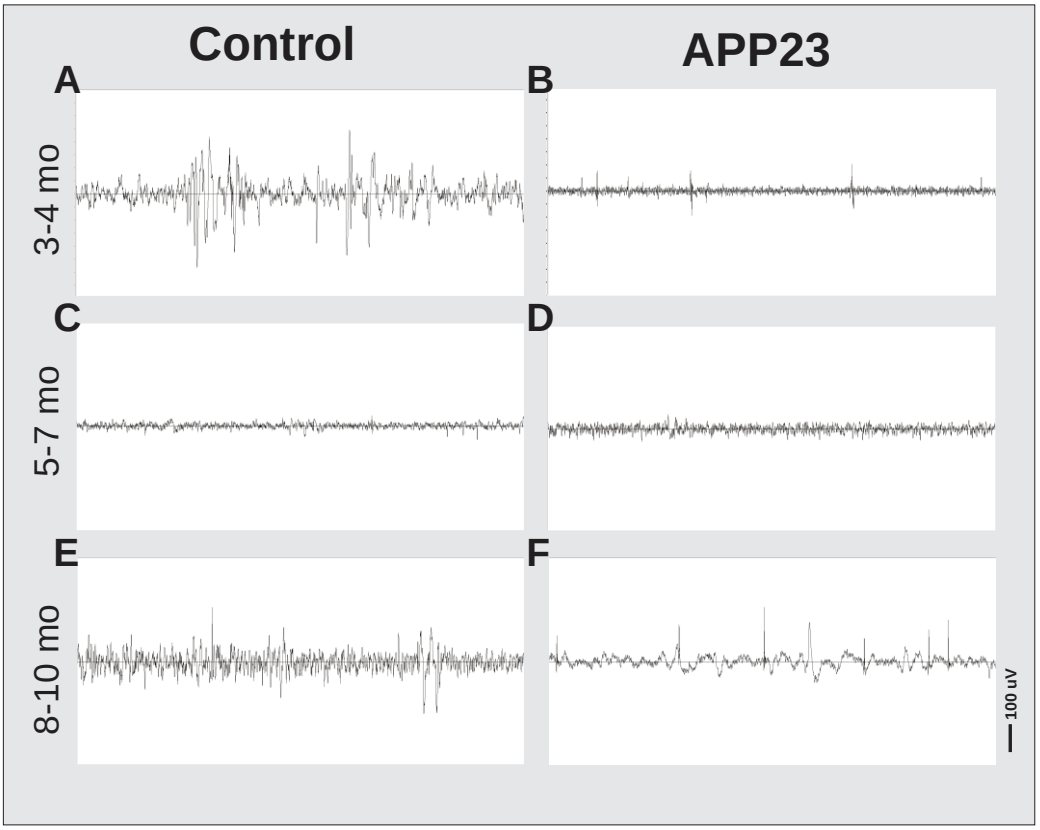

Figure 19: EEG Comparison of APP23 Mice. Raw EEG recordings of APP23 mice display visibly different characteristics. Figure shows 1-minute intervals of EEG2 extracted from 3-4-month-old mice (A-B), 5-7-month-old mice (C-D), and 8-10-month-old mice (E-F). Recordings shown start 10 minutes following the initiation of isoflurane exposure. Control mice shown on left and APP23 mice shown on right. EEG scale 100 µV.

Raw samples of EEG2 recordings of the tenth minute of isoflurane exposure display visible differences in 3-4-month-old Control and APP23 mice (**Figure 19 A-B**) and 8-10-month-old (**Figure 19 E-F**). Minimal differences are observable in 5-7-month-old mice (**Figure 19 C-D**).

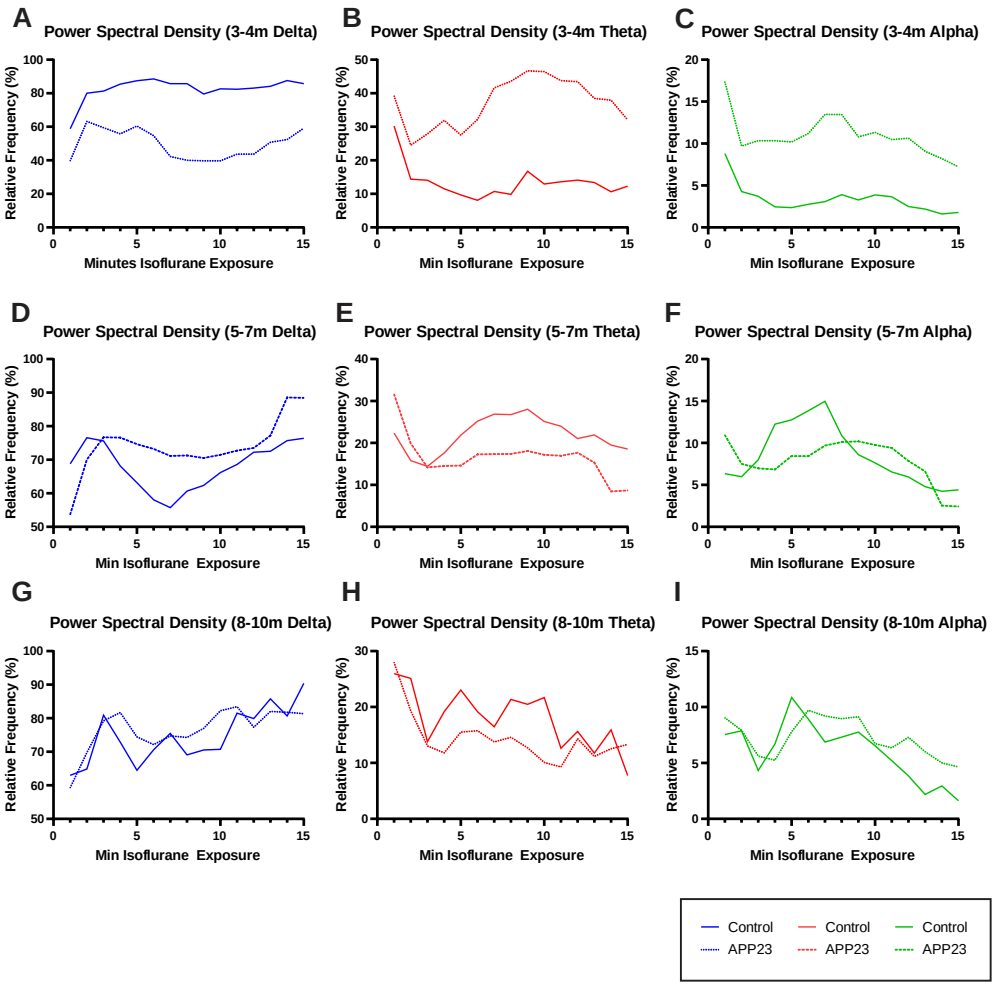

Figure 20: Power Spectral Density of APP23 Mice. Brainstorm was used to derive Welch's Power Spectral Density per minute of isoflurane exposure into frequency bins. A-C: 3-4-month-old mice; D-F: 5-7-month-old mice; G-I: 8-10-month-old mice. A-C. Delta: blue; Theta: red; Alpha: green. Control: solid line; APP23: dashed line.

At 3-4 months of age, relative frequency of Delta was lower in APP23 mice compared to controls during Isoflurane exposure (**Figure 20 A**). Theta and Alpha were higher in APP23 mice than in controls in this age range (**Figure 20 B-C**). Fluctuations in power frequency bands were found in both 5-7- and 8-10-month age groups throughout the duration of isoflurane exposure (**Figure 20 D-I**). This variation was especially notable in the eldest age range (**Figure 20 G-I**).

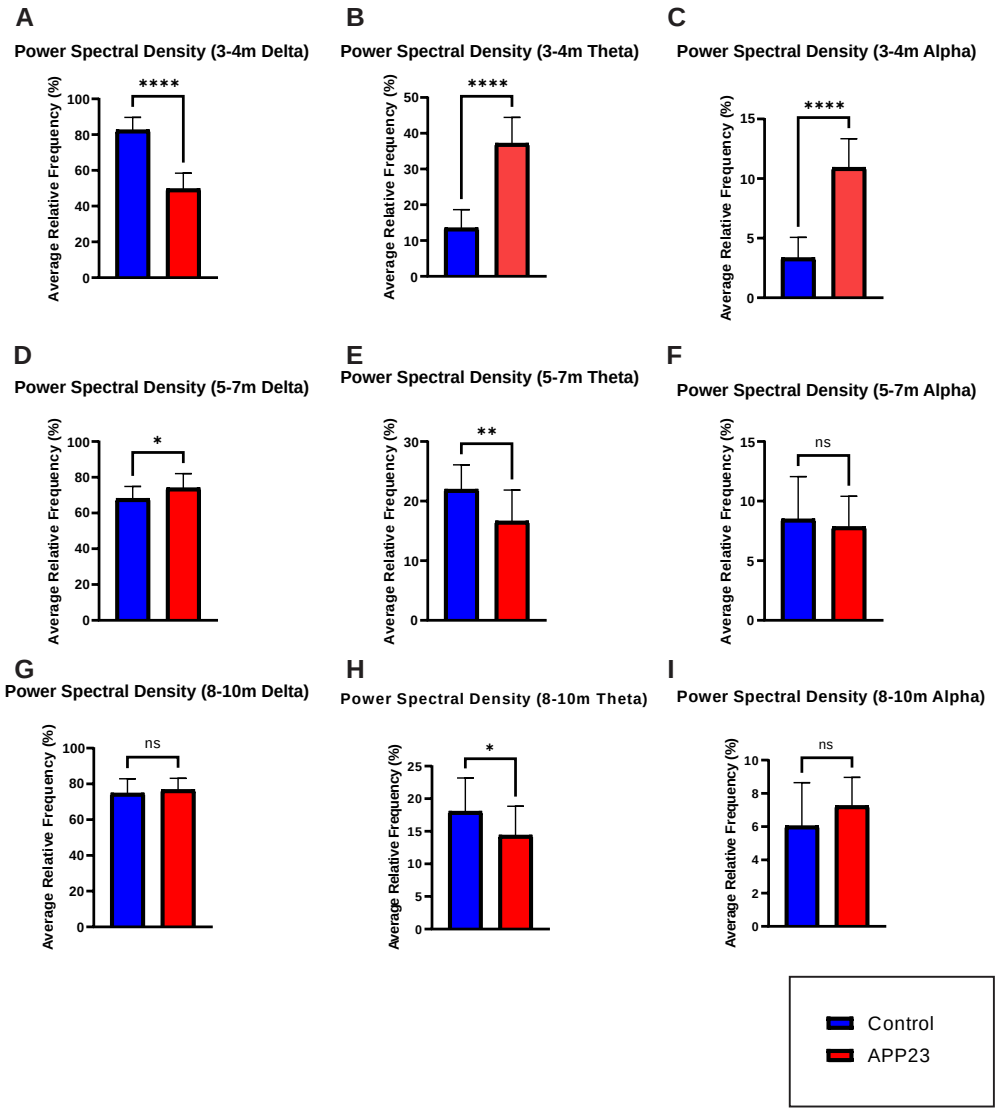

Figure 21: Average Power Spectral Density of APP23 Mice. Average relative frequency of different powers was compared for its average over the duration of isoflurane administration. Brainstorm was used to derive Welch's Power Spectral Density per minute of isoflurane exposure into frequency bins and these numbers were averaged over the total 15 minutes. A-C: 3-4-month-old mice; D-F: 5-7-month-old mice; G-I: 8-10-month-old mice. A-C. Control: blue; APP23 red. Significance was calculated using the Mann-Whitney test.

At 3-4 months of age, the average of Delta was significantly ($p < 0.0001$) lower in APP23 mice (**Figure 21 A**) while the averages of Theta and Alpha were significantly higher ($p < 0.0001$) in APP23 mice (**Figure 21 B-C**). At 5-7 months of age, there was a significantly higher average of Delta ($p<0.05$) (**Figure 21 D**); significantly lower average

of Theta p<0.01) (E); and no significant difference in Alpha (**Figure 21 F**). At 8-10 months, APP23 mice showed a significantly (p<0.05) lower average of Theta (**Figure 21 H**), but no significance in the other frequencies shown.

The highest degree of statistical significance was found in the 3-4-month age range (**Figure 21 A-C**), further supporting the visual difference seen in **Figure 20**. Statistical significance was also found in 5-7-month-old mice in Delta and Theta and 8-10-month-old mice in Theta (**Figure 21 D, E, H**). The variations based on age, similarly to the results of BSD can possibly be attributed to the aging brain, but the distinction in young mice is highly relevant to the potential for early evaluation of AD prior to the onset of symptoms.

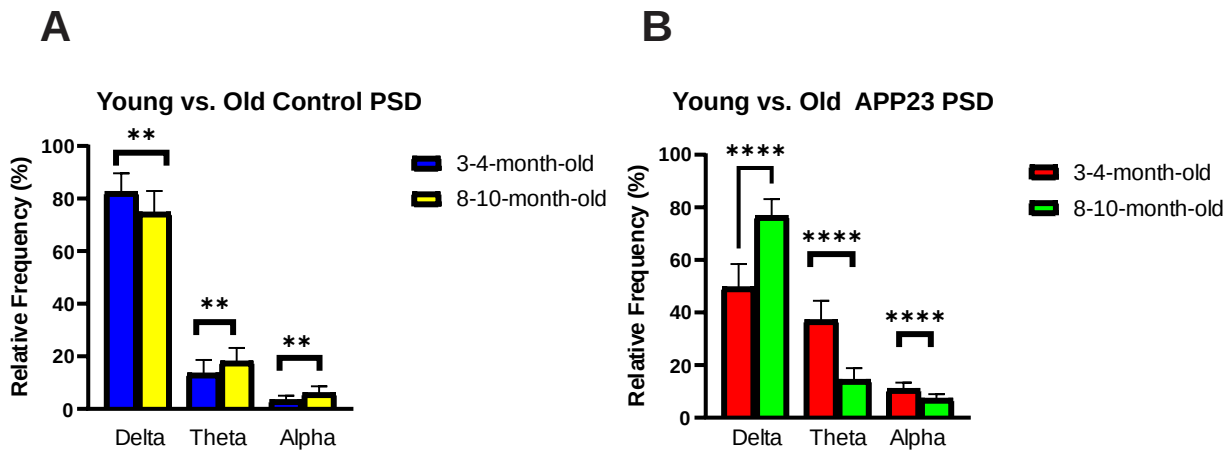

Figure 22: Comparison of PSD Between Young and Old APP23 Mice. Average PSD over isoflurane administration was compared between groups of mice. A. 3-4-month-old Controls (blue) compared to 8-10-month-old Controls (yellow). B. 3-4-month-old APP23 (red) compared to 8-10-month-old APP23 (green). Statistical difference calculated with the Mann-Whitney test.

Comparison of average PSD during isoflurane exposure between young and old mice showed statistically significant differences in frequencies examined. 8-10-month-old Control mice have significantly lower Delta (p<0.01), higher Theta (p<0.01), and

higher Alpha ($p<0.01$) than 3-4-month-old Controls (**Figure 22 A**). 8-10-month-old APP23 mice showed significantly higher Delta ($p<0.0001$), lower Theta ($p<0.001$), and lower Alpha ($p<0.001$) than 3-4-month-old APP23 mice (**Figure 22 B**).

iii. PHASE AMPLITUDE COUPLING OF APP23 MICE

Phase Amplitude Coupling (PAC) is a type of cross frequency analysis founded on the patterning of high frequency bands nested within low frequency bands. PAC shows fast oscillations propelled by slow oscillations, thereby being a measure of the cohesion across different bands. This behavior indicates synchrony in populations of firing neurons and consequently underlying mechanisms of neurological functioning [191].

Results

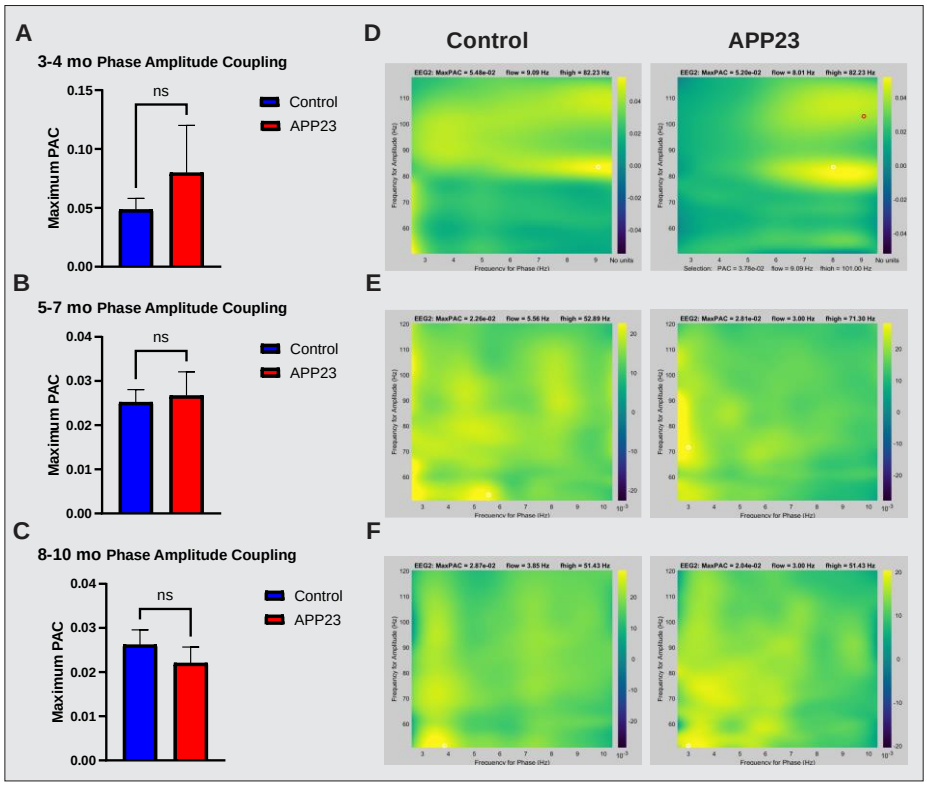

Figure 23: Phase Amplitude Coupling of APP23 Mice. Maximum PAC was processed via Brainstorm and analyzed between age groups. A: 3-4-month-old; B: 5-7-month-old; C.8-10-month-old. Control (blue); APP23 (red). Samples of PAC extracted from Brainstorm are shown on right panel, correspondent with the relevant age (D-F). Control – left; APP23– right. Significance calculated with the Mann-Whitney test.

Evaluation and comparison of maximum phase amplitude coupling of high frequency gamma against low frequency Theta as derived from the MATLAB GUI Brainstorm of young, mid-aged, and older mice did not elicit statistically significant results (**Figure 23**). It is possible that the commonly used nested and nesting frequencies (Gamma and Theta) were not relevant during anesthesia conditions. It has been reported the PAC of Gamma and Alpha disrupt PAC [192]. Furthermore, it is possible that the isoflurane sedation altered the presence of statistically significant Gamma and Theta PAC detectable in EEG2 of APP23 mutants and Controls.

CHAPTER 6

DISCUSSION & CONCLUSIONS

These studies aimed to elucidate the functionality of primary cilia and Arl13B in the reactive mouse brain, as well as evaluate EEG waveform of a mouse model of Alzheimer's Disease. The subsequent sections discuss the conclusions of each project.

Part 1: CILIA LENGTH VARIANCE

This study began with exploring morphological differences between primary cilium types, regions, and strains of mice. We hypothesized that primary cilia morphology would be impacted by cell type and disease-like conditions. Investigations moved forward to use epilepsy and cortical injury to produce different forms of reactivity induction to trigger astrocytic change and determine what morphological changes occur in primary cilia under reactive conditions.

Immunohistochemistry was first used as the primary tool to determine morphological differences between astrocytic and neuronal primary cilia, as well as regional differences in cilia type and strain of mouse. Results from these investigations support evidence from other studies that neuronal cilia are significantly longer than astrocytic cilia. This variation is likely attributed to the non-mitotic nature of neurons and the maintained proliferative capacity of astrocytes. Astrocytes need for more dynamic plasticity in primary cilia to support mitosis and are thus likely to exhibit shorter cilia.

These studies went further to demonstrate that both neuronal and astrocytic primary cilia display variations in length based on hippocampal region, and this variation is partly dependent on murine strain. Neurons showed regional variance in all regions of the hippocampus, while astrocytes displayed a marked shortening only in the dentate gyrus of Arl13B-mCherry; Centrin2-GFP mice. It is possible that the regional variation of neurons is due to region-specific function, although the difference in astrocytic cilia length only in one strain of mice is unique and unexpected. It is possible that the overexpression of Arl13B shown in this transgenic strain influences the cellular function and likewise the ciliary function of astrocytes in this region. Staining and imaging showed that differences in cilia length exist between strains. Staining was used to further support the unreported elongation of both neuronal and astrocytic primary cilia in the transgenic strain of Arl13B-mCherry; Centrin2-GFP mice, thereby identifying the potential for this strain to bias results of morphological studies.

The structural dynamics of astrocytic and neuronal primary cilia were shown to be influenced by spontaneously occurring seizures. This study is the first to verify a morphological change is astrocytic cilia based on spontaneous seizure occurrence. It further is the first to report that spontaneous audiogenic seizures reduce neuronal cilia length as well. The systemic reactivity throughout the brain influenced by repetitive seizure activity is also reported to propagate epileptic behavior. The heightened effect on astrocytic cilia may be a result of the influence of long-term seizure activity or an effector of the activity itself.

The first project in this thesis underscores the dichotomy between neuronal and astrocytic cilia, with respect to brain region, strain of mouse, and pathogenic condition.

These published results substantiate the hypothesis that primary cilia vary in morphology based on cell-type and the presence and/or type of disease. They additionally show that genotype can influence ciliary length. These findings illustrate the significance of primary cilia in disease, thereby supporting their potential as a therapeutic target.

Part 2: ARL13B IN BRAIN INJURY

The second project in this dissertation research sought out to evaluate the presence of a role of the Ras GTPase Arl13B in reactive gliosis and the formation of glial scarring, as indicated by altered GFAP expression. The project was founded on findings from data collected from the first study, indicating that Arl13B expression is enhanced near cortical injury following the reduction of Arl13B-positive primary cilia. From these results, I developed the hypothesis that Arl13B overexpression or reduced expression could be used to manipulate the degree of astrocyte reactivity.

Cortical injury resulted in undetectable Arl13B-primary cilia proximal to the injury site and a marked decrease of neuronal ciliary length. IFT88, an additional ciliary marker, was also unable to identify astrocytic cilia in these regions. Absence of astrocytic primary cilia supports the hypothesis that astrocytes in the vicinity of damaged tissue must proliferate, and consequently resorb their primary cilia, in order to mitose and form a glial scar. The reduction in neuronal cilia length suggests signaling differences potentially related to reparatory functions.

Immunohistochemistry was then analyzed for differences in protein expression proximal to and distal to cortical location (ipsilateral and contralateral hemisphere,

respectively) and genotype. Loss-of-Function, Gain-of-Function, Ciliary Knockout, and Controls were compared at seven days post injury for Arl13B and GFAP. Our hypothesis that Arl13B influences astrocyte reactivity in the form of altered GFAP expression at seven days post injury was not substantiated by results from this study.

It is possible that a longer period of time from lesion induction may have produced a difference in GFAP expression based on genotype, but seven days post injury was selected due to reports of heightened GFAP expression at this time and the ease in visualization of the injured cortex. Future studies may warrant focus on mice fourteen days following lesion to determine potential links between Arl13B and GFAP.

These studies did not substantiate the role of Arl13B in neurological repair and gliosis. Arl13B, a unique member of the Arl family, is still functionally unclear. Immunostaining results showed that Arl13B protein expression is heightened proximal to the injury site in all strains of mice used in this experimental design, but ablation and overexpression of Arl13B did not enhance or reduce glial scarring at seven days following cortical lesion.

This second research project did not support our hypothesis and did not establish the relevance of protein Arl13B in reactive gliosis and neurological homeostasis. Ergo, these findings do not provide evidence of Arl13B as a therapeutic target in gliosis-based brain injury reparations of Arl13B GOF, Arl13B LOF, IFT88-based ciliary KO, or C57BL/6BControl mice,

PART 3: EEG WAVEFORM ANALYSIS OF A MOUSE MODEL OF AD

The aim of the third project in this dissertation research was designed to expand the investigation of the pathogenic brain. This project was constructed to evaluate if EEG recordings can be used to identify hallmarks indicative of the presence of the AD prior to the onset of the AD phenotype. We hypothesized that while in a sedated state, the uninterrupted waveform would yield characteristics that could contribute to early diagnosis of AD.

APP23 mice, a mouse model of AD, were exposed to isoflurane anesthesia to reduce the noise of neuronal firing seen in the roused and even sleeping brain. The graphical user interface Brainstorm, a MATLAB-based platform, was used to filter waveforms of young, middle-aged, and old mice and process for differences in power spectral density, burst suppression density, and phase amplitude coupling.

During isoflurane administration, 3-4-month-old APP23 mice displayed a significantly higher level of Burst Suppression Density than Controls in the same age range. This age group also displayed significantly lower Delta Power Spectral Density and higher Theta and Alpha averages. There was limited statistical difference found in 5-7- and 8-10-month-old mice, likely attributed to normal cognitive changes that can occur with senescent change.

This third research project supported our hypothesis that while under anesthesia, APP23 mice would show significant differences in EEG waveform as substantiated with Burst Suppression Density quantification. Additionally, Power Spectral Density analysis of this age group yielded statistically significant differences in Delta, Theta, and Alpha frequencies, the powers relevant to relaxation and sleep.

The findings of this third project are relevant in the development of clinical evaluation of AD. EEG recordings during short procedures requiring anesthesia could be introduced to evaluate risk of this disease and therefore offer the potential for early intervention. These results are important in scientific understanding and implications of Alzheimer's.

CHAPTER 7:

CONSIDERATIONS OF FUTURE WORK

This dissertation research focused on enhancing our understanding of the pathogenic brain. Although the experiments yielded findings that elucidate the involvement of primary cilia epilepsy and brains injury, the relevance of Arl13B in cortical injury, and the identification of unique characteristics of EEG activity in early Alzheimer's, further work is needed to augment the importance and our understanding of these results.

For the evaluation of ciliary variance, it would be appropriate to investigate the difference in astrocyte and neuronal primary cilia in additional strains. The results included in this dissertation explore neuronal and astrocytic primary cilia of Arl13B-mCherry; Centrin2-GFP mice and two controls from their genetic background. A comparison of strains that do not share the same degree of genetics would aid in a better understanding of the strain-based variations that exist in mice.

Secondly, our findings of the previously described experiments consistently showed Arl13B as intensifying in the region of cortical injury. Investigation of its expression seven days following the lesion of cortical tissue of mice with an overexpression or ablation of Arl13B did not show an upregulation or down-regulation of GFAP expression. These findings do not support the hypothesis that Arl13B affects GFAP-based reactive gliosis. Investigation of expression by a different means of evaluation, such as qPCR could be relevant, but ineffective primers were a limiting factor during the time of this study. It is also possible that Arl13B may play a role in a

different feature of gliosis, such as the fibrotic tissue matrix that develops. Targeting this tissue and examining a correlation with Arl13B may be a promising pursuit.

Finally, the investigations of AD discussed in this dissertation are the foundation of a potentially important and large research project. In APP23 mice, the EEG waveform could also be investigated for differences in the cortical region. Due to the strength of signal, only EEG2 (prefrontal cortex) was used for analysis. EEG1, which transduces activity from the occipital lobe, was not included. Furthermore, investigation of human cortical activity would be very interesting and would require the collaboration of medical doctors and continued participation of patients over time to identify cognitive changes. The possibilities of investigating AD are highly extensive, and it is my hope that the methods and results shown here provide a research foundation on which development of early diagnostic tools for AD can be built.

APPENDIX

i. SUPPORTING TABLES

a. Table 3: Primary Antibodies used in Immunohistochemistry

Primary Antibody	Species	Dilution	Catalog #	Binding
Arl13B	Mouse	1:250	Neuromab, 75–287	Astrocytic primary cilia
GFAP	Rabbit	1:750	Dako, 2024-05-31	Astrocytes, Reactivity measurement
AC3	Rabbit	1:10,000	EnCorBiotechnology, AB2572219	Neuronal primary cilia
IBA1	Goat	1:250	Abcam, ab5076	Microglia
Ki67	Mouse	1:150	BD Biosciences, 550609	Proliferation marker (any stage of mitosis)

b. Table 4: Modified Racine Scale

Score	Behavior
0	No difference in behavior
1	Repetitive jaw twitch/chewing
2	Cranial bobbing and repetitive nodding
3	Involuntary movements accompanied with tremors
4	Involuntary movements accompanied by falling
5	Loss of muscle tone followed by death

ii. APPROVED IACUC PROTOCOLS

University of New Hampshire

Research Integrity Services, Service Building
51 College Road, Durham, NH 03824-3585
Fax: 603-862-3564

13-Sep-2019

Chen, Xuanmao
Molecular, Cellular, & Biomedical Sciences
Rudman Hall Rm 389
Durham, NH 03824-2618

IACUC #: 160701
Project: AC3 and Primary Cilia of Astrocytes
Modification Approval Date: 09-Sep-2019
Annual Approval Expiration Date: 14-Sep-2020
Protocol Three-Year Approval Expiration Date: 14-Sep-2020

The Institutional Animal Care and Use Committee (IACUC) has reviewed and approved the requested modification to the protocol for this study:

Significant modification - addition of mouse strain and surgical procedure

If you have any questions, please contact either Dean Elder at 862-4629 or Susan Jalbert at 862-3536.

For the IACUC,

Julie Simpson, Ph.D.
Director

cc: File

University *of* New Hampshire

Research Integrity Services, Service Building
51 College Road, Durham, NH 03824-3585
Fax: 603-862-3564

16-Apr-2019

Chen, Xuanmao
Molecular, Cellular, & Biomedical Sciences
Rudman Hall Rm 389
Durham, NH 03824-2618

IACUC #: 180603
Project: Primary Cilia of Neurons and Astrocytes
Modification Approval Date: 15-Apr-2019
Annual Approval Expiration Date: 25-Jul-2019
Protocol Three-Year Approval Expiration Date: 25-Jul-2021

The Institutional Animal Care and Use Committee (IACUC) has reviewed and approved the requested modification to the protocol for this study:

Changes per 4/1/19 memo

If you have any questions, please contact either Dean Elder at 862-4629 or Julie Simpson at 862-2003.

For the IACUC,

Rebecca Rowe, Ph.D.
Chair

cc: File

University *of* New Hampshire

Research Integrity Services, Service Building
51 College Road, Durham, NH 03824-3585
Fax: 603-862-3564

31-Jul-2019

Chen, Xuanmao
Molecular, Cellular, & Biomedical Sciences
Rudman Hall Rm 389
Durham, NH 03824-2618

IACUC #: 180603
Project: Primary Cilia of Neurons and Astrocytes
Modification Approval Date: 30-Jul-2019
Annual Approval Expiration Date: 25-Jul-2020
Protocol Three-Year Approval Expiration Date: 25-Jul-2021

The Institutional Animal Care and Use Committee (IACUC) has reviewed and approved the requested modification to the protocol for this study:

VVC change, carprofen injection to meloxicam tablet

If you have any questions, please contact either Dean Elder at 862-4629 or Susan Jalbert at 862-3536.

For the IACUC,

Julie Simpson, Ph.D.
Director

cc: File

University *of* New Hampshire

Research Integrity Services, Service Building
51 College Road, Durham, NH 03824-3585
Fax: 603-862-3564

27-Jul-2018

Chen, Xuanmao
Molecular, Cellular, & Biomedical Sciences
Rudman Hall Rm 389
Durham, NH 03824-2618

IACUC #: 180603
Project: Primary Cilia of Neurons and Astrocytes

The Institutional Animal Care and Use Committee (IACUC) has reviewed and recommended approval of the protocol submitted for this study contingent upon your response to the following:

1. *The investigator needs to work with the ARO veterinarians to revise the information in the application to add the possibility of using isoflurane for anesthesia in surgeries, if available.*

As soon as the IACUC receives an appropriate response to its concerns, above, it will issue you an approval letter for this protocol. **You may not commence activities in this protocol involving vertebrate animals until you have received IACUC approval.**

If you have any questions, please contact either Dean Elder at 862-4629 or Julie Simpson at 862-2003.

For the IACUC,

Rebecca Rowe

Rebecca Rowe, Ph.D.
Chair

cc: File

University *of* New Hampshire

Research Integrity Services, Service Building
51 College Road, Durham, NH 03824-3585
Fax: 603-862-3564

13-Sep-2019

Chen, Xuanmao
Molecular, Cellular, & Biomedical Sciences
Rudman Hall Rm 389
Durham, NH 03824-2618

IACUC #: 180901
Project: In vivo Imaging on Living Mice
Modification Approval Date: 09-Sep-2019
Annual Approval Expiration Date: 23-Oct-2019
Protocol Three-Year Approval Expiration Date: 23-Oct-2021

The Institutional Animal Care and Use Committee (IACUC) has reviewed and approved the requested modification to the protocol for this study:

VVC modification - add temporal anesthesia

If you have any questions, please contact either Dean Elder at 862-4629 or Susan Jalbert at 862-3536.

For the IACUC,

Julie Simpson, Ph.D.
Director

cc: File

University of New Hampshire

Research Integrity Services, Service Building
51 College Road, Durham, NH 03824-3585
Fax: 603-862-3564

26-Aug-2021

Chen, Xuanmao
Molecular, Cellular, & Biomedical Sciences
Rudman Hall Rm 389
Durham, NH 03824-2618

IACUC #: 210801
Project: Conditioning-Induced Alteration of Brain Waveform
Approval Date: 25-Aug-2021

The Institutional Animal Care and Use Committee (IACUC) reviewed and approved the protocol submitted for this study under Category E in Section V of the Application for Review of Vertebrate Animal Use in Research or Instruction - *Animal use activities that involve accompanying pain or distress to the animals for which appropriate anesthetic, analgesic, tranquilizing drugs or other methods for relieving pain or distress are not used.*

Approval is granted for a period of three years from the approval date above. Continued approval throughout the three year period is contingent upon completion of annual reports on the use of animals. At the end of the three year approval period you may submit a new application and request for extension to continue this project. Requests for extension must be filed prior to the expiration of the original approval.

Please Note:
1. All cage, pen, or other animal identification records must include your IACUC # listed above.
2. Use of animals in research and instruction is approved contingent upon participation in the UNH Occupational Health Program for persons handling animals. Participation is mandatory for all principal investigators and their affiliated personnel, employees of the University and students alike. Information about the program, including forms, is available at http://unh.edu/research/occupational-health-program-animal-handlers.

If you have any questions, please contact either Dean Elder at 862-4629 or Susan Jalbert at 862-3536.

For the IACUC,

Julie Simpson, Ph.D.
Director

cc: File

LIST OF REFERENCES

1. Liddelow, S.A. and B.A. Barres, *Reactive Astrocytes: Production, Function, and Therapeutic Potential.* Immunity, 2017. **46**(6): p. 957-967.
2. Chen, Y. and R.A. Swanson, *Astrocytes and brain injury.* J Cereb Blood Flow Metab, 2003. **23**(2): p. 137-49.
3. de Lanerolle, N.C., T.S. Lee, and D.D. Spencer, *Astrocytes and epilepsy.* Neurotherapeutics, 2010. **7**(4): p. 424-38.
4. Sofroniew, M.V. and H.V. Vinters, *Astrocytes: biology and pathology.* Acta Neuropathol, 2010. **119**(1): p. 7-35.
5. Scheib, J. and C. Byrd-Jacobs, *Zebrafish Astroglial Morphology in the Olfactory Bulb Is Altered With Repetitive Peripheral Damage.* Front Neuroanat, 2020. **14**: p. 4.
6. Sterpka, A., et al., *Diverged morphology changes of astrocytic and neuronal primary cilia under reactive insults.* Mol Brain, 2020. **13**(1): p. 28.
7. Sterpka, A. and X. Chen, *Neuronal and astrocytic primary cilia in the mature brain.* Pharmacol Res, 2018. **137**: p. 114-121.
8. Kasahara, K., et al., *Visualization of astrocytic primary cilia in the mouse brain by immunofluorescent analysis using the cilia marker Arl13b.* Acta Med Okayama, 2014. **68**(6): p. 317-22.
9. Phua, S.C., et al., *Dynamic Remodeling of Membrane Composition Drives Cell Cycle through Primary Cilia Excision.* Cell, 2019. **178**(1): p. 261.
10. Bay, S.N., A.B. Long, and T. Caspary, *Disruption of the ciliary GTPase Arl13b suppresses Sonic hedgehog overactivation and inhibits medulloblastoma formation.* Proc Natl Acad Sci U S A, 2018. **115**(7): p. 1570-1575.
11. Amankulor, N.M., et al., *Sonic hedgehog pathway activation is induced by acute brain injury and regulated by injury-related inflammation.* J Neurosci, 2009. **29**(33): p. 10299-308.
12. Kumar, A., et al., *Alzheimer Disease*, in *StatPearls*. 2022: Treasure Island (FL).
13. Thalhauser, C.J. and N.L. Komarova, *Alzheimer's disease: rapid and slow progression.* J R Soc Interface, 2012. **9**(66): p. 119-26.
14. Sorokin, S.P., *Reconstructions of centriole formation and ciliogenesis in mammalian lungs.* J Cell Sci, 1968. **3**(2): p. 207-30.
15. Park, S.M., H.J. Jang, and J.H. Lee, *Roles of Primary Cilia in the Developing Brain.* Front Cell Neurosci, 2019. **13**: p. 218.
16. Breunig, J.J., et al., *Primary cilia regulate hippocampal neurogenesis by mediating sonic hedgehog signaling.* Proc Natl Acad Sci U S A, 2008. **105**(35): p. 13127-32.
17. Pan, J. and W. Snell, *The primary cilium: keeper of the key to cell division.* Cell, 2007. **129**(7): p. 1255-7.
18. Singla, V. and J.F. Reiter, *The primary cilium as the cell's antenna: signaling at a sensory organelle.* Science, 2006. **313**(5787): p. 629-33.
19. Waters, A.M. and P.L. Beales, *Ciliopathies: an expanding disease spectrum.* Pediatr Nephrol, 2011. **26**(7): p. 1039-56.
20. Mitchison, H.M. and E.M. Valente, *Motile and non-motile cilia in human pathology: from function to phenotypes.* J Pathol, 2017. **241**(2): p. 294-309.
21. Venkatesh, D., *Primary cilia.* J Oral Maxillofac Pathol, 2017. **21**(1): p. 8-10.
22. Hsiao, Y.C., K. Tuz, and R.J. Ferland, *Trafficking in and to the primary cilium.* Cilia, 2012. **1**(1): p. 4.

23. Taschner, M. and E. Lorentzen, *The Intraflagellar Transport Machinery.* Cold Spring Harb Perspect Biol, 2016. **8**(10).
24. Goncalves, J. and L. Pelletier, *The Ciliary Transition Zone: Finding the Pieces and Assembling the Gate.* Mol Cells, 2017. **40**(4): p. 243-253.
25. Di Pietro, C., et al., *Primary Cilia in the Murine Cerebellum and in Mutant Models of Medulloblastoma.* Cell Mol Neurobiol, 2017. **37**(1): p. 145-154.
26. Han, Y.G., et al., *Dual and opposing roles of primary cilia in medulloblastoma development.* Nat Med, 2009. **15**(9): p. 1062-5.
27. Sarkisian, M.R., et al., *Detection of primary cilia in human glioblastoma.* J Neurooncol, 2014. **117**(1): p. 15-24.
28. Moser, J.J., M.J. Fritzler, and J.B. Rattner, *Ultrastructural characterization of primary cilia in pathologically characterized human glioblastoma multiforme (GBM) tumors.* BMC Clin Pathol, 2014. **14**: p. 40.
29. Loskutov, Y. and E.N. Pugacheva, *Targeting primary cilia - associated signaling in glioblastoma: guided approach for drug development.* Oncoscience, 2019. **6**(1-2): p. 289-290.
30. Seeley, E.S., et al., *Pancreatic cancer and precursor pancreatic intraepithelial neoplasia lesions are devoid of primary cilia.* Cancer Res, 2009. **69**(2): p. 422-30.
31. Nielsen, S.K., et al., *Characterization of primary cilia and Hedgehog signaling during development of the human pancreas and in human pancreatic duct cancer cell lines.* Dev Dyn, 2008. **237**(8): p. 2039-52.
32. Higgins, M., I. Obaidi, and T. McMorrow, *Primary cilia and their role in cancer.* Oncol Lett, 2019. **17**(3): p. 3041-3047.
33. Yoder, B.K., *Role of primary cilia in the pathogenesis of polycystic kidney disease.* J Am Soc Nephrol, 2007. **18**(5): p. 1381-8.
34. Kathem, S.H., A.M. Mohieldin, and S.M. Nauli, *The Roles of Primary cilia in Polycystic Kidney Disease.* AIMS Mol Sci, 2014. **1**(1): p. 27-46.
35. Tadel, F., et al., *Brainstorm: a user-friendly application for MEG/EEG analysis.* Comput Intell Neurosci, 2011. **2011**: p. 879716.
36. Revenkova, E., et al., *The Joubert syndrome protein ARL13B binds tubulin to maintain uniform distribution of proteins along the ciliary membrane.* J Cell Sci, 2018. **131**(9).
37. Cantagrel, V., et al., *Mutations in the cilia gene ARL13B lead to the classical form of Joubert syndrome.* Am J Hum Genet, 2008. **83**(2): p. 170-9.
38. Novas, R., et al., *Bardet-Biedl syndrome: Is it only cilia dysfunction?* FEBS Lett, 2015. **589**(22): p. 3479-91.
39. Pazour, G.J. and G.B. Witman, *The vertebrate primary cilium is a sensory organelle.* Curr Opin Cell Biol, 2003. **15**(1): p. 105-10.
40. Fulda, S., et al., *Rapid eye movements during sleep in mice: high trait-like stability qualifies rapid eye movement density for characterization of phenotypic variation in sleep patterns of rodents.* BMC Neurosci, 2011. **12**: p. 110.
41. Antal, M.C., et al., *Adenylate Cyclase Type III Is Not a Ubiquitous Marker for All Primary Cilia during Development.* PLoS One, 2017. **12**(1): p. e0170756.
42. Gascue, C., et al., *Direct role of Bardet-Biedl syndrome proteins in transcriptional regulation.* J Cell Sci, 2012. **125**(Pt 2): p. 362-75.
43. Williams, C.L., et al., *Gene Therapeutic Reversal of Peripheral Olfactory Impairment in Bardet-Biedl Syndrome.* Mol Ther, 2017. **25**(4): p. 904-916.
44. Babu, D. and S. Roy, *Left-right asymmetry: cilia stir up new surprises in the node.* Open Biol, 2013. **3**(5): p. 130052.

45. Guadiana, S.M., et al., *Type 3 Adenylyl Cyclase and Somatostatin Receptor 3 Expression Persists in Aged Rat Neocortical and Hippocampal Neuronal Cilia.* Front Aging Neurosci, 2016. **8**: p. 127.
46. Valente, E.M., et al., *Primary cilia in neurodevelopmental disorders.* Nat Rev Neurol, 2014. **10**(1): p. 27-36.
47. Narita, K., et al., *Multiple primary cilia modulate the fluid transcytosis in choroid plexus epithelium.* Traffic, 2010. **11**(2): p. 287-301.
48. Sipos, E., S. Komoly, and P. Acs, *Quantitative Comparison of Primary Cilia Marker Expression and Length in the Mouse Brain.* J Mol Neurosci, 2018. **64**(3): p. 397-409.
49. Falcon-Urrutia, P., et al., *Shh Signaling through the Primary Cilium Modulates Rat Oligodendrocyte Differentiation.* PLoS One, 2015. **10**(7): p. e0133567.
50. Bowie, E. and S.C. Goetz, *TTBK2 and primary cilia are essential for the connectivity and survival of cerebellar Purkinje neurons.* Elife, 2020. **9**.
51. Lee, J., et al., *Loss of Primary Cilia Results in the Development of Cancer in the Murine Thyroid Gland.* Mol Cells, 2019. **42**(2): p. 113-122.
52. Bangs, F.K., et al., *Lineage specificity of primary cilia in the mouse embryo.* Nat Cell Biol, 2015. **17**(2): p. 113-22.
53. Weiner, L.P., *Definitions and criteria for stem cells.* Methods Mol Biol, 2008. **438**: p. 3-8.
54. Kriegstein, A. and A. Alvarez-Buylla, *The glial nature of embryonic and adult neural stem cells.* Annu Rev Neurosci, 2009. **32**: p. 149-84.
55. Myster, D.L. and R.J. Duronio, *To differentiate or not to differentiate?* Curr Biol, 2000. **10**(8): p. R302-4.
56. Moser, J.J., M.J. Fritzler, and J.B. Rattner, *Primary ciliogenesis defects are associated with human astrocytoma/glioblastoma cells.* BMC Cancer, 2009. **9**: p. 448.
57. Qiu, L., et al., *Type 3 adenylyl cyclase: a key enzyme mediating the cAMP signaling in neuronal cilia.* Int J Physiol Pathophysiol Pharmacol, 2016. **8**(3): p. 95-108.
58. Ott, C., *Research Presentation*, in *SRC*, FASEB, Editor. 2019, Janelia Research Campus: Snowmass CO.
59. Pekny, M., et al., *Astrocytes: a central element in neurological diseases.* Acta Neuropathol, 2016. **131**(3): p. 323-45.
60. Schiweck, J., B.J. Eickholt, and K. Murk, *Important Shapeshifter: Mechanisms Allowing Astrocytes to Respond to the Changing Nervous System During Development, Injury and Disease.* Front Cell Neurosci, 2018. **12**: p. 261.
61. Farhy-Tselnicker, I. and N.J. Allen, *Astrocytes, neurons, synapses: a tripartite view on cortical circuit development.* Neural Dev, 2018. **13**(1): p. 7.
62. Allen, N.J. and C. Eroglu, *Cell Biology of Astrocyte-Synapse Interactions.* Neuron, 2017. **96**(3): p. 697-708.
63. Perea, G., M. Navarrete, and A. Araque, *Tripartite synapses: astrocytes process and control synaptic information.* Trends Neurosci, 2009. **32**(8): p. 421-31.
64. Mangia, S., et al., *The in vivo neuron-to-astrocyte lactate shuttle in human brain: evidence from modeling of measured lactate levels during visual stimulation.* J Neurochem, 2009. **109 Suppl 1**: p. 55-62.
65. Belanger, M. and P.J. Magistretti, *The role of astroglia in neuroprotection.* Dialogues Clin Neurosci, 2009. **11**(3): p. 281-95.
66. Allahyari, R.V., et al., *Sonic hedgehog signaling is negatively regulated in reactive astrocytes after forebrain stab injury.* Sci Rep, 2019. **9**(1): p. 565.
67. Pekny, M. and M. Nilsson, *Astrocyte activation and reactive gliosis.* Glia, 2005. **50**(4): p. 427-34.
68. Burda, J.E., A.M. Bernstein, and M.V. Sofroniew, *Astrocyte roles in traumatic brain injury.* Exp Neurol, 2016. **275 Pt 3**: p. 305-315.

69. Moeton, M., et al., *GFAP isoforms control intermediate filament network dynamics, cell morphology, and focal adhesions.* Cell Mol Life Sci, 2016. **73**(21): p. 4101-20.
70. Nishiyama, H., et al., *Glial protein S100B modulates long-term neuronal synaptic plasticity.* Proc Natl Acad Sci U S A, 2002. **99**(6): p. 4037-42.
71. Gos, T., et al., *S100B-immunopositive astrocytes and oligodendrocytes in the hippocampus are differentially afflicted in unipolar and bipolar depression: a postmortem study.* J Psychiatr Res, 2013. **47**(11): p. 1694-9.
72. Steiner, J., et al., *Evidence for a wide extra-astrocytic distribution of S100B in human brain.* BMC Neurosci, 2007. **8**: p. 2.
73. Chaboub, L.S. and B. Deneen, *Developmental origins of astrocyte heterogeneity: the final frontier of CNS development.* Dev Neurosci, 2012. **34**(5): p. 379-88.
74. Tabata, H., *Diverse subtypes of astrocytes and their development during corticogenesis.* Front Neurosci, 2015. **9**: p. 114.
75. Dallerac, G. and N. Rouach, *Astrocytes as new targets to improve cognitive functions.* Prog Neurobiol, 2016. **144**: p. 48-67.
76. Wetherington, J., G. Serrano, and R. Dingledine, *Astrocytes in the epileptic brain.* Neuron, 2008. **58**(2): p. 168-78.
77. Eng, L.F. and R.S. Ghirnikar, *GFAP and astrogliosis.* Brain Pathol, 1994. **4**(3): p. 229-37.
78. Chen, S.D., et al., *Emerging Roles of Sonic Hedgehog in Adult Neurological Diseases: Neurogenesis and Beyond.* Int J Mol Sci, 2018. **19**(8).
79. Zbesko, J.C., et al., *Glial scars are permeable to the neurotoxic environment of chronic stroke infarcts.* Neurobiol Dis, 2018. **112**: p. 63-78.
80. Vargas-Sanchez, K., et al., *Astroglial role in the pathophysiology of status epilepticus: an overview.* Oncotarget, 2018. **9**(42): p. 26954-26976.
81. Li, Y., et al., *The small GTPases ARL-13 and ARL-3 coordinate intraflagellar transport and ciliogenesis.* J Cell Biol, 2010. **189**(6): p. 1039-51.
82. Fisher, S., et al., *ARF family GTPases with links to cilia.* Am J Physiol Cell Physiol, 2020. **319**(2): p. C404-C418.
83. Johnson, D.S. and Y.H. Chen, *Ras family of small GTPases in immunity and inflammation.* Curr Opin Pharmacol, 2012. **12**(4): p. 458-63.
84. Donaldson, J.G. and A. Honda, *Localization and function of Arf family GTPases.* Biochem Soc Trans, 2005. **33**(Pt 4): p. 639-42.
85. Pasqualato, S., L. Renault, and J. Cherfils, *Arf, Arl, Arp and Sar proteins: a family of GTP-binding proteins with a structural device for 'front-back' communication.* EMBO Rep, 2002. **3**(11): p. 1035-41.
86. Barral, D.C., et al., *Arl13b regulates endocytic recycling traffic.* Proc Natl Acad Sci U S A, 2012. **109**(52): p. 21354-9.
87. Casalou, C., et al., *Arl13b Regulates Breast Cancer Cell Migration and Invasion by Controlling Integrin-Mediated Signaling.* Cancers (Basel), 2019. **11**(10).
88. Higginbotham, H., et al., *Arl13b in primary cilia regulates the migration and placement of interneurons in the developing cerebral cortex.* Dev Cell, 2012. **23**(5): p. 925-38.
89. Toma-Fukai, S. and T. Shimizu, *Structural Insights into the Regulation Mechanism of Small GTPases by GEFs.* Molecules, 2019. **24**(18).
90. Kahn, R.A., et al., *Nomenclature for the human Arf family of GTP-binding proteins: ARF, ARL, and SAR proteins.* J Cell Biol, 2006. **172**(5): p. 645-50.
91. Roy, K., et al., *Palmitoylation of the ciliary GTPase ARL13b is necessary for its stability and its role in cilia formation.* J Biol Chem, 2017. **292**(43): p. 17703-17717.

92. Alvarez-Satta, M. and A. Matheu, *Primary cilium and glioblastoma.* Ther Adv Med Oncol, 2018. **10**: p. 1758835918801169.
93. Casalou, C., A. Ferreira, and D.C. Barral, *The Role of ARF Family Proteins and Their Regulators and Effectors in Cancer Progression: A Therapeutic Perspective.* Front Cell Dev Biol, 2020. **8**: p. 217.
94. Donaldson, J.G. and C.L. Jackson, *ARF family G proteins and their regulators: roles in membrane transport, development and disease.* Nat Rev Mol Cell Biol, 2011. **12**(6): p. 362-75.
95. Kahn, R.A., M.P. East, and J.W. Francis, *ARF-Like (ARL) Proteins*, in *Ras Superfamily Small G Proteins: Biology and Mechanisms 2: Transport*, A. Wittinghofer, Editor. 2014, Springer International Publishing: Cham. p. 215-251.
96. Gotthardt, K., et al., *A G-protein activation cascade from Arl13B to Arl3 and implications for ciliary targeting of lipidated proteins.* Elife, 2015. **4**.
97. Gigante, E.D., et al., *ARL13B regulates Sonic hedgehog signaling from outside primary cilia.* Elife, 2020. **9**.
98. Ferent, J., et al., *The Ciliary Protein Arl13b Functions Outside of the Primary Cilium in Shh-Mediated Axon Guidance.* Cell Rep, 2019. **29**(11): p. 3356-3366 e3.
99. *Correction for Arl13b regulates Shh signaling from both inside and outside the cilium.* Mol Biol Cell, 2017. **28**(7): p. 996.
100. Song, P. and B.D. Perkins, *Developmental expression of the zebrafish Arf-like small GTPase paralogs arl13a and arl13b.* Gene Expr Patterns, 2018. **29**: p. 82-87.
101. Parisi, M.A., *The molecular genetics of Joubert syndrome and related ciliopathies: The challenges of genetic and phenotypic heterogeneity.* Transl Sci Rare Dis, 2019. **4**(1-2): p. 25-49.
102. Ivanova, A.A., et al., *Biochemical characterization of purified mammalian ARL13B protein indicates that it is an atypical GTPase and ARL3 guanine nucleotide exchange factor (GEF).* J Biol Chem, 2017. **292**(26): p. 11091-11108.
103. Hardee, I., et al., *Defective ciliogenesis in INPP5E-related Joubert syndrome.* Am J Med Genet A, 2017. **173**(12): p. 3231-3237.
104. Alkanderi, S., et al., *ARL3 Mutations Cause Joubert Syndrome by Disrupting Ciliary Protein Composition.* Am J Hum Genet, 2018. **103**(4): p. 612-620.
105. Dilan, T.L., et al., *ARL13B, a Joubert Syndrome-Associated Protein, Is Critical for Retinogenesis and Elaboration of Mouse Photoreceptor Outer Segments.* J Neurosci, 2019. **39**(8): p. 1347-1364.
106. Ware, S.M., M.G. Aygun, and F. Hildebrandt, *Spectrum of clinical diseases caused by disorders of primary cilia.* Proc Am Thorac Soc, 2011. **8**(5): p. 444-50.
107. Fansa, E.K., et al., *PDE6delta-mediated sorting of INPP5E into the cilium is determined by cargo-carrier affinity.* Nat Commun, 2016. **7**: p. 11366.
108. Humbert, M.C., et al., *ARL13B, PDE6D, and CEP164 form a functional network for INPP5E ciliary targeting.* Proc Natl Acad Sci U S A, 2012. **109**(48): p. 19691-6.
109. Choudhry, Z., et al., *Sonic hedgehog signalling pathway: a complex network.* Ann Neurosci, 2014. **21**(1): p. 28-31.
110. Nozaki, S., et al., *Regulation of ciliary retrograde protein trafficking by the Joubert syndrome proteins ARL13B and INPP5E.* J Cell Sci, 2017. **130**(3): p. 563-576.
111. Higginbotham, H., et al., *Arl13b-regulated cilia activities are essential for polarized radial glial scaffold formation.* Nat Neurosci, 2013. **16**(8): p. 1000-7.
112. Armato, U., et al., *Alzheimer's disease: an update of the roles of receptors, astrocytes and primary cilia (review).* Int J Mol Med, 2013. **31**(1): p. 3-10.
113. Mariani, L.E., et al., *Arl13b regulates Shh signaling from both inside and outside the cilium.* Mol Biol Cell, 2016.

114. Hurley, J.H., *Structure, mechanism, and regulation of mammalian adenylyl cyclase.* J Biol Chem, 1999. **274**(12): p. 7599-602.
115. Nicol, X. and P. Gaspar, *Routes to cAMP: shaping neuronal connectivity with distinct adenylate cyclases.* Eur J Neurosci, 2014. **39**(11): p. 1742-51.
116. Sadana, R. and C.W. Dessauer, *Physiological roles for G protein-regulated adenylyl cyclase isoforms: insights from knockout and overexpression studies.* Neurosignals, 2009. **17**(1): p. 5-22.
117. Nordman, S., et al., *Genetic variation of the adenylyl cyclase 3 (AC3) locus and its influence on type 2 diabetes and obesity susceptibility in Swedish men.* Int J Obes (Lond), 2008. **32**(3): p. 407-12.
118. Chen, X., et al., *Ablation of Type III Adenylyl Cyclase in Mice Causes Reduced Neuronal Activity, Altered Sleep Pattern, and Depression-like Phenotypes.* Biol Psychiatry, 2016. **80**(11): p. 836-848.
119. Wang, Z., et al., *Adult type 3 adenylyl cyclase-deficient mice are obese.* PLoS One, 2009. **4**(9): p. e6979.
120. Wang, Z., T. Phan, and D.R. Storm, *The type 3 adenylyl cyclase is required for novel object learning and extinction of contextual memory: role of cAMP signaling in primary cilia.* J Neurosci, 2011. **31**(15): p. 5557-61.
121. Breijyeh, Z. and R. Karaman, *Comprehensive Review on Alzheimer's Disease: Causes and Treatment.* Molecules, 2020. **25**(24).
122. Picciotto, M.R., M.J. Higley, and Y.S. Mineur, *Acetylcholine as a neuromodulator: cholinergic signaling shapes nervous system function and behavior.* Neuron, 2012. **76**(1): p. 116-29.
123. Chen, G.F., et al., *Amyloid beta: structure, biology and structure-based therapeutic development.* Acta Pharmacol Sin, 2017. **38**(9): p. 1205-1235.
124. O'Brien, R.J. and P.C. Wong, *Amyloid precursor protein processing and Alzheimer's disease.* Annu Rev Neurosci, 2011. **34**: p. 185-204.
125. Medeiros, R., D. Baglietto-Vargas, and F.M. LaFerla, *The role of tau in Alzheimer's disease and related disorders.* CNS Neurosci Ther, 2011. **17**(5): p. 514-24.
126. Weller, J., et al., *Accounting for Individual Differences in Decision-Making Competence: Personality and Gender Differences.* Front Psychol, 2018. **9**: p. 2258.
127. Weller, J. and A. Budson, *Current understanding of Alzheimer's disease diagnosis and treatment.* F1000Res, 2018. **7**.
128. Jeong, J., *EEG dynamics in patients with Alzheimer's disease.* Clin Neurophysiol, 2004. **115**(7): p. 1490-505.
129. Ittner, A.A., et al., *p38 MAP kinase-mediated NMDA receptor-dependent suppression of hippocampal hypersynchronicity in a mouse model of Alzheimer's disease.* Acta Neuropathol Commun, 2014. **2**: p. 149.
130. Vaisse, C., J.F. Reiter, and N.F. Berbari, *Cilia and Obesity.* Cold Spring Harb Perspect Biol, 2017. **9**(7).
131. Seixas, C., et al., *Arl13b and the exocyst interact synergistically in ciliogenesis.* Mol Biol Cell, 2016. **27**(2): p. 308-20.
132. Wang, R., et al., *Power spectral density and coherence analysis of Alzheimer's EEG.* Cogn Neurodyn, 2015. **9**(3): p. 291-304.
133. Goelz, M.F., et al., *Neuropathologic findings associated with seizures in FVB mice.* Lab Anim Sci, 1998. **48**(1): p. 34-7.
134. Kohnken, R.A. and D.J. Schwahn, *Lack of Chronic Histologic Lesions Supportive of Sublethal Spontaneous Seizures in FVB/N Mice.* Comp Med, 2016. **66**(2): p. 105-11.
135. Silva-Fernandes, A.O., Pedro & Sousa, Nuno & Maciel, Patricia, *Motor and Behavioural Abnormalities Associated with Persistent Spontaneous Epilepsy in the fvb/n Mouse Strain*

Scandinavian Journal of Laboratory Animal Science. , 2010. **37.** : p. 213-222. .
136. de Cheveigne, A. and I. Nelken, *Filters: When, Why, and How (Not) to Use Them.* Neuron, 2019. **102**(2): p. 280-293.
137. Jia, W., et al., *Spike separation from EEG/MEG data using morphological filter and wavelet transform.* Conf Proc IEEE Eng Med Biol Soc, 2006. **2006**: p. 6137-40.
138. Sharmila, A. and P. Geethanjali, *Effect of filtering with time domain features for the detection of epileptic seizure from EEG signals.* J Med Eng Technol, 2018. **42**(3): p. 217-227.
139. Leske, S. and S.S. Dalal, *Reducing power line noise in EEG and MEG data via spectrum interpolation.* Neuroimage, 2019. **189**: p. 763-776.
140. Tadel, F., et al., *MEG/EEG Group Analysis With Brainstorm.* Front Neurosci, 2019. **13**: p. 76.
141. Niso, G., et al., *Brainstorm Pipeline Analysis of Resting-State Data From the Open MEG Archive.* Front Neurosci, 2019. **13**: p. 284.
142. Groppe, D.M., et al., *Dominant frequencies of resting human brain activity as measured by the electrocorticogram.* Neuroimage, 2013. **79**: p. 223-33.
143. Maheshwari, A., et al., *Persistent aberrant cortical phase-amplitude coupling following seizure treatment in absence epilepsy models.* J Physiol, 2017. **595**(23): p. 7249-7260.
144. Florin, E. and S. Baillet, *Commentary: Evaluation of Phase-Amplitude Coupling in Resting State Magnetoencephalographic Signals: Effect of Surrogates and Evaluation Approach.* Front Comput Neurosci, 2018. **12**: p. 26.
145. Kenny, J.D., et al., *Propofol and sevoflurane induce distinct burst suppression patterns in rats.* Front Syst Neurosci, 2014. **8**: p. 237.
146. Taketo, M., et al., *FVB/N: an inbred mouse strain preferable for transgenic analyses.* Proc Natl Acad Sci U S A, 1991. **88**(6): p. 2065-9.
147. Bryant, C.D., *The blessings and curses of C57BL/6 substrains in mouse genetic studies.* Ann N Y Acad Sci, 2011. **1245**: p. 31-3.
148. Zurita, E., et al., *Genetic polymorphisms among C57BL/6 mouse inbred strains.* Transgenic Res, 2011. **20**(3): p. 481-9.
149. Su, C.Y., et al., *Temporal deletion of Arl13b reveals that a mispatterned neural tube corrects cell fate over time.* Development, 2012. **139**(21): p. 4062-71.
150. Van Dam, D., et al., *APP23 mice as a model of Alzheimer's disease: an example of a transgenic approach to modeling a CNS disorder.* CNS Spectr, 2005. **10**(3): p. 207-22.
151. Chen, Z., et al., *An empirical EEG analysis in brain death diagnosis for adults.* Cogn Neurodyn, 2008. **2**(3): p. 257-71.
152. Yang, Y. and K. Herrup, *Cell division in the CNS: protective response or lethal event in post-mitotic neurons?* Biochim Biophys Acta, 2007. **1772**(4): p. 457-66.
153. Liddelow, S.A., et al., *Neurotoxic reactive astrocytes are induced by activated microglia.* Nature, 2017. **541**(7638): p. 481-487.
154. Tian, G.F., et al., *An astrocytic basis of epilepsy.* Nat Med, 2005. **11**(9): p. 973-81.
155. Farrell, J.S., M.D. Wolff, and G.C. Teskey, *Neurodegeneration and Pathology in Epilepsy: Clinical and Basic Perspectives.* Adv Neurobiol, 2017. **15**: p. 317-334.
156. Chatzikonstantinou, A., *Epilepsy and the hippocampus.* Front Neurol Neurosci, 2014. **34**: p. 121-42.
157. Parker, A.K., et al., *Neonatal seizures induced by pentylenetetrazol or kainic acid disrupt primary cilia growth on developing mouse cortical neurons.* Exp Neurol, 2016. **282**: p. 119-27.
158. Kirschen, G.W., et al., *The radial organization of neuronal primary cilia is acutely disrupted by seizure and ischemic brain injury.* Front Biol (Beijing), 2017. **12**(2): p. 124-138.
159. Borges, K., et al., *Degeneration and proliferation of astrocytes in the mouse dentate gyrus after pilocarpine-induced status epilepticus.* Exp Neurol, 2006. **201**(2): p. 416-27.

160. Jahanshahi, M., et al., *The similarity of astrocytes number in dentate gyrus and CA3 subfield of rats hippocampus.* Pak J Biol Sci, 2007. **10**(1): p. 186-8.
161. Zhou, Y., et al., *Dual roles of astrocytes in plasticity and reconstruction after traumatic brain injury.* Cell Commun Signal, 2020. **18**(1): p. 62.
162. Wang, H., et al., *Portrait of glial scar in neurological diseases.* Int J Immunopathol Pharmacol, 2018. **31**: p. 2058738418801406.
163. Moeendarbary, E., et al., *The soft mechanical signature of glial scars in the central nervous system.* Nat Commun, 2017. **8**: p. 14787.
164. Nishimura, Y., et al., *Primary Cilia as Signaling Hubs in Health and Disease.* Adv Sci (Weinh), 2019. **6**(1): p. 1801138.
165. Renault-Mihara, F., et al., *Regulation of RhoA by STAT3 coordinates glial scar formation.* J Cell Biol, 2017. **216**(8): p. 2533-2550.
166. Larkins, C.E., et al., *Arl13b regulates ciliogenesis and the dynamic localization of Shh signaling proteins.* Mol Biol Cell, 2011. **22**(23): p. 4694-703.
167. Fisher, S.P., et al., *Rapid assessment of sleep-wake behavior in mice.* J Biol Rhythms, 2012. **27**(1): p. 48-58.
168. Soltani, S., et al., *Sleep-Wake Cycle in Young and Older Mice.* Front Syst Neurosci, 2019. **13**: p. 51.
169. Oishi, Y., et al., *Polygraphic Recording Procedure for Measuring Sleep in Mice.* J Vis Exp, 2016(107): p. e53678.
170. Patel, A.K., V. Reddy, and J.F. Araujo, *Physiology, Sleep Stages*, in *StatPearls*. 2020: Treasure Island (FL).
171. Yamada, R.G. and H.R. Ueda, *Molecular Mechanisms of REM Sleep.* Front Neurosci, 2019. **13**: p. 1402.
172. Hutchison, I.C. and S. Rathore, *The role of REM sleep theta activity in emotional memory.* Front Psychol, 2015. **6**: p. 1439.
173. Wimmer, M.E., et al., *Aging in mice reduces the ability to sustain sleep/wake states.* PLoS One, 2013. **8**(12): p. e81880.
174. Kumar, P. and T.R. Raju, *Seizure susceptibility decreases with enhancement of rapid eye movement sleep.* Brain Res, 2001. **922**(2): p. 299-304.
175. Ng, M. and M. Pavlova, *Why are seizures rare in rapid eye movement sleep? Review of the frequency of seizures in different sleep stages.* Epilepsy Res Treat, 2013. **2013**: p. 932790.
176. Bazil, C.W., L.H. Castro, and T.S. Walczak, *Reduction of rapid eye movement sleep by diurnal and nocturnal seizures in temporal lobe epilepsy.* Arch Neurol, 2000. **57**(3): p. 363-8.
177. Miller, J.W., G.M. Turner, and B.C. Gray, *Anticonvulsant effects of the experimental induction of hippocampal theta activity.* Epilepsy Res, 1994. **18**(3): p. 195-204.
178. Gigli, G.L. and J. Gotman, *Effects of seizures, kindling, and carbamazepine on sleep organization in cats.* Epilepsia, 1992. **33**(1): p. 14-22.
179. Andra, K., et al., *Expression of APP in transgenic mice: a comparison of neuron-specific promoters.* Neurobiol Aging, 1996. **17**(2): p. 183-90.
180. Kelly, P.H., et al., *Progressive age-related impairment of cognitive behavior in APP23 transgenic mice.* Neurobiol Aging, 2003. **24**(2): p. 365-78.
181. Fitz, N.F., et al., *Improvement of memory deficits and amyloid-beta clearance in aged APP23 mice treated with a combination of anti-amyloid-beta antibody and LXR agonist.* J Alzheimers Dis, 2014. **41**(2): p. 535-49.
182. Van Erum, J., et al., *Sleep architecture changes in the APP23 mouse model manifest at onset of cognitive deficits.* Behav Brain Res, 2019. **373**: p. 112089.

183. Hoffman, W.E. and G. Edelman, *Comparison of isoflurane and desflurane anesthetic depth using burst suppression of the electroencephalogram in neurosurgical patients.* Anesth Analg, 1995. **81**(4): p. 811-6.
184. Shanker, A., et al., *Etiology of Burst Suppression EEG Patterns.* Front Psychol, 2021. **12**: p. 673529.
185. Kratzer, S., et al., *Age-Related EEG Features of Bursting Activity During Anesthetic-Induced Burst Suppression.* Front Syst Neurosci, 2020. **14**: p. 599962.
186. Akerstedt, T. and M. Gillberg, *Sleep duration and the power spectral density of the EEG.* Electroencephalogr Clin Neurophysiol, 1986. **64**(2): p. 119-22.
187. Dressler, O., et al., *Awareness and the EEG power spectrum: analysis of frequencies.* Br J Anaesth, 2004. **93**(6): p. 806-9.
188. Basar, E. and B. Guntekin, *Review of delta, theta, alpha, beta, and gamma response oscillations in neuropsychiatric disorders.* Suppl Clin Neurophysiol, 2013. **62**: p. 303-41.
189. Jia, X. and A. Kohn, *Gamma rhythms in the brain.* PLoS Biol, 2011. **9**(4): p. e1001045.
190. Roohi-Azizi, M., et al., *Changes of the brain's bioelectrical activity in cognition, consciousness, and some mental disorders.* Med J Islam Repub Iran, 2017. **31**: p. 53.
191. Munia, T.T.K. and S. Aviyente, *Time-Frequency Based Phase-Amplitude Coupling Measure For Neuronal Oscillations.* Sci Rep, 2019. **9**(1): p. 12441.
192. Poza, J., et al., *Phase-amplitude coupling analysis of spontaneous EEG activity in Alzheimer's disease.* Annu Int Conf IEEE Eng Med Biol Soc, 2017. **2017**: p. 2259-2262.

iii. PUBLICATIONS

- **Sterpka, A**., Yang, J., Strobel, M., Zhou, Y., Pauplis, C., Chen, X. Diverged morphology changes of astrocytic and neuronal primary cilia under reactive insults. Mol Brain, 2020. 13(1): p. 28.

- Zhou, Y., Qiu, L., **Sterpka, A**., Wang, H., Chu, F., Chen, X. Comparative Phosphoproteomic Profiling of Type III Adenylyl Cyclase Knockout and Control, Male, and Female Mice. Frontiers in Cellular Neuroscience, 2019. 13(34).

- Kristen Fuda, & Mary Katherine Lockwood. Contributors: **Ashley Sterpka** & Michael Goulet. Laboratory Manual for Human Anatomy and Physiology II. University of New Hampshire: Fountainhead Press. 2020.ISBN 978-1-64485-027-5.

- **Sterpka, A**. and X. Chen, Neuronal and astrocytic primary cilia in the mature brain. Pharmacol Res, 2018. 137: p. 114-121.

The following is sourced from Pharmacological Research, Sterpka and Chen 2018 [7]

HHS Public Access

Author manuscript

Pharmacol Res. Author manuscript; available in PMC 2019 November 01.

Published in final edited form as:

Pharmacol Res. 2018 November ; 137: 114–121. doi:10.1016/j.phrs.2018.10.002.

Neuronal and Astrocytic Primary Cilia in the Mature Brain

Ashley Sterpka and **Xuanmao Chen***

Department of Molecular, Cellular and Biomedical Sciences, University of New Hampshire, Durham, NH 03824

Abstract

Primary cilia are tiny microtubule-based signaling devices that regulate a variety of physiological functions, including metabolism and cell division. Defects in primary cilia lead to a myriad of diseases in humans such as obesity and cancers. In the mature brain, both neurons and astrocytes contain a single primary cilium. Although neuronal primary cilia are not directly involved in synaptic communication, their pathophysiological impacts on obesity and mental disorders are well recognized. In contrast, research on astrocytic primary cilia lags far behind. Currently, little is known about their functions and molecular pathways in the mature brain. Unlike neurons, postnatal astrocytes retain the capacity of cell division and can become reactive and proliferate in response to various brain insults such as epilepsy, ischemia, traumatic brain injury, and neurodegenerative β-amyloid plaques. Since primary cilia derive from the mother centrioles, astrocyte proliferation must occur in coordination with the dismantling and ciliogenesis of astrocyte cilia. In this regard, the functions, signal pathways, and structural dynamics of neuronal and astrocytic primary cilia are fundamentally different. Here we discuss and compare the current understanding of neuronal and astrocytic primary cilia.

Graphical Abstract

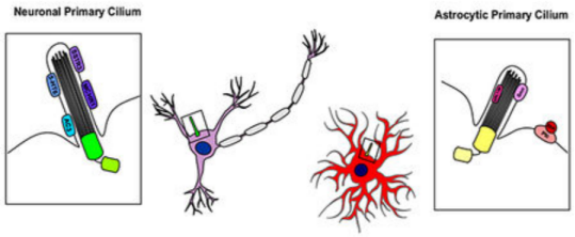

Keywords

Primary Cilia; Astrocytes; Type 3 Adenylyl Cyclase (AC3); ARL13B; Sonic Hedgehog

*Correspondence should be addressed to: 46 College Road, Rudman hall, Department of Molecular, Cellular, and Biomedical Sciences, College of Life Sciences and Agriculture, University of New Hampshire, NH 03824; Xuanmao.Chen@unh.edu; Phone: 603 862 4542; Fax: 603 862 4013.

Declarations of Interest: None

Introduction

The primary cilium is a centriole-derived, membrane-ensheathed process present in most mammalian cells [1]. It relies on a highly conserved intraflagellar transport (IFT) system for trafficking select protein cargo into and out of the ciliary compartment [2]. There is a diffusion barrier at the base of the primary cilium, which restricts the free diffusion of unselected molecules into the compartment [3]. Hence, the microenvironment in the primary cilium is insulated from the main cytosolic compartment. Moreover, the volume of the primary cilium is very tiny compared to other cellular compartments, but it has a high ratio of plasma membrane to cytosol and can enrich a high density of membrane receptors. Second messengers such as cAMP can easily reach high concentrations in the narrow ciliary compartment. Given this, cilia are exquisitely sensitive to extracellular signals, including nutrients, neuropeptides, morphogens, and hormones [1, 4, 5]. As such, primary cilia are considered cellular “antennae” to detect extracellular signals [1, 4, 5].

The primary cilium emanates from the basal body residing underneath the plasma membrane, which is a special form of the mother centriole [6]. It maintains stability during interphase of the cell cycle, but dismantling the primary cilium is a prerequisite for the progression of mitosis [7]. Accordingly, primary cilia regulate cell division [7], development [4, 8, 9], and tissue regeneration [10]. Vigorous research in the past two decades has collected a great deal of evidence supporting the significance of primary cilia in both physiology and pathology [11, 12]. It is well recognized that malfunction of primary cilia causes numerous disorders, including polycystic kidney disease, obesity, cognitive impairment, developmental disorders [8], and certain cancers [11, 13, 14], which are collectively termed “ciliopathies” [11].

The brain is mainly comprised of neurons and glial cells. Glial cells in the brain include astrocytes, ependymal cells, microglia, and oligodendrocytes. It is known that neurons and astrocytes possess a single, non-motile primary cilium [8]. Ependymal cells, which line the ventricles of the brain and aid in the circulation of cerebrospinal fluid, have multiple motile cilia. Microglia, the resident macrophages in the central nervous system (CNS), do not display primary cilia [15] (see Figure 1). Primary cilia are observable in young oligodendrocyte precursor cells, but are lost as these cells differentiate [16]. Putatively, mature oligodendrocytes may also have primary cilia [17], but no direct evidence has been shown thus far. Additionally, adult neural stem cells (or astrocyte-like type 1 radial glial cells) in the subgranular zone (SGZ) in the dentate gyrus of the hippocampus and likely the subventricular zone (SVZ) of the lateral ventricles [18] possess primary cilia, which are essential for Sonic hedgehog (Shh) signaling and adult neurogenesis [19–21].

Astrocytes comprise the largest number of glia in the mature brain and maintain a great level of heterogeneity in function and morphology [22, 23]. Astrocytes perform a wide variety of functions, including regulation of synaptic function by recycling neurotransmitters [22], supplying neurons with neurotransmitter precursors [23], and regulating synaptic pruning by marking neuronal junctions for degradation via complement proteins [24]. In the event of neuropathologies, astrocytes are altered phenotypically to become reactive. When this occurs, these cells act to repair the blood brain barrier [25], support neuronal survival, and

restore homeostasis within the brain via creation of a glial scar followed by metabolite and chemical control [26].

While astrocytes and neurons derive from the same origin (neuroepithelial cells and radial glial cells) in the early stage of neurodevelopment [27], research on astrocytic cilia in the mature brain lags far behind that of neuronal cilia. Neuronal primary cilia in the adult brain have been the most extensively studied compared to other cilia [4, 8, 17, 28, 29]. They have been found to regulate metabolism [13, 30, 31], mood state [32], and cognitive function [33, 34]. To date, very little, except for a role in adult neurogenesis, is known regarding the function and molecular pathways of astrocytic primary cilia in the mature brain. Nevertheless, as postnatal astrocytes maintain the ability to proliferate throughout life [25, 26, 35–37], astrocyte cell division should occur in coordination with the resorption and ciliogenesis of primary cilia. Herein represents a fundamental difference between neuronal and astrocyte cilia. Neuronal primary cilia in the brain have been well described in several elegant review articles [4, 17, 28, 38]. Here in this review, we aim to describe some fundamentals related to primary cilia and compare neuronal and astrocytic primary cilia in the adult brain (Summarized in Table 1).

Cilia Markers and Transgenic Mouse Strains to Label Primary Cilia with Fluorescent Proteins or Calcium Sensors

The necessity for visualizing primary cilia and detecting ciliary molecules has grown as studies on primary cilia have rapidly expanded. To date, primary cilia in the brain can be visualized in immunofluorescence staining using commercial antibodies to target type 3 adenylyl cyclase (AC3), type 3 somatostatin receptor (SSTR3), ADP-ribosylation factor-like 13B (ARL13B) [15], type 6 serotonin receptor (5-HT6) [39], and melanin-concentrating hormone receptor 1 (MCHR1) [40]. However, it has been recognized that these cilia markers are not ubiquitously expressed, and their expression levels can vary. For example, 5-HT6 has a focal expression and is enriched in neuronal primary cilia in the striatum region [39]. MCHR1 expression is detected in neuronal primary cilia in the hippocampus, amygdala, piriform cortex, and hypothalamus [40, 41]. In a comparison of primary cilia markers, Sipos et al. showed regional differences in expression of AC3, ARL13B, and SSTR3 [15]. A high level of AC3 expression in the primary cilia of mature neurons was detected. In contrast, AC3 is only faintly expressed in a small number of glial fibrillary acidic protein (GFAP)-positive astrocytes and absent in adenomatous polyposis coli (APC)-positive oligodendrocytes and ionizing calcium-binding adaptor molecule 1 (IBA1)-labeled microglia [15] (confirmed by our observations, see Figure 1). SSTR3 was found to be expressed in mature neuronal primary cilia [15]. Several studies have demonstrated that SSTR3 is co-expressed with AC3 in neuronal primary cilia in the hippocampus [34] and the olfactory bulb [42]. It is noteworthy that AC3 is also distributed to other tissues and is highly expressed in olfactory sensory cilia, primary cilia of kidney epithelial cells [43], and primary cilia of brown and white adipose tissue [44]. Generally, AC3 is a commonly accepted neuronal primary cilia marker protein and ARL13B antibody is commonly used to label astrocytic primary cilia (Figure 1), but neither is universally localized in primary cilia. A study focusing on visualization of astrocytic primary cilia in mice showed differential

expression based on age [45]. This study detected a high expression of AC3 in the primary cilia of both astrocytes and neurons ten days after birth, but by postnatal day 56, neuronal primary cilia highly expressed AC3 and astrocytic primary cilia showed high levels of ARL13B expression [45].

Utilizing cilia-specific proteins, strains of mice with fluorescent proteins restricted to primary cilia have been generated. These strains have proven effective in visualizing cilia or detecting calcium levels. For example, O'Connor et al. generated an inducible cilia-GFP model of mice to enable direct visualization primary cilia [46]. This strain linked GFP with the ciliary protein SSTR3. In observations of deeply anesthetized adult mice, primary cilia were found to be expressed in numerous cells within the mature brain, including neurons and in choroid plexus epithelial cells [46]. In 2016, Delling et al. developed an imaging tool to study calcium signaling in response to mechanical force. They engineered a strain of mouse with ARL13B marked with mCherry and genetically encoded calcium indicator 1.2 localized in primary cilia. This tool allows for detection of calcium influx into ciliary compartment responding to mechanical stimuli. They discovered that calcium signaling is not responsible for the mechano-sensation of renal cilia in both embryonic and adult murine cilia models [47]. Additionally, in 2015, Bangs et al. conducted a study using a strain of mice that had both primary cilia and centrosomes labeled with mCherry and GFP, respectively. This model, *ARL13B-mCerry;Centrin2-GFP*, allowed for visualization of primary cilia and centrioles throughout embryonic development. Using that strain, primary cilia were found to arise from epiblast cells at E6, and cells arising from the visceral endoderm and trophoectoderm maintained centrosomes, but lack cilia through development [48]. The *ARL13B-pmCerry;Centrin2-GFP* strain marks primary cilia of many epiblast-derived cells including neuroepithelial cells in the neural tube very clearly [48]. However, we observed that although ARL13-mCherry also labels astrocytes very well, but not well on neurons, in the mature brain. Thus, ARL13B is not a ubiquitous ciliary maker in mature. Presently, research tools to visualize primary cilia or detect ciliary molecules are far from adequate. Consequently, there remains the need to develop novel tools (or mouse strains) to detect key messenger molecules in cilia such as cAMP, as the explorations of primary cilia grow.

Ciliogenesis

Ciliogenesis is the process by which the microtubule-based cilium arises from the basal body within the cell [49]. Ciliogenesis is generally inhibited in actively dividing cells [50]. Initiation of ciliogenesis requires that a cell exit its mitotic cell cycle to allow the centriole to dock at the plasma membrane by fusing with a ciliary vesicle [49]. At this point, IFT begins to transport protein complexes in anterograde and retrograde directions to promote the growth of the cilium [51]. Due to the terminally differentiating nature of neurons and the consequential loss of mitotic ability [52], there is little need for neuronal primary cilia to destabilize and retract into the soma. This results in the absence of *de novo* ciliogenesis in mature neurons. Thus, studies exploring neuronal ciliogenesis are primarily limited to the early embryonic development stage or in cultured cells.

The ciliogenesis of astrocytes occurs in the embryonic development stage as well as in the mature brain. Human astrocytes have five stages of ciliogenesis [53, 54]. The first stage can be identified by the localization and fusion of vesicles with the distal end of the basal body. During the second stage, the non-motile 9+0 axoneme begins to arise from the basal body. This structure continues to grow in the third stage and fuses with the plasma membrane. At this point, a ciliary bud can be detected on the surface of the cell. The fourth stage consists of continued growth and extension of the cilium past the surface of the cell due to IFT. In the fifth and final stage of astrocyte ciliogenesis, a fully formed primary cilium can be observed on the surface of the cell [54, 55]. Once fully mature, astrocyte-like neural precursors display a primary cilium with a length significantly shorter than that of a neuronal primary cilium [56] (see table 1). Moser et al. also explored the potential effects of disruption of the mammalian processing body, namely the GW/P body, on ciliogenesis of human astrocytes [57]. Greater than half of transcriptional silencing of mRNA occurs within GW/P bodies. The early stages of ciliogenesis were observed in astrocytes studied in this experiment, but GW/P small interfering RNA-transfected cells failed to display a matured cilium that extended properly out of the soma. This study demonstrates that inhibition of GW/P body components and the RNAi microprocessor disrupts ciliogenesis of astrocytes [57]. To date, there is limited understanding of the structural dynamics of astrocyte cilia. We postulate that elucidating the molecular mechanisms of ciliogenesis will help unravel the contributions of astrocyte cilia to astrocyte reactivity and pathology in the mature brain.

Primary Cilia are Required for Sonic Hedgehog Signal Transduction in Vertebrate Cells

Shh signal transduction is essential for proper embryonic development and morphogenesis of vertebrates. The components within this pathway are required for patterning and organization of the notochord, floorplate, and cells within the zone of polarizing activity [58]. This patterning is needed for embryonic organization of tissue that is required not simply for symmetry, but also appropriate organogenesis. Hence, the Shh pathway is necessary for proper CNS development. Conceivably, malfunction of Shh pathway is also implicated in certain forms of cancer [59]. Shh mediates cell signaling and also regulates cell survival. The best-known components in the Shh pathway are the Shh ligand, Smoothened (Smo), and Patched1 (Ptch1) [59]. Binding of Shh to Ptch1 leads to translocation of Smo from the plasma membrane into primary ciliary compartment and activation of the Shh pathway, promoting the Gli transcription factors to translocate to the nucleus, where they can stimulate cell proliferation and encourage cell survival [60].

In vertebrate cells, primary cilia constitute key modulators for Shh transduction, which is essential for embryonic development of neural cells [61]. In the developing notochord, neural progenitor cells are guided in proliferation and differentiation by the Shh signaling [61]. Many key components of the Shh pathway localize in the primary cilium and can shift regionally upon receipt of the Shh ligand [62]. Patched1 localizes in the primary cilium in the absence of Shh and regulates the activity of Smoothened [63]. *Suppressor of Fused*, a downstream regulator of this pathway, localizes in the tip of the primary cilia of cells in the neural tube [61]. The G-protein-coupled receptor GPR161 is expressed on the primary

cilium in the neural tube and can suppress Shh signaling and inhibit the growth of medulloblastomas [64].

Extensive evidence has underscored the importance of primary cilia in Shh signaling. Transgenic mice lacking cilia in astrocyte-like neural precursors have abnormal development and disruption in Shh signaling [56]. Disturbance of ARL13B in primary cilia can result in lessened Shh signaling in mouse medulloblastoma cultures [65]. Ablation of ciliary genes or Smoothened results in interrupted development of radial astrocytes (the postnatal progenitors in the dentate gyrus), while constitutive expression of these genes results in an enlargement of the dentate gyrus [66]. SAG, a Shh agonist, can act in a protective fashion via ciliary signaling for astrocytes under starving conditions [67]. However, most research focuses on the aspect of neurodevelopment or neurogenesis (and adult neurogenesis). To date, there are few reports directly addressing the Shh pathway in neuronal and astrocytic primary cilia in the mature brain. This is possibly because the Shh pathway in neuronal primary cilia is more prominent in neurodevelopment, not so much in adulthood, and astrocyte cilia in the mature brain is generally under-studied.

Potential Function of Astrocytic Primary Cilia in the Mature Brain

Many studies have emphasized the importance of primary cilia in cell division [4, 8, 9]. Evidence is emerging to associate astrocyte cilia with brain pathophysiology, particularly brain tumorigenesis. As primary cilia must first destabilize and retract into the cell to allow for the movement of the centriole and cell division, inability to stabilize the primary cilium can be related with abnormal proliferation of cells. Indeed, dysfunction of the primary cilium is recognized in the development of some types of tumors [12, 64, 68]. For example, glioblastomas, brain tumors arising from abnormal proliferation of astrocytes, are highly related to loss of or malformed primary cilia [68]. In an experiment characterizing the tissue of seven human glioblastoma samples from mature brains [53], defects in the early stages of ciliogenesis of astrocytes have been identified. These abnormalities included absent vesicle pairs, non-mature axonemes, and other morphological differences that impeded ciliary maturation and normal function. Lisophosphatidic acid receptor 1 (LPAR1), a G-protein coupled receptor, localizes on the primary cilia of astrocytes, but when the primary cilium is absent, LPAR1 transitions into the plasma membrane. This regionalization is accompanied by an increase of association with $G\alpha_{12}$ and Gαq [68], which have been reported to be associated with cancer proliferation [69]. Consequently, glioblastoma proliferation is enhanced [68].

Remarkably, adult neurogenesis is well recognized as occurring in the mature brain [18]. Generation of new neurons arises from adult neural stem cells in the subventricular zone and dentate gyrus, rather than from neurons [18]. Adult neural stem cells exhibit glial nature [27] and astrocyte-like adult neural stem cells are maintained in the subgranular layer (SGL) of the dentate gyrus (DG) and in the subventricular zone (SGZ) in the mammalian brain, and they give rise to new neurons in the adult mammalian brain throughout life [18, 70]. The primary cilium and Shh signaling of adult neural stem cells were found to be required for adult neurogenesis and regulate the proliferation of progenitors in the adult hippocampus, implicating in learning and memory [19]. Moreover, the dendritic refinement and synaptic

integration of adult-born neurons in the dentate gyrus's subgranular zone was reported to be modulated by primary cilia [71].

In contrast to neurons, which terminally differentiate and lose proliferative capacity upon maturation, astrocytes throughout the brain maintain the capacity of cell division following differentiation and new astrocytes are continuously generated during postnatal development. Astrocytes have the ability to become reactive and a proportion of reactive astrocytes proliferate in response to various neuropathological conditions such as ischemia, traumatic injury, and epilepsy, as well as neurodegenerative amyloid plaques [25, 35, 72, 73]. During the process of astrocyte proliferation, astrocyte primary cilia need to be resorbed to liberate the centriole and allow the centrosomes to form the mitotic spindle. Thus, astrocyte cilia are conceivably subjected to a dynamic change in conjunction with astrocyte proliferation. However, to date, how astrocytic primary cilia modulate astrocyte reactivity *in vivo* and how astrocytic primary cilia dynamically change their structure in accordance with astrocyte proliferation remain to be elusive. We postulate that investigation into molecular fundamentals of astrocyte cilia in the context of reactive astrogliosis will advance our understanding of how the "antenna" of astrocytes senses pathological milieu and how astrocyte cilia regulate the initiation and termination of astrocytes.

ARL13B, a Ciliary Protein Essential for Cilia Structure, is Implicated in Joubert Syndrome and Developmental Abnormalities

ADP-ribosylation factor-like 13B (ARL13B) is a member of the monomeric small GTPase superfamily [74, 75] and selectively expressed in many primary cilia including astrocytic primary cilia [45]. ARL13B is required for ciliogenesis in certain organs [76]. Studies have shown that ARL13B modulates ciliary protein trafficking and cilia length [62, 77], and supports connectivity between neurons [78]. ARL13B is required for radial glial polarity, disruption of which causes abnormal formation of the cerebral cortex [79]. Notably, ARL13B also regulates ciliary targeting of inositol polyphosphate-5-phosphatase E (INPP5E) [80]. INPP5E is a ciliary protein which prevents actin polymerization in primary cilia [81]. Prior to ciliary destabilization, INPP5E is depleted in cilia, allowing for the re-localization of phosphatidylinositol 4,5-bisphosphate into the primary cilium, which triggers actin polymerization and cilia decapitation, and consequently drives the cell cycle [81].

Joubert syndrome is an autosomal recessive ciliopathy featured by the "molar tooth sign" [82] and characterized by dysfunction in different viscera, eyes, digits, and the brain [74, 83]. ARL13B mutations cause Joubert syndrome, which was first identified in two families [74, 84]. Joubert syndrome patients demonstrate cerebral disorder, mental retardation and developmental delay as well as other variable common-shared ciliopathy manifestations such as cystic kidney, blindness, and polydactyly. Many mutations in ARL13B have been identified in Joubert syndrome patients, all having impeded neural development to some degree. A homozygous missense variant c.[223G>A] (p.(Gly75Arg) identified in the ARL13B gene cause intellectual disability, ataxia, ocular defects, and epilepsy in Jourbert syndrome patients [85]. Interestingly, ARL13B-c.[223G>A] (p.(Gly75Arg) displayed a marked loss of ARL13B guanine nucleotide-exchange factor activity, with retention of its

GTPase activities [85]. A crystal structure of *Chlamydomonas rheinhardtii* ARL13B shows that R79Q as well as R200C, two missense ARL13B mutations identified in Joubert syndrome patients, are involved in stabilizing important intramolecular interactions [86].

ARL13B also plays a critical role in supporting the activity of Shh signaling and acts to regulate the trafficking of its signaling components into the primary cilium [87]. It can induce cell proliferation and survival [87]. Given the localization of Shh components to primary cilia [16, 62], disruption of ARL13B results in abrogated Shh signaling [62]. Consequently, ablation of ARL13B leads to medulloblastoma formation, due to the correlated deletion of cilia and Shh components [65].

AC3, a Key Enzyme Mediating the cAMP Signaling in Neuronal Cilia, is Associated with Obesity and Psychiatric Diseases

Neuronal primary cilia are commonly fortified with G protein-coupled receptors (GPCRs) [40] including Smoothened, SSTR3, 5-HT6, MCHR1, and many others [88]. Some types of GPCRs, such as Smoothened, do not continuously reside in primary cilia and can transition into and out of the cilium [88]. Interestingly, at this time all ciliary GPCRs are found to be either Gαs- or Gαi-protein coupled receptors, which depend on adenylyl cyclases (ACs) to generate cAMP and transduce a signal into the cell. AC3 is widely recognized as a key enzyme mediating the cAMP signaling in neuronal cilia [89]. AC3 was first established as an obligate protein in olfactory cilia mediating olfactory signal transduction in the main olfactory epithelium [90–92]. In 2007, Bishop et al. reported that AC3 predominantly localizes to neuronal primary cilia throughout the mature mouse brain [93], expanding the AC3's fame originally as the olfactory adenylyl cyclase to a well-known neuronal cilia marker in the CNS.

The most prominent function of AC3 in the CNS is to regulate metabolism [94]. Many lines of evidence support the pathological role of AC3 in obesity. First, numerous human genetic analyses have clearly defined *ADCY3* as a gene associated with obesity [95–101]. Second, obesity is also one of the most common symptoms for ciliopathies including Bardet-Biedl Syndrome [9, 102], and Joubert Syndrome [83]. Third, both conventional and tamoxifen-induced conditional AC3 KO mice exhibit adult-onset obesity [44, 103]. Conversely, a gain-of-function mutation of AC3 in mice can protect the animals from diet-induced obesity [104]. Hence, AC3 plays a critical role in regulating energy balance, and defects in the ciliary cAMP pathway lead to obesity [89, 94]. This is in line with the evidence demonstrating that neuronal primary cilia play a critical role in regulating energy balance. Specifically, ablations of many ciliary proteins including KIF3a [105], Bbip10 [106], IFT88 [107], Tubby [108], BBS1, and BBS4 [107, 109] all lead to obesity in mouse models [89].

However, it is not well understood how cAMP in neuronal primary cilia regulates energy balance. It has been postulated that AC3 functionally couples to melanocortin 4 receptor (MC4R) in the hypothalamus [89, 103], because activation of adenylyl cyclase by alpha-melanocyte stimulating hormone (α-MSH) downstream in the leptin pathway is required for the anorectic activity of leptin[110, 111]. Siljee at al. have recently shown that MC4R co-localizes with *ADCY3* at the primary cilia of a subset of neurons of the paraventricular

nucleus (PVN) of the hypothalamus [31]. They also discovered that obesity-associated MC4R mutations impair ciliary localization and that suppression of cAMP production using GPR88, a constitutively active version of the cilia-specific Gαi-protein-coupled receptor [112], at the primary cilia in these neurons increases body weight. The findings of Siljee et al. suggest that MC4R may couple to AC3 and positively regulate cAMP generation in neuronal primary cilia in a subset of neurons in the PVN, and impaired cAMP signaling in the primary cilia of MC4R-positive neurons lead to obesity [31]. However, further research is warranted to clearly address how leptin, α-MSH, MC4R and ciliary cAMP signaling in different sublocations of the hypothalamus hook up to regulate feeding and energy balance.

Another pathological role of AC3 relates to mental disorders. A genome-wide association study based on over five thousand patients with major depressive disorder (MDD) and healthy subjects identified AC3 (*ADCY3)* as a top-ranked gene for MDD [113]. In animal model, we discovered that constitutive AC3 knockout (KO) mice exhibit strong depression-like phenotypes in several behavioral assays [32]. Disturbances of sleep including alterations in sleep architecture and increased REM sleep are one of the core symptoms associated with MDD [114]. Our sleep analysis based on electroencephalogram-electromyogram showed that AC3 KO mice have altered sleep patterns characterized by an increased percentage of rapid eye movement sleep [32]. Moreover, MDD also is associated with neuronal atrophy [115]. We further found that basal synaptic activity at CA3-CA1 synapses was significantly lower in AC3 KO mice, and they also exhibited attenuated long-term potentiation as well as deficits in spatial navigation [32]. Conditional knockout mice with AC3 ablated in the mature brain also exhibit depression-like phenotypes [32]. In addition to MDD, human genetic studies have also associated AC3 with autism [116, 117] and intellectual disability [118], Although the underlying molecular mechanisms remain to be elucidated. In summary, AC3 in the mature brain mediates olfactory signal transduction, regulates energy balance and mood state, and contributes to psychiatric diseases.

Conclusion

Neurons are terminally differentiated excitable cells that lose mitotic ability in maturity [52]. Neuronal primary cilia are relatively stable and apparently lack de novo ciliogenesis. Moreover, no synaptic structures, ionotropic glutamate receptors, or $GABA_A$ receptors have been identified in neuronal primary cilia thus far. But many types of GPCRs have been found in neuronal primary cilia [88] (Table 1). Therefore, neuronal primary cilia mostly depend on these metabotropic receptors and downstream effector proteins to send a signal to regulate neuronal activity [89]. Hence, AC3 represents a key enzyme to mediate the cAMP signaling in neuronal primary cilia in the mature brain and regulate energy balance, mood state, and probably cognitive function.

In contrast, astrocytes are non-excitable cells and do not electrically wire to one another via chemical synapses. They are not terminally differentiated cells and maintain proliferative ability throughout life (Table 1). Presently, little is known about the function, signaling pathways, and structural dynamics of astrocytic primary cilia in the mature brain, although astrocytes fulfill a wide range of functions including providing trophic support, maintaining homeostasis, and protecting neurons from acute insults or brain injury [36]. Since astrocytes

can proliferate under certain pathological conditions [26], astrocytic primary cilia are not static but subject to dynamic changes. Hence, it is not surprising that ARL13B, a protein regulating cilia protein trafficking, Shh pathway and cell division, prevails over AC3 in astrocytic cilia as a protein marker.

In summary, the function, molecular markers, signaling pathways, and structural dynamics of neuronal primary cilia and astrocytic cilia are fundamentally distinct (Table 1). Conceivably, ciliary GPCR- and AC3-mediated cAMP signaling in neurons provide excellent targets to design therapeutics to combat obesity, depression and cognitive disorders. In the long term, research on astrocytic primary cilia will provide useful clues to intervene in astrocyte-proliferation and reactive astrogliosis to combat various neuropathologies such as ischemia and brain injury.

Acknowledgements:

We thank the members of the Chen Laboratory for critical review of the manuscript. This work is supported by National Institutes of Health Grants MH105746, AG054729 and GM113131 to X.C.; a Cole Neuroscience and Behavior Faculty Research Award to X.C.; and UNH Summer TA Research Fellowship (STAF) to A.S.

References:

1. Singla V, and Reiter JF (2006). The primary cilium as the cell's antenna: signaling at a sensory organelle. Science 313, 629–633. [PubMed: 16888132]
2. Rosenbaum JL, and Witman GB (2002). Intraflagellar transport. Nat Rev Mol Cell Biol 3, 813–825. [PubMed: 12415299]
3. Endicott SJ, and Brueckner M (2018). NUP98 Sets the Size-Exclusion Diffusion Limit through the Ciliary Base. Curr Biol.
4. Lee JH, and Gleeson JG (2010). The role of primary cilia in neuronal function. Neurobiol Dis 38, 167–172. [PubMed: 20097287]
5. Goetz SC, and Anderson KV (2010). The primary cilium: a signalling centre during vertebrate development. Nat Rev Genet 11, 331–344. [PubMed: 20395968]
6. Nigg EA, and Stearns T (2011). The centrosome cycle: Centriole biogenesis, duplication and inherent asymmetries. Nat Cell Biol 13, 1154–1160. [PubMed: 21968988]
7. Pan J, and Snell W (2007). The primary cilium: keeper of the key to cell division. Cell 129, 1255–1257. [PubMed: 17604715]
8. Guemez-Gamboa A, Coufal NG, and Gleeson JG (2014). Primary cilia in the developing and mature brain. Neuron 82, 511–521. [PubMed: 24811376]
9. Valente EM, Rosti RO, Gibbs E, and Gleeson JG (2014). Primary cilia in neurodevelopmental disorders. Nat Rev Neurol 10, 27–36. [PubMed: 24296655]
10. Jackson PK (2012). TTBK2 kinase: linking primary cilia and cerebellar ataxias. Cell 151, 697–699. [PubMed: 23141531]
11. Braun DA, and Hildebrandt F (2017). Ciliopathies. Cold Spring Harb Perspect Biol 9.
12. Youn YH, and Han YG (2018). Primary Cilia in Brain Development and Diseases. Am J Pathol 188, 11–22. [PubMed: 29030052]
13. Green JA, and Mykytyn K (2010). Neuronal ciliary signaling in homeostasis and disease. Cell Mol Life Sci 67, 3287–3297. [PubMed: 20544253]
14. Marley A, and von Zastrow M (2012). A simple cell-based assay reveals that diverse neuropsychiatric risk genes converge on primary cilia. PLoS One 7, e46647. [PubMed: 23056384]
15. Sipos E, Komoly S, and Acs P (2018). Quantitative Comparison of Primary Cilia Marker Expression and Length in the Mouse Brain. J Mol Neurosci.

16. Falcon-Urrutia P, Carrasco CM, Lois P, Palma V, and Roth AD (2015). Shh Signaling through the Primary Cilium Modulates Rat Oligodendrocyte Differentiation. PLoS One 10, e0133567. [PubMed: 26218245]
17. Louvi A, and Grove EA (2011). Cilia in the CNS: the quiet organelle claims center stage. Neuron 69, 1046–1060. [PubMed: 21435552]
18. Ming GL, and Song H (2011). Adult neurogenesis in the mammalian brain: significant answers and significant questions. Neuron 70, 687–702. [PubMed: 21609825]
19. Amador-Arjona A, Elliott J, Miller A, Ginbey A, Pazour GJ, Enikolopov G, Roberts AJ, and Terskikh AV (2011). Primary cilia regulate proliferation of amplifying progenitors in adult hippocampus: implications for learning and memory. J Neurosci 31, 9933–9944. [PubMed: 21734285]
20. Han YG, Spassky N, Romaguera-Ros M, Garcia-Verdugo JM, Aguilar A, Schneider-Maunoury S, and Alvarez-Buylla A (2008). Hedgehog signaling and primary cilia are required for the formation of adult neural stem cells. Nat Neurosci 11, 277–284. [PubMed: 18297065]
21. Tong CK, Han YG, Shah JK, Obernier K, Guinto CD, and Alvarez-Buylla A (2014). Primary cilia are required in a unique subpopulation of neural progenitors. Proc Natl Acad Sci U S A 111, 12438–12443. [PubMed: 25114218]
22. Zuchero JB, and Barres BA (2015). Glia in mammalian development and disease. Development 142, 3805–3809. [PubMed: 26577203]
23. Verkhratsky A, and Nedergaard M (2018). Physiology of Astroglia. Physiol Rev 98, 239–389. [PubMed: 29351512]
24. Stephan AH, Barres BA, and Stevens B (2012). The complement system: an unexpected role in synaptic pruning during development and disease. Annu Rev Neurosci 35, 369–389. [PubMed: 22715882]
25. Liddelow SA, and Barres BA (2017). Reactive Astrocytes: Production, Function, and Therapeutic Potential. Immunity 46, 957–967. [PubMed: 28636962]
26. Sofroniew MV, and Vinters HV (2010). Astrocytes: biology and pathology. Acta Neuropathol 119, 7–35. [PubMed: 20012068]
27. Kriegstein A, and Alvarez-Buylla A (2009). The glial nature of embryonic and adult neural stem cells. Annu Rev Neurosci 32, 149–184. [PubMed: 19555289]
28. Lepanto P, Badano JL, and Zolessi FR (2016). Neuron's little helper: The role of primary cilia in neurogenesis. Neurogenesis (Austin) 3, e1253363. [PubMed: 28090545]
29. Lee JE, and Gleeson JG (2011). Cilia in the nervous system: linking cilia function and neurodevelopmental disorders. Curr Opin Neurol 24, 98–105. [PubMed: 21386674]
30. Song DK, Choi JH, and Kim MS (2018). Primary Cilia as a Signaling Platform for Control of Energy Metabolism. Diabetes Metab J 42, 117–127. [PubMed: 29676541]
31. Siljee JE, Wang Y, Bernard AA, Ersoy BA, Zhang S, Marley A, Von Zastrow M, Reiter JF, and Vaisse C (2018). Subcellular localization of MC4R with ADCY3 at neuronal primary cilia underlies a common pathway for genetic predisposition to obesity. Nat Genet 50, 180–185. [PubMed: 29311635]
32. Chen X, Luo J, Leng Y, Yang Y, Zweifel LS, Palmiter RD, and Storm DR (2016). Ablation of Type III Adenylyl Cyclase in Mice Causes Reduced Neuronal Activity, Altered Sleep Pattern, and Depression-like Phenotypes. Biol Psychiatry 80, 836–848. [PubMed: 26868444]
33. Berbari NF, Malarkey EB, Yazdi SM, McNair AD, Kippe JM, Croyle MJ, Kraft TW, and Yoder BK (2014). Hippocampal and cortical primary cilia are required for aversive memory in mice. PLoS One 9, e106576. [PubMed: 25184295]
34. Wang Z, Phan T, and Storm DR (2011). The type 3 adenylyl cyclase is required for novel object learning and extinction of contextual memory: role of cAMP signaling in primary cilia. J Neurosci 31, 5557–5561. [PubMed: 21490195]
35. Liddelow S, and Barres B (2015). SnapShot: Astrocytes in Health and Disease. Cell 162, 1170–1170 e1171. [PubMed: 26317476]
36. Molofsky AV, Krencik R, Ullian EM, Tsai HH, Deneen B, Richardson WD, Barres BA, and Rowitch DH (2012). Astrocytes and disease: a neurodevelopmental perspective. Genes Dev 26, 891–907. [PubMed: 22549954]

37. Pekny M, and Pekna M (2016). Reactive gliosis in the pathogenesis of CNS diseases. Biochim Biophys Acta 1862, 483–491. [PubMed: 26655603]
38. Sarkisian MR, and Guadiana SM (2015). Influences of primary cilia on cortical morphogenesis and neuronal subtype maturation. Neuroscientist 21, 136–151. [PubMed: 24740576]
39. Brodsky M, Lesiak AJ, Croicu A, Cohenca N, Sullivan JM, and Neumaier JF (2017). 5-HT6 receptor blockade regulates primary cilia morphology in striatal neurons. Brain Res 1660, 10–19. [PubMed: 28087224]
40. Green JA, Gu C, and Mykytyn K (2012). Heteromerization of ciliary G protein-coupled receptors in the mouse brain. PLoS One 7, e46304. [PubMed: 23029470]
41. Sun X, Haley J, Bulgakov OV, Cai X, McGinnis J, and Li T (2012). Tubby is required for trafficking G protein-coupled receptors to neuronal cilia. Cilia 1, 21. [PubMed: 23351594]
42. Luo J, Chen X, Pan YW, Lu S, Xia Z, and Storm DR (2015). The type 3 adenylyl cyclase is required for the survival and maturation of newly generated granule cells in the olfactory bulb. PLoS One 10, e0122057. [PubMed: 25807252]
43. Pluznick JL, Zou DJ, Zhang X, Yan Q, Rodriguez-Gil DJ, Eisner C, Wells E, Greer CA, Wang T, Firestein S, et al. (2009). Functional expression of the olfactory signaling system in the kidney. Proc Natl Acad Sci U S A 106, 2059–2064. [PubMed: 19174512]
44. Wang Z, Li V, Chan GC, Phan T, Nudelman AS, Xia Z, and Storm DR (2009). Adult type 3 adenylyl cyclase-deficient mice are obese. PLoS One 4, e6979. [PubMed: 19750222]
45. Kasahara K, Miyoshi K, Murakami S, Miyazaki I, and Asanuma M (2014). Visualization of astrocytic primary cilia in the mouse brain by immunofluorescent analysis using the cilia marker Arl13b. Acta Med Okayama 68, 317–322. [PubMed: 25519025]
46. O'Connor AK, Malarkey EB, Berbari NF, Croyle MJ, Haycraft CJ, Bell PD, Hohenstein P, Kesterson RA, and Yoder BK (2013). An inducible CiliaGFP mouse model for in vivo visualization and analysis of cilia in live tissue. Cilia 2, 8. [PubMed: 23819925]
47. Delling M, Indzhykulian AA, Liu X, Li Y, Xie T, Corey DP, and Clapham DE (2016). Primary cilia are not calcium-responsive mechanosensors. Nature 531, 656–660. [PubMed: 27007841]
48. Bangs FK, Schrode N, Hadjantonakis AK, and Anderson KV (2015). Lineage specificity of primary cilia in the mouse embryo. Nat Cell Biol 17, 113–122. [PubMed: 25599390]
49. Ishikawa H, and Marshall WF (2011). Ciliogenesis: building the cell's antenna. Nat Rev Mol Cell Biol 12, 222–234. [PubMed: 21427764]
50. Kasahara K, Aoki H, Kiyono T, Wang S, Kagiwada H, Yuge M, Tanaka T, Nishimura Y, Mizoguchi A, Goshima N, et al. (2018). EGF receptor kinase suppresses ciliogenesis through activation of USP8 deubiquitinase. Nat Commun 9, 758. [PubMed: 29472535]
51. Avasthi P, and Marshall WF (2012). Stages of ciliogenesis and regulation of ciliary length. Differentiation 83, S30–42. [PubMed: 22178116]
52. Myster DL, and Duronio RJ (2000). To differentiate or not to differentiate? Curr Biol 10, R302–304. [PubMed: 10801410]
53. Moser JJ, Fritzler MJ, and Rattner JB (2014). Ultrastructural characterization of primary cilia in pathologically characterized human glioblastoma multiforme (GBM) tumors. BMC Clin Pathol 14, 40. [PubMed: 25228849]
54. Moser JJ, Fritzler MJ, and Rattner JB (2009). Primary ciliogenesis defects are associated with human astrocytoma/glioblastoma cells. BMC Cancer 9, 448. [PubMed: 20017937]
55. Ou Y, Ruan Y, Cheng M, Moser JJ, Rattner JB, and van der Hoorn FA (2009). Adenylate cyclase regulates elongation of mammalian primary cilia. Exp Cell Res 315, 2802–2817. [PubMed: 19576885]
56. Breunig JJ, Sarkisian MR, Arellano JI, Morozov YM, Ayoub AE, Sojitra S, Wang B, Flavell RA, Rakic P, and Town T (2008). Primary cilia regulate hippocampal neurogenesis by mediating sonic hedgehog signaling. Proc Natl Acad Sci U S A 105, 13127–13132. [PubMed: 18728187]
57. Moser JJ, Fritzler MJ, and Rattner JB (2011). Repression of GW/P body components and the RNAi microprocessor impacts primary ciliogenesis in human astrocytes. BMC Cell Biol 12, 37. [PubMed: 21880135]
58. Ingham PW, and McMahon AP (2001). Hedgehog signaling in animal development: paradigms and principles. Genes Dev 15, 3059–3087. [PubMed: 11731473]

59. Carballo GB, Honorato JR, de Lopes GPF, and Spohr T (2018). A highlight on Sonic hedgehog pathway. Cell Commun Signal 16, 11. [PubMed: 29558958]
60. Rimkus TK, Carpenter RL, Qasem S, Chan M, and Lo HW (2016). Targeting the Sonic Hedgehog Signaling Pathway: Review of Smoothened and GLI Inhibitors. Cancers (Basel) 8.
61. Zhang Z, Shen L, Law K, Zhang Z, Liu X, Hua H, Li S, Huang H, Yue S, Hui CC, et al. (2017). Suppressor of Fused Chaperones Gli Proteins To Generate Transcriptional Responses to Sonic Hedgehog Signaling. Mol Cell Biol 37.
62. Larkins CE, Aviles GD, East MP, Kahn RA, and Caspary T (2011). Arl13b regulates ciliogenesis and the dynamic localization of Shh signaling proteins. Mol Biol Cell 22, 4694–4703. [PubMed: 21976698]
63. Rohatgi R, Milenkovic L, and Scott MP (2007). Patched1 regulates hedgehog signaling at the primary cilium. Science 317, 372–376. [PubMed: 17641202]
64. Shimada IS, Hwang SH, Somatilaka BN, Wang X, Skowron P, Kim J, Kim M, Shelton JM, Rajaram V, Xuan Z, et al. (2018). Basal Suppression of the Sonic Hedgehog Pathway by the G-Protein-Coupled Receptor Gpr161 Restricts Medulloblastoma Pathogenesis. Cell Rep 22, 1169–1184. [PubMed: 29386106]
65. Bay SN, Long AB, and Caspary T (2018). Disruption of the ciliary GTPase Arl13b suppresses Sonic hedgehog overactivation and inhibits medulloblastoma formation. Proc Natl Acad Sci U S A 115, 1570–1575. [PubMed: 29378965]
66. Han YG, and Alvarez-Buylla A (2010). Role of primary cilia in brain development and cancer. Curr Opin Neurobiol 20, 58–67. [PubMed: 20080044]
67. Yoshimura K, Kawate T, and Takeda S (2011). Signaling through the primary cilium affects glial cell survival under a stressed environment. Glia 59, 333–344. [PubMed: 21125655]
68. Loskutov YV, Griffin CL, Marinak KM, Bobko A, Margaryan NV, Geldenhuys WJ, Sarkaria JN, and Pugacheva EN (2018). LPA signaling is regulated through the primary cilium: a novel target in glioblastoma. Oncogene 37, 1457–1471. [PubMed: 29321663]
69. Park J, Jang JH, Oh S, Kim M, Shin C, Jeong M, Heo K, Park JB, Kim SR, and Oh YS (2018). LPA-induced migration of ovarian cancer cells requires activation of ERM proteins via LPA1 and LPA2. Cell Signal 44, 138–147. [PubMed: 29329782]
70. Seri B, Garcia-Verdugo JM, McEwen BS, and Alvarez-Buylla A (2001). Astrocytes give rise to new neurons in the adult mammalian hippocampus. J Neurosci 21, 7153–7160. [PubMed: 11549726]
71. Kumamoto N, Gu Y, Wang J, Janoschka S, Takemaru K, Levine J, and Ge S (2012). A role for primary cilia in glutamatergic synaptic integration of adult-born neurons. Nat Neurosci 15, 399–405, S391. [PubMed: 22306608]
72. Frost GR, and Li YM (2017). The role of astrocytes in amyloid production and Alzheimer's disease. Open Biol 7.
73. Khakh BS, and Sofroniew MV (2015). Diversity of astrocyte functions and phenotypes in neural circuits. Nat Neurosci 18, 942–952. [PubMed: 26108722]
74. Cantagrel V, Silhavy JL, Bielas SL, Swistun D, Marsh SE, Bertrand JY, Audollent S, Attie-Bitach T, Holden KR, Dobyns WB, et al. (2008). Mutations in the cilia gene ARL13B lead to the classical form of Joubert syndrome. Am J Hum Genet 83, 170–179. [PubMed: 18674751]
75. Wennerberg K, Rossman KL, and Der CJ (2005). The Ras superfamily at a glance. J Cell Sci 118, 843–846. [PubMed: 15731001]
76. Seixas C, Choi SY, Polgar N, Umberger NL, East MP, Zuo X, Moreiras H, Ghossoub R, Benmerah A, Kahn RA, et al. (2016). Arl13b and the exocyst interact synergistically in ciliogenesis. Mol Biol Cell 27, 308–320. [PubMed: 26582389]
77. Mariani LE, Bijlsma MF, Ivanova AI, Suciu SK, Kahn RA, and Caspary T (2016). Arl13b regulates Shh signaling from both inside and outside the cilium. Mol Biol Cell.
78. Higginbotham H, Eom TY, Mariani LE, Bachleda A, Hirt J, Gukassyan V, Cusack CL, Lai C, Caspary T, and Anton ES (2012). Arl13b in primary cilia regulates the migration and placement of interneurons in the developing cerebral cortex. Dev Cell 23, 925–938. [PubMed: 23153492]

79. Higginbotham H, Guo J, Yokota Y, Umberger NL, Su CY, Li J, Verma N, Hirt J, Ghukasyan V, Caspary T, et al. (2013). Arl13b-regulated cilia activities are essential for polarized radial glial scaffold formation. Nat Neurosci 16, 1000–1007. [PubMed: 23817546]
80. Humbert MC, Weihbrecht K, Searby CC, Li Y, Pope RM, Sheffield VC, and Seo S (2012). ARL13B, PDE6D, and CEP164 form a functional network for INPP5E ciliary targeting. Proc Natl Acad Sci U S A 109, 19691–19696. [PubMed: 23150559]
81. Phua SC, Chiba S, Suzuki M, Su E, Roberson EC, Pusapati GV, Setou M, Rohatgi R, Reiter JF, Ikegami K, et al. (2017). Dynamic Remodeling of Membrane Composition Drives Cell Cycle through Primary Cilia Excision. Cell 168, 264–279 e215. [PubMed: 28086093]
82. Doherty D (2009). Joubert syndrome: insights into brain development, cilium biology, and complex disease. Semin Pediatr Neurol 16, 143–154. [PubMed: 19778711]
83. Thomas S, Cantagrel V, Mariani L, Serre V, Lee JE, Elkhartoufi N, de Lonlay P, Desguerre I, Munnich A, Boddaert N, et al. (2015). Identification of a novel ARL13B variant in a Joubert syndrome-affected patient with retinal impairment and obesity. Eur J Hum Genet 23, 621–627. [PubMed: 25138100]
84. Parisi MA (2009). Clinical and molecular features of Joubert syndrome and related disorders. Am J Med Genet C Semin Med Genet 151C, 326–340. [PubMed: 19876931]
85. Rafiullah R, Long AB, Ivanova AA, Ali H, Berkel S, Mustafa G, Paramasivam N, Schlesner M, Wiemann S, Wade RC, et al. (2017). A novel homozygous ARL13B variant in patients with Joubert syndrome impairs its guanine nucleotide-exchange factor activity. Eur J Hum Genet 25, 1324–1334. [PubMed: 29255182]
86. Miertzschke M, Koerner C, Spoerner M, and Wittinghofer A (2014). Structural insights into the small G-protein Arl13B and implications for Joubert syndrome. Biochem J 457, 301–311. [PubMed: 24168557]
87. Shao J, Xu L, Chen L, Lu Q, Xie X, Shi W, Xiong H, Shi C, Huang X, Mei J, et al. (2017). Arl13b Promotes Gastric Tumorigenesis by Regulating Smo Trafficking and Activation of the Hedgehog Signaling Pathway. Cancer Res 77, 4000–4013. [PubMed: 28611043]
88. Schou KB, Pedersen LB, and Christensen ST (2015). Ins and outs of GPCR signaling in primary cilia. EMBO Rep 16, 1099–1113. [PubMed: 26297609]
89. Qiu L, LeBel RP, Storm DR, and Chen X (2016). Type 3 adenylyl cyclase: a key enzyme mediating the cAMP signaling in neuronal cilia. Int J Physiol Pathophysiol Pharmacol 8, 95–108. [PubMed: 27785336]
90. Challis RC, Tian H, Wang J, He J, Jiang J, Chen X, Yin W, Connelly T, Ma L, Yu CR, et al. (2015). An Olfactory Cilia Pattern in the Mammalian Nose Ensures High Sensitivity to Odors. Curr Biol 25, 2503–2512. [PubMed: 26365258]
91. Chen X, Xia Z, and Storm DR (2012). Stimulation of electro-olfactogram responses in the main olfactory epithelia by airflow depends on the type 3 adenylyl cyclase. J Neurosci 32, 15769–15778. [PubMed: 23136416]
92. Wong ST, Trinh K, Hacker B, Chan GC, Lowe G, Gaggar A, Xia Z, Gold GH, and Storm DR (2000). Disruption of the type III adenylyl cyclase gene leads to peripheral and behavioral anosmia in transgenic mice. Neuron 27, 487–497. [PubMed: 11055432]
93. Bishop GA, Berbari NF, Lewis J, and Mykytyn K (2007). Type III adenylyl cyclase localizes to primary cilia throughout the adult mouse brain. J Comp Neurol 505, 562–571. [PubMed: 17924533]
94. Wu L, Shen C, Seed Ahmed M, Ostenson CG, and Gu HF (2016). Adenylate cyclase 3: a new target for anti-obesity drug development. Obes Rev 17, 907–914. [PubMed: 27256589]
95. Nordman S, Abulaiti A, Hilding A, Langberg EC, Humphreys K, Ostenson CG, Efendic S, and Gu HF (2008). Genetic variation of the adenylyl cyclase 3 (AC3) locus and its influence on type 2 diabetes and obesity susceptibility in Swedish men. Int J Obes (Lond) 32, 407–412. [PubMed: 17895882]
96. Wen W, Cho YS, Zheng W, Dorajoo R, Kato N, Qi L, Chen CH, Delahanty RJ, Okada Y, Tabara Y, et al. (2012). Meta-analysis identifies common variants associated with body mass index in east Asians. Nat Genet 44, 307–311. [PubMed: 22344219]

97. Warrington NM, Howe LD, Paternoster L, Kaakinen M, Herrala S, Huikari V, Wu YY, Kemp JP, Timpson NJ, St Pourcain B, et al. (2015). A genome-wide association study of body mass index across early life and childhood. Int J Epidemiol 44, 700–712. [PubMed: 25953783]

98. Felix JF, Bradfield JP, Monnereau C, van der Valk RJ, Stergiakouli E, Chesi A, Gaillard R, Feenstra B, Thiering E, Kreiner-Moller E, et al. (2015). Genome-wide association analysis identifies three new susceptibility loci for childhood body mass index. Hum Mol Genet.

99. Cousminer DL, Berry DJ, Timpson NJ, Ang W, Thiering E, Byrne EM, Taal HR, Huikari V, Bradfield JP, Kerkhof M, et al. (2013). Genome-wide association and longitudinal analyses reveal genetic loci linking pubertal height growth, pubertal timing and childhood adiposity. Hum Mol Genet 22, 2735–2747. [PubMed: 23449627]

100. Stergiakouli E, Gaillard R, Tavare JM, Balthasar N, Loos RJ, Taal HR, Evans DM, Rivadeneira F, St Pourcain B, Uitterlinden AG, et al. (2014). Genome-wide association study of height-adjusted BMI in childhood identifies functional variant in ADCY3. Obesity (Silver Spring) 22, 2252–2259. [PubMed: 25044758]

101. Volkov P, Olsson AH, Gillberg L, Jorgensen SW, Brons C, Eriksson KF, Groop L, Jansson PA, Nilsson E, Ronn T, et al. (2016). A Genome-Wide mQTL Analysis in Human Adipose Tissue Identifies Genetic Variants Associated with DNA Methylation, Gene Expression and Metabolic Traits. PLoS One 11, e0157776. [PubMed: 27322064]

102. Fliegauf M, Benzing T, and Omran H (2007). When cilia go bad: cilia defects and ciliopathies. Nat Rev Mol Cell Biol 8, 880–893. [PubMed: 17955020]

103. Cao H, Chen X, Yang Y, and Storm DR (2016). Disruption of type 3 adenylyl cyclase expression in the hypothalamus leads to obesity. Integr Obes Diabetes 2, 225–228. [PubMed: 27942392]

104. Pitman JL, Wheeler MC, Lloyd DJ, Walker JR, Glynne RJ, and Gekakis N (2014). A gain-of-function mutation in adenylate cyclase 3 protects mice from diet-induced obesity. PLoS One 9, e110226. [PubMed: 25329148]

105. Davenport JR, Watts AJ, Roper VC, Croyle MJ, van Groen T, Wyss JM, Nagy TR, Kesterson RA, and Yoder BK (2007). Disruption of intraflagellar transport in adult mice leads to obesity and slow-onset cystic kidney disease. Curr Biol 17, 1586–1594. [PubMed: 17825558]

106. Loktev AV, and Jackson PK (2013). Neuropeptide Y Family Receptors Traffic via the Bardet-Biedl Syndrome Pathway to Signal in Neuronal Primary Cilia. Cell Rep.

107. Berbari NF, Pasek RC, Malarkey EB, Yazdi SM, McNair AD, Lewis WR, Nagy TR, Kesterson RA, and Yoder BK (2013). Leptin resistance is a secondary consequence of the obesity in ciliopathy mutant mice. Proc Natl Acad Sci U S A 110, 7796–7801. [PubMed: 23599282]

108. Mukhopadhyay S, and Jackson PK (2013). Cilia, tubby mice, and obesity. Cilia 2, 1. [PubMed: 23351214]

109. Mok CA, Heon E, and Zhen M (2010). Ciliary dysfunction and obesity. Clin Genet 77, 18–27. [PubMed: 19968672]

110. Klok MD, Jakobsdottir S, and Drent ML (2007). The role of leptin and ghrelin in the regulation of food intake and body weight in humans: a review. Obes Rev 8, 21–34. [PubMed: 17212793]

111. Oswal A, and Yeo G (2010). Leptin and the control of body weight: a review of its diverse central targets, signaling mechanisms, and role in the pathogenesis of obesity. Obesity (Silver Spring) 18, 221–229. [PubMed: 19644451]

112. Alavi MS, Shamsizadeh A, Azhdari-Zarmehri H, and Roohbakhsh A (2018). Orphan G protein-coupled receptors: The role in CNS disorders. Biomed Pharmacother 98, 222–232. [PubMed: 29268243]

113. Wray NR, Pergadia ML, Blackwood DH, Penninx BW, Gordon SD, Nyholt DR, Ripke S, MacIntyre DJ, McGhee KA, Maclean AW, et al. (2012). Genome-wide association study of major depressive disorder: new results, meta-analysis, and lessons learned. Mol Psychiatry 17, 36–48. [PubMed: 21042317]

114. Pillai V, Kalmbach DA, and Ciesla JA (2011). A meta-analysis of electroencephalographic sleep in depression: evidence for genetic biomarkers. Biol Psychiatry 70, 912–919. [PubMed: 21937023]

115. Sapolsky RM (2001). Depression, antidepressants, and the shrinking hippocampus. Proc Natl Acad Sci U S A 98, 12320–12322. [PubMed: 11675480]

116. Skafidas E, Testa R, Zantomio D, Chana G, Everall IP, and Pantelis C (2014). Predicting the diagnosis of autism spectrum disorder using gene pathway analysis. Mol Psychiatry 19, 504–510. [PubMed: 22965006]

117. C.Y. RK, Merico D, Bookman M, L.H. J, Thiruvahindrapuram B, Patel RV, Whitney J, Deflaux N, Bingham J, Wang Z, et al. (2017). Whole genome sequencing resource identifies 18 new candidate genes for autism spectrum disorder. Nat Neurosci 20, 602–611. [PubMed: 28263302]

118. Saeed S, Bonnefond A, Tamanini F, Mirza MU, Manzoor J, Janjua QM, Din SM, Gaitan J, Milochau A, Durand E, et al. (2018). Loss-of-function mutations in ADCY3 cause monogenic severe obesity. Nat Genet 50, 175–179. [PubMed: 29311637]

119. Weiner LP (2008). Definitions and criteria for stem cells. Methods Mol Biol 438, 3–8. [PubMed: 18369744]

120. Bennett MV, Contreras JE, Bukauskas FF, and Saez JC (2003). New roles for astrocytes: gap junction hemichannels have something to communicate. Trends in neurosciences 26, 610–617. [PubMed: 14585601]

121. Porter JT, and McCarthy KD (1997). Astrocytic neurotransmitter receptors in situ and in vivo. Progress in neurobiology 51, 439–455. [PubMed: 9106901]

122. Di Pietro C, Marazziti D, La Sala G, Abbaszadeh Z, Golini E, Matteoni R, and Tocchini-Valentini GP (2017). Primary Cilia in the Murine Cerebellum and in Mutant Models of Medulloblastoma. Cell Mol Neurobiol 37, 145–154. [PubMed: 26935062]

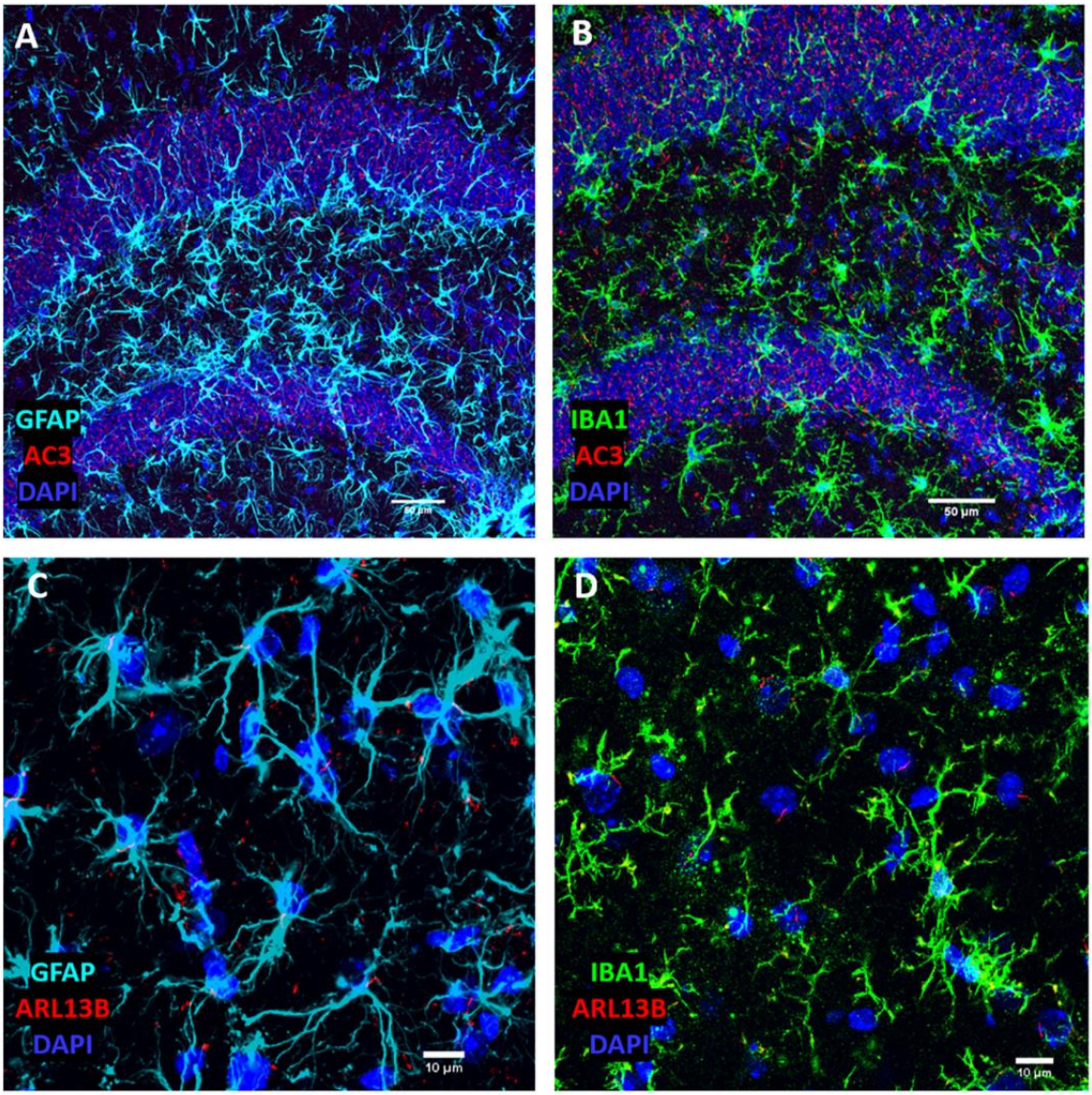

Figure 1.

Neuronal and astrocytic primary cilia are marked by AC3 and ARL13B, respectively, while microglia do not posess primary cilia. **(A)** AC3 is highly expressed in neuronal primary cilia, but not well expressed GFAP-labeled astrocyte cilia. **(B)** IBA1-marked microglia lack AC3-stained primary cilia. **(C)** ARL13B is highly expressed in astrocyte primary cilia. **(D)** IBA1-marked microglia lack ARL13B-stained primary cilia. All images were taken from the mouse hippocampus.

Table 1.

Comparision of Neuronal and Astrocytic Primary Cilia in the Mature Brain

Features	Neurons	Astrocytes
Origination	Ectoderm [119] Neuroepithelial Cells and Radial Glial Cells [27]	Ectoderm [119] Neuroepithelial Cells and Radial Glial Cells[27]
Excitability	Excitable	Non-excitable
Connectivity	Highly connected via synapses	Not wired to one another via chemical synapses; albeit gap junctions found [120, 121]
Differentiation	Terminally differentiate upon maturation	Regional differentiation & become reactive in response to insults
Proliferative Capacity	Lose mitotic ability in maturation [52]	Maintain proliferative capacity throughout life [26]
Primary Cilia Markers	AC3 (Figure 1), SSTR3, 5-HT6, & MCHR1 [15]	Arl13B (Figure 1) [15]
AC3	Highly expressed in neuronal primary cilia [45]	Faintly expressed in immature astrocyte cilia, few in adult astrocyte cilia [45]
ARL13B	Faintly expressed in immature neurons, not prominent in mature neurons [45]	Highly expressed in astrocyte primary cilia in the mature brain [45] (Figure 1)
Cilia Length (Hippocampus)	5.0–5.91 μm (AC3-positive) [15]	2.8–3.2 μm (ARL13B-positive) [15]
Shh Components	Smoothened [17], Patched1 [63], GPR161 [64,56] and Gli transcription factors [63] detected in primary cilia in the neural tube. Presence in primary cilia of mature neurons not shown.	Smoothened and Patched1 detected in primary cilia of astrocytes in the postnatal brain [122]
Structural Dynamics	Relatively stable	Subject to dynamic change during astrocyte proliferation
Ciliogenesis	Research confined to embryonic neuronal ciliogenesis; Lack of *de novo* ciliogenesis in mature neurons	5 known stages of ciliogenesis in adult astrocytes [53, 54]
Ciliary Disease Implications	Obesity, cognitive impairment & mental disorders [89]	Astrocytoma/glioblastoma [53, 54]

The following is sourced from the Molecular Brain, Sterpka et al 2020 [6]

Sterpka et al. Molecular Brain (2020) 13:28
https://doi.org/10.1186/s13041-020-00571-y

Molecular Brain

RESEARCH Open Access

Diverged morphology changes of astrocytic and neuronal primary cilia under reactive insults

Ashley Sterpka, Juan Yang, Matthew Strobel, Yuxin Zhou, Connor Pauplis and Xuanmao Chen*

Abstract

Primary cilia are centriole-derived sensory organelles that are present in most mammalian cells, including astrocytes and neurons. Evidence is emerging that astrocyte and neuronal primary cilia demonstrate a dichotomy in the mature mouse brain. However, it is unknown how astrocytic and neuronal primary cilia change their morphology and ciliary proteins when exposed to reactive insults including epilepsy and traumatic brain injury. We used a double transgenic mouse strain (Arl13b-mCherry; Centrin2-GFP), in which we found spontaneous seizures, and a cortical injury model to examine the morphological changes of astrocytic and neuronal primary cilia under reactive conditions. Transgenic overexpression of Arl13b drastically increases the length of astrocytic and neuronal primary cilia in the hippocampus, as well as the cilia lengths of cultured astrocytes and neurons. Spontaneous seizures shorten Arl13b-positive astrocytic cilia and AC3-positive neuronal cilia in the hippocampus. In a cortical injury model, Arl13b is not detectable in primary cilia, but Arl13b protein relocates to the cell body and has robust expression in the proximity of injured tissues. In contrast, the number of AC3-positive cilia near injured tissues remains unchanged, but their lengths become shorter. These results on astrocytic cilia implicate Arl13b in regulating astrocyte proliferation and tissue regeneration, while the shortening of AC3-positive cilia suggests adaptive changes of neuronal primary cilia under excitotoxicity.

Keywords: Primary cilia, Astrocytes, Arl13b, AC3, Traumatic brain injury, Epilepsy

Introduction

Primary cilia are microtubule-based sensory organelles present in most mammalian cells, including neurons and astrocytes in the brain [1, 2]. The microenvironment of primary cilia is distinct from actin-based microdomains such as microvilli and synapses. During the G0 phase, the primary cilium emanates from the basal body, which is a special form of the mother centriole [3]. In quiescent cells, primary cilia are exquisitely sensitive to extracellular signals, serving as a hub to integrate signals to modulate a variety of cellular functions including neuronal activity [2, 4, 5]. In dividing cells, primary cilia engage directly with the cell cycle, and dismantling primary cilia is a prerequisite for the release of centrioles and formation of the mitotic spindle [6]. Thus, primary cilia have two diverged classes of function: to serve as the "cell antenna" [2, 7] to detect extracellular signals and to function as the "keeper of the key for cell division" [3] to regulate mitosis. In accordance, primary cilia play critical roles in sensory perception, and detection of neurotransmitters and hormones, regulation of cell division, development, and tissue regeneration [8–11]. Currently, little is known about the physiological and pathological function of neuronal and astrocytic primary cilia, despite their strong association with many human diseases

* Correspondence: Xuanmao.Chen@unh.edu
Department of Molecular, Cellular and Biomedical Sciences, College of Life Sciences and Agriculture, University of New Hampshire, 389 Rudman Hall, 46 College Road, Durham, NH 03824, USA

including cognitive impairment [12], obesity [13], developmental disorders [14], and glioblastomas [15, 16].

Although neurons and astrocytes originate from the same precursors in early neurodevelopment, their primary cilia demonstrate a dichotomy in the mature brain [1]: their signaling pathways and molecular components, marker proteins [1, 17], ciliary nanoscale structure (communicated by Carolyn Ott from Janelia Research Campus in 2019), and functionality, as well as disease associations, are markedly diverged. In the adult brain, neuronal and astrocytic primary cilia are generally marked by type 3 adenylyl cyclase (AC3) [18] and ADP-ribosylation factor-like protein 13b (*Arl13b*), respectively [1]. AC3 represents a key enzyme mediating cAMP signaling in neuronal primary cilia throughout the mature brain [4]. Neurons are terminally differentiated and excitable cells that lose mitotic ability in maturity [19]. Neuronal primary cilia are relatively stable and lack de novo ciliogenesis in the adult brain. While no synaptic structures have been identified in neuronal primary cilia, many types of G protein-coupled receptors are detected in these tiny organelles [20]. Hence, neuronal cilia largely rely on metabotropic receptors and often AC3 to transduce a signal into the cell to regulate neuronal activity [4, 21, 22]. In contrast, astrocytes are non-excitable and generally do not intertwine with one another via chemical synapses. Moreover, they are not terminally differentiated cells and maintain proliferative capacity throughout life [23–25]. Since astrocytes can proliferate during reactive astrogliosis in the event of excitotoxic insults [23], astrocytic primary cilia are not static, but subject to dynamic change. Hence, it is not surprising that Arl13b, which regulates ciliary protein trafficking, the Sonic Hedgehog (Shh) pathway, and neural development, prevails over AC3 in astrocytic cilia as a protein marker [17, 26–29].

While neurons generally mediate electrical activity and neural communication in the mammalian brain [30], astrocytes are the most abundant cell type. Astrocytes support neurons by forming a part of the tripartite synapse [25], shuttling lactate for the supplementation of glucose [31], recycling neurotransmitters, maintaining homeostasis, and remodeling synapses [24]. In addition to providing neurotrophic factors, astrocytes play major roles in reducing and halting the progression of toxicity. In the event of harmful insults, astrocytes become reactive, and alter expression to protect healthy parts of the brain. Under these conditions, they change morphology by hypertrophying and extending processes towards the insults and sometimes proliferating to demarcate injury and form glial scarring [32]. These physical changes are accompanied by a heightened expression of GFAP in astrocyte processes [23]. Yet, it is unknown how astrocytic primary cilia change morphology and signaling components in the event of excitotoxic insults.

This study aimed to determine morphological changes and molecular alterations of neuronal and astrocytic primary cilia when the mouse brain is exposed to epileptic conditions and traumatic injury. We employed a double transgenic mouse strain, Arl13b-mCherry; Centrin2-GFP (named "Arl mice" henceforth), in which mCherry labels Arl13b-positive primary cilia, and GFP marks centrosomes via fusion with Centrin2 (a marker protein of centrosomes). This strain allows for direct visualization of Arl13b-positive primary cilia and centrosomes [33]. Serendipitously, we observed that the Arl mice exhibit a high incidence of spontaneously occurring seizures, which provided an excellent mouse model to examine the impact of spontaneous seizure activity on neuronal and astrocytic primary cilia. Additionally, we examined injured brain tissues and assessed the morphological changes of neuronal and astrocytic cilia after brain injury. Here we show that AC3-positive neuronal cilia shorten following reactive insults. Intriguingly, Arl13b-positive astrocytic cilia are not detectable, while Arl13b protein relocates to the cell body and has robust expression in the proximity of injured tissues.

Methods and materials

Mice

The Arl mice were introduced from the Jackson Laboratory (Stock No: 027967) and bred in house. The expression of Arl13b-mCherry and Centrin2-GFP was driven by CAG promoters [33–35]. This mouse strain has C57BL/6, FVB/N, and BALB/c mixed genetic background. Due to the strong activity of the CAG promoter, Arl13b was also found to be highly expressed in neurons in the hippocampus in adult Arl mice and prolong the length of neuronal primary cilia. Wild type FVB/N and C57BL/6 strains were purchased from the Jackson Laboratory and bred in house. Groups of mice were maintained on a 12 h light/dark cycle at 22 °C and had access to food and water ad libitum. Both male and female mice were used for all experiments to prevent sexual bias. All animal procedures were approved by the Institutional Animal Care and Use Committee of the University of New Hampshire and conducted in accordance with their guidelines.

Observation of seizure activity

To determine the presence of the intermittent seizure activity, all Arl mice were observed individually for 30 s to 1 min in a new, clean cage after being removed from their home cage by their tail. Mice exhibiting seizure activity were marked with an animal marker, while mice without seizure expression were not labeled. Observations were repeated for 10 days over 2 consecutive weeks with additional observations occurring intermittently throughout the duration of this experiment. All mice

were returned to their home cage after observation. A modified Racine scale was used to quantify seizure severity [36, 37]: 0, no change in behavior; 1, repetitive chewing; 2, head bobbing; 3, involuntary movement of forelimbs with tremors; 4, involuntary movement of all limbs with rearing and falling; and 5, hypertonia, loss of movement, and death.

Primary astrocyte and neuronal cultures

P0-P3 pups were euthanized with sterile surgical scissors and isolated tissues were placed in ice cold HBSS (Corning, Reference: 21–040-CV). Meninges were removed fully while tissue remained immersed and chilled. Under sterile conditions, cortices were placed in prewarmed papain (Worthington-Biochem, Cat#: LS003127) in DMEM. DNAase was then added to mixture. Tissue was incubated at 37 °C for 15–20 min with inversion every 5 min. Tissue was then transferred to sterile conditions and washed three times in DMEM. Following this, tissue was dissociated into a single cell suspension by repeated pipetting with HBSS and settling of tissue. HBSS containing dissociated cells was centrifuged and pellet resuspended in astrocyte medium. To generate astrocyte cultures, cells were grown to confluence in flask for about 1 week and then split twice to produce pure astrocyte cultures. To produce neuronal cultures, media was removed after 2–4 h and cells were grown with neuronal media, following procedures as described previously [38]. Astrocytes and neurons were cultured in vitro for 7–10 days.

Electroencephalogram/electromyogram (EEG/EMG) surgery, recordings, and analyses

Adult mice undergoing EEG/EMG surgeries were anesthetized with 1.5–3% isoflurane (Henry Schein, NDC 11695–6776-2) and secured in a stereotaxic device (Kopf Instruments). While under anesthesia, mice were prepared for surgery by hair removal, sterilization of skin with alcohol and 4% chlorhexidine (Phoenix, NDC 57319–612-09), and injections of 1 mg/kg lidocaine (Phoenix, NDC 57319–533-05) and 5 mg/kg carprofen (Putney, NDC 26637–521-02). Corneal drying was prevented by the application of sterile ophthalmic ointment (Solutions, Alta lube Ointment, X0020S6KF) prior to surgery. Once secured in the stereotaxic frame, the surface of the cranium was exposed with a single sagittal incision. The cranial surface was cleaned with saline and sterile gauze. Once dry, the EEG/EMG headmount (Pinnacle Technology Inc., Cat # 8201) was secured to the cranium with VetBond (3 M VetBond, 1469SB). Holes were drilled into the skull by hand with a 24-gauge sterile needle. Corners of the headmount were secured into the skull with Resin (Resin lab, SEC 12334GR) placed between the micro-screws (Pinnacle Technology Inc., Cat # 8209). After screws were tightened, the two probes attached to the back of the mount were placed directly into the spinotrapezius of the nuchal region of the mouse. Skin was then sutured around the base of the headmount. The mount and surrounding screws and wires were then stabilized with dental cement and allowed to dry. Mice recovered from surgery on a heating pad and were monitored until awake and active. Mice received carprofen administration for 1–3 days following surgery and were monitored for activity and weight fluctuations. To prevent sexual bias in our data, each phenotypic group had equal sexes of mice. Sirenia Seizure Pro software (Pinnacle Technology Inc. Version 1.8.3) was used to identify seizure activity. All events greater than 5 s were confirmed and interpreted through visual analysis.

Cortical injury

Animals which underwent cranial surgery for device implantation were euthanized and their brain tissue was collected for immunohistochemistry. Following induction of sedation through isoflurane administration, animals were secured in a stereotaxic frame. A single incision was made along the sagittal suture and the cranium was exposed. Bone was cleaned with sterile cotton swabs and saline. Three holes were drilled into cranium with a sterile needle, and microscrews then secured an implant into place. Microscrews resulted in cortical damage and glial scarring not exceeding 2 mm. Microprobe implants were then attached to screws with dental acrylic for fixation. Mice were administered analgesics as necessary during their recovery prior to their use for other experiments.

Transcardial perfusion and tissue fixation

Mice were deeply anesthetized with an intraperitoneal injection of ketamine (Ved Co, KetaVed, NDC 50989–161-06,)/xylazine (AKORN, NDC 59399–111-50). After confirmed assessment for lack of palpebral or tail pinch reflexes, they were transcardially perfused with phosphate buffered saline (PBS) followed by 4% paraformaldehyde (PFA) (Sigma-Aldrich, 252,549-1 L). In brief, a catheter was inserted into their left ventricle and the right atrium was punctured. PBS was administered at a rate of approximately 20 ml/min for 5 min, followed by PFA for roughly 7 min. Whole brains were extracted and then placed into 4% PFA overnight at 4 °C. The following day, brains were rinsed in PBS and placed into 30% sucrose in PBS for 48 h or until fully dehydrated. Tissue was then frozen directly on dry ice and stored at − 80 °C until use.

Immunohistochemistry

After being embedded with tissue-tek optimal cutting temperature compound, brain tissue was sliced on a

Leica CM3050 S cryostat to 30 μM sections at − 18 °C. For immunostaining, tissue was washed for 5–10 min 3 times in PBS while on an orbital shaker at room temperature. Tissue was then permeabilized in 0.5% PBST (PBS + Triton X-100) 3 times for 10 min during shaking. Tissue was then blocked for 2 h while shaking at room temperature in blocking solution (10% donkey serum (Sigma, D9663–10 ML), 2% bovine serum albumin (Sigma-Aldrich, A7906-100G), and 0.1 M glycine (Apex, 18–109) in 0.5% PBST). Tissue was then placed in new blocking buffer and incubated overnight while rocking at 4 °C with primary antibodies: anti-AC3 rabbit antibody (EnCor Biotechnology, AB2572219, 1:10,000 dilution), anti-Arl13b mouse (Neuromab, 75–287, 1:250), anti-GFAP rabbit (Dako, 2024-05-31, 1:750), and anti-GFAP mouse (Sigma, G3893-100UL, 1:500). After incubation, tissue was washed for 10 min 3 times in 0.5% PBST and then incubated with Alexa Fluor secondary antibodies 546 and 647 at 1:500 dilution. After incubation, tissue was washed once in 0.5% PBST for 10 min and then twice in PBS for 10 min. Floating sections were mounted on gelatin coated slides, allowed to moderately dry, and then fixed with DAPI mounting solution (Southern Biotech, 0100–20). Coverslips were secured with clear nail polish and allowed to dry fully before being stored at − 20 °C.

Confocal microscopy and ImageJ analysis

Following immunofluorescence staining, tissue was imaged with a Nikon A1R HD25 confocal microscope, and tiled or non-tiled Z-stacks were taken for quantitative analysis. Fiji ImageJ was used to measure primary cilia, determine intensity of Arl13b with pixel analysis, and examine morphological differences of astrocytes and cilia within the hippocampus or injured cortical tissue. Cilia length was measured in the cornu ammonis 1 (CA1), cornu ammonis 3 (CA3), and dentate gyrus (DG) regions, and cortical injury sites of different strains and phenotypes of mice. Somatic differences characteristic of astrocyte reactivity were confirmed visually in the hippocampus or injured cortical tissue. Arl13b intensity was measured in 3–4500 μm lengths per region of the brain and then averaged per site.

Data analysis

All length and intensity data were analyzed with GraphPad Prism and JMP statistical analysis software. Analyses included unpaired Student's t-test, correlation analysis, Kolmogorov-Smirnov test, one-way ANOVA with Bonferroni correction, and density analysis. Significance was determined by a p value less than 0.05 (*), less than 0.01 (**), and less than 0.001 (***). Data in the graphs are presented as mean ± standard error of the mean.

Results

Arl mice have much longer astrocytic and neuronal primary cilia than wild type FVB/N and C57BL/6 mice

Double transgenic Arl mice have become a useful mouse model to study primary cilia and centrosomes [33]. While this strain has been commonly used in developmental studies [33–35], little is known about their morphological features and cilia expression pattern in the mature mouse brain. To characterize cilia morphology of Arl mice, we first measured cilia length in the hippocampus. We chose FVB/N and C57BL/6 control mice for comparison, owing to the mixed genetic background of the Arl mice. The Arl mice have mCherry linked with Arl13b and do not require additional staining to detect Arl13b-postive primary cilia [33]. Thus, immunofluorescence staining for AC3 was completed in brain tissues of three strains of mice, while Arl13b immunostaining was only applied to FVB/N and C57BL/6 samples. We focused on the CA1, CA3, and DG regions in the hippocampus and measured cilia length in the three regions. Confocal imaging first revealed that Arl13b-positive cilia were longer in the CA3 region of Arl mice than that of both control strains (Fig. 1a-c). Cilia length quantification indicated that Arl mice have significantly longer Arl13b-positive cilia in the CA1, CA3, and DG regions than both control strains (Fig. 1g). Cumulative distribution frequency plots (CDFs) and histogram density comparisons also show a marked difference in cilia length in the three regions between Arl mice and the two control strains (Fig. 1i). Similar to Arl13b-positive cilia, AC3-positive neuronal primary cilia were also found to be longer in Arl mice than in FVB/N and C57BL/6 controls (Fig. 1d-f). Moreover, cilia length analysis revealed that Arl mice had significantly longer AC3-positive cilia in the hippocampal CA1, CA3, and DG regions than both control strains (Fig. 1h). CDFs and histogram density comparisons of AC3-positive cilia lengths also supported this conclusion (Fig. 1j). Interestingly, Arl13b overexpression affected Arl13b-positive cilia more intensely than AC3-positive cilia in adult mice (4–8 months old). Comparison of the ratios of Arl13b- and AC3-positive cilia length of Arl mice relative to that of C57BL/6 mice yielded a range of 1.9 to 2.1 for Arl13b-positive cilia, and 1.1 to 1.4 for AC3-positive cilia in the CA1, CA3, and DG regions, respectively (Fig. 1k). However, in primary astrocyte cultures derived from Arl mice, Arl13b-positive astrocytic cilia length was almost doubled compared to that derived from C57BL/6 mice (Fig. 1l&m). Primarily cultured neurons displayed a similar trend of lengthening in Arl mice when compared to controls, and the length of AC3-postive neuronal cilia were also doubled in neurons of derived from Arl mice (Fig. 1n&o). These data indicate that overexpression of Arl13b significantly increases the length of both astrocytic and

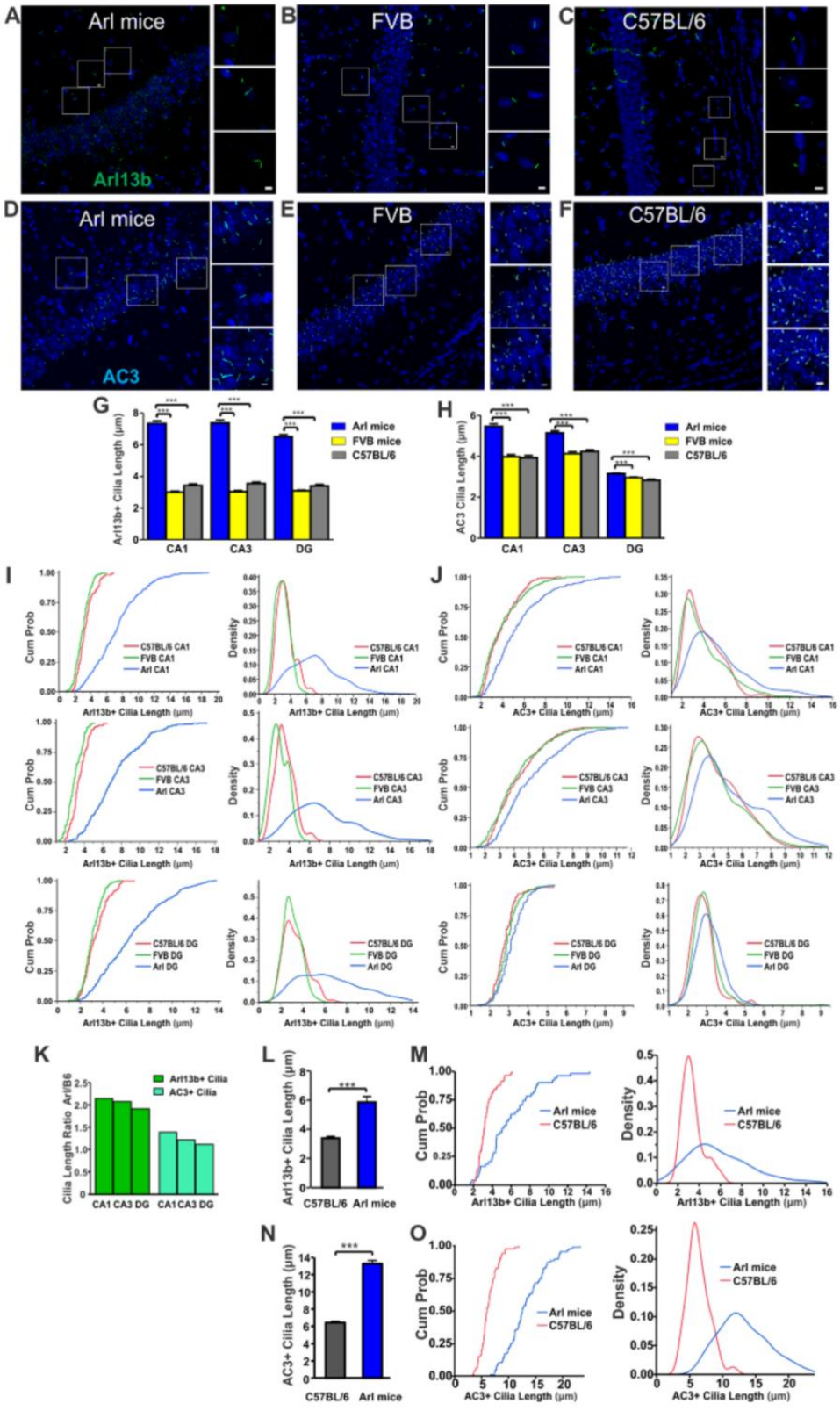

Fig. 1 (See legend on next page.)

(See figure on previous page.)
Fig. 1 Arl13b-positive and AC3-positive primary cilia of Arl mice are longer than those of FVB/N and C57BL/6 wildtype mice. **a-c, g** Arl mice had longer Arl13b-positive primary cilia than control mice in the hippocampal CA1, CA3, and DG regions. **a** Arl mice, **b** FVB/N controls, **c** C57BL/6 controls. Representative images were taken from the CA1 region. Scale bar, 5 μm. **g** Comparison of Arl13b + cilia length in the hippocampal CA1, CA3, and DG of three mouse strains. Arl mice, $N = 8$; FVB/N mice, $N = 5$; C57BL/6, $N = 4$. Cilia number: Arl mice: 399, 230, and 435; FVB/N: 213, 146, and 254; C57BL/6: 144, 118, and 116. Data were compared with one-way ANOVA test with post hoc Tukey test. CA1: $F(2, 753) = 307$, $p < 0.001$; CA3: $F(2, 491) = 251$, $p < 0.001$; DG: $F(2, 802) = 241$, $p < 0.001$. (**d-f**, **h**) Arl mice had longer AC3-positive primary cilia in three subregions in the hippocampus. **d** Arl mice, **e** FVB/N controls, **f** C57BL/6 controls. Scale bar, 5 μm. **h** Comparison of AC3+ primary cilia length in hippocampal CA1, CA3, and DG regions. Arl mice, $N = 4$; FVB/N, $N = 5$; C57BL/6, $N = 3$. Cilia number: Arl mice, 403, 471, and 527; FVB/N mice: 386, 343, and 555; C57BL/6: 202, 422, and 180. Data were analyzed with one-way ANOVA test with post hoc Tukey test. CA1: $F(2, 988) = 58$, $p < 0.001$; CA3: $F(2, 1233) = 40$, $p < 0.001$; DG: $(2, 1259) = 21$, $p < 0.001$. **i** CDFs and histogram density of cilia length show the distribution differences of Arl13b-positive cilia length in different hippocampal regions of the three mouse strains. **j** CDFs and histogram density of cilia length demonstrate the distribution differences of AC3-positive cilia length in different regions of three mouse strains. **k** Ratios of Arl13b- and AC3-positive cilia length in Arl mice relative to those of C57BL/6 mice. Cilia length ratios for Arl13b-positive primary cilia: CA1: 2.1; CA3: 2.1; and DG: 1.9; Cilia length ratios for AC3-positive primary cilia: CA1: 1.4; CA3: 1.2; and DG: 1.1. For (**a-k**), cilia length data were collected from 4 to 8 months old mice. **l-m** Primary cultures of astrocytes from Arl mice had much longer Arl13b-positive primary cilia than those from C57BL/6 mice. **l** Arl13b-positive cilia in primarily cultured astrocytes were significantly longer than those derived from C57BL/6 mice (***, $p < 0.001$, unpaired Student's t-test). Data were collected from 6 Arl cultures, 5 C57BL/6 cultures. Cilia number: Arl mice, 50; C57BL/6 mice, 57. **m** CDFs and density comparisons demonstrate the differences in Arl13b-positive cilia length between Arl mice and C57BL/6 mice. **n** AC3-positive cilia in primarily cultured cortical neurons (~ 10 days in vitro) were significantly longer than those derived from C57BL/6 mice (***, $p < 0.001$, unpaired Student's t-test). Data were collected from 6 Arl cultures, 6 C57BL/6 cultures. Cilia number: Arl mice, 87; C57BL/6 mice, 87. **o** CDFs and density comparisons demonstrate the differences in AC3-positive cilia length between Arl mice and C57BL/6 mice

neuronal primary cilia. These results are consistent with previous reports, showing that Arl13b regulates ciliary protein trafficking and promotes ciliogenesis [27, 29].

Cilia length variation in the hippocampal CA1, CA3, and DG regions in three mouse strains

To examine the length variation of Arl13b-positive and AC3-positive cilia in different regions of the hippocampus among different mouse strains, we compared the cilia lengths in the CA1, CA3, and DG regions. Arl13b-positive and AC3-positive cilia of Arl mice are significantly shorter in the DG than in the CA1 and CA3 regions (Fig. 2a&d). Additionally, AC3-positive cilia in CA3 were moderately shorter than those in the CA1 in Arl mice (Fig. 2d). However, there was no significant regional difference in Arl13b-positive cilia length in FVB/N or C57BL/6 mice (Fig. 2b-c). Moreover, AC3-positive cilia were found to be significantly shorter in the DG than in the CA1 and CA3 regions in FVB/N and C57BL/6 mice, and moderately longer in the CA3 when compared to the CA1 in C57BL/6 mice (Fig. 2e-f). These results on regional cilia length differences are in line with another study, reporting that AC3-positive neuronal cilia are shortest in the DG region in the hippocampus [39].

Centrin2-GFP centrosome protein does not consistently localize at the base of primary cilia in the adult brain

The mother centriole forms the base of the primary cilium, and comprises the centrosome with the daughter centriole during interphase [1, 40]. It has been widely thought that Centrin2 is a marker protein of the centrosome, and the Centrin2-GFP of Arl mice has been used to mark the centrosome in multiple developmental studies [33, 41–44]. Nevertheless, it has not been assessed if Centrin2-GFP can mark the centrosomes of all primary cilia in the mature brain. We determined the co-expression percentage of Centrin2 with Arl13b and AC3 (Fig. 3). Centrin2 was expected to be found at the base of neuronal primary cilia. However, the image quantification of percentages of co-expression shows a significantly higher amount of non-ciliated Centrin2 than Arl13b-Centrin2 or AC3-Centrin2 co-expression (Fig. 3a-c). These data suggest that Centrin2-GFP does not always localize to the base of neuronal primary cilia or astrocytic cilia, and thus cannot be always used as a protein marker to mark the location of centrosomes of primary cilia in the hippocampus of Arl mice.

Arl mice exhibit a high incidence of spontaneous seizure

Likely due to the hybrid background strains of the Arl mice, we also observed spontaneous seizure activity in Arl mice (Fig. 4a). This epileptic activity is short-lived and rarely correlated with sudden death or chronic incapacity in mice. To determine the prevalence of this phenotype in our cohort, all adult mice were first observed daily for 10 days over 2 consecutive weeks. During observations, we removed mice from their home cage by a tail lift and then placed them individually in a new, clean cage for 30 s to 1 min. These standard husbandry procedures were usually enough to initiate seizure activity in Arl mice. This epileptic activity manifested in mice more as they aged and was non-existent in mice under 2 months old. Seizure activity occurred among 42% of a population of 78 Arl mice (4–8 months). Epileptic activity often lasted from 5 to 15 s, and after roughly 10 s following the event, the mouse would return to normal activity. There was no significant sexual

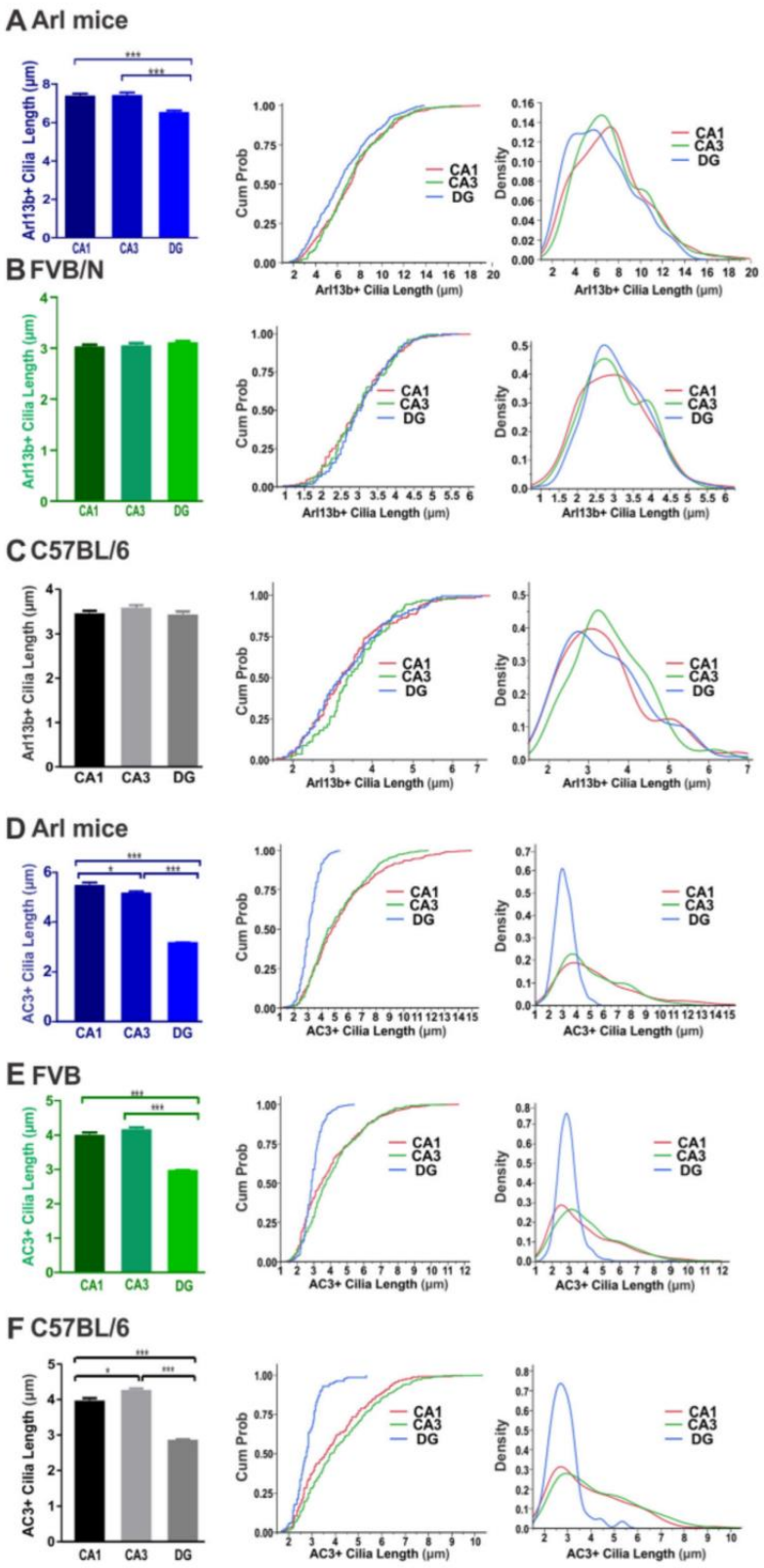

Fig. 2 (See legend on next page.)

(See figure on previous page.)
Fig. 2 Regional cilia length variations in the hippocampal CA1, CA3 and DG in Arl mice, FVB/N and C57BL/6 mice. **a** Arl13b-positive cilia in hippocampal regions of Arl mice were significantly shorter cilia in the DG than in CA1 or CA3 (***, $p < 0.001$, unpaired Student's t-test). $N = 8$ mice. Cilia number: 399, 230, and 435. **b** Arl13b-positive cilia of FVB/N mice had no significant differences in length among hippocampal CA1, CA3, and DG regions. $N = 5$ mice. Cilia number: 213, 146, and 254. **c** Arl13b-positive cilia of C57BL/6 mice had no significant differences in length among the hippocampal CA1, CA3, and DG regions. $N = 4$ mice. Cilia number: 144, 118, and 116. **d** AC3-positive cilia in the hippocampal DG region of Arl mice were significantly (***, $p < 0.001$) shorter than in the CA1 and CA3 regions, and significantly shorter in the CA3 than in the CA1 (*, $p < 0.05$). $N = 4$ mice. Cilia number: 403, 471, and 527. **e** AC3-positive cilia in hippocampal DG regions of FVB/N control mice were significantly (***, $p < 0.001$) shorter than in the CA1 and CA3 regions. $N = 5$ mice. Cilia number: 386, 343, and 555. **f** AC3-positive cilia in hippocampal DG regions of C57BL/6 mice were significantly (***, $p < 0.001$) shorter than in the CA1 and CA3 regions. $N = 4$. Cilia number: 202, 422, and 180. Data were analyzed with one-way ANOVA with post hoc Tukey test. Arl13b: Arl strain: $F(2, 1061) = 11.05$, $p < 0.001$; FVB: $F(2, 610) = 0.5850$, $p = 0.4632$; C57BL/6: $F(F(2, 3775) = 0.7700$, $p = 0.4632$; AC3: Arl Strain: $F(2, 1398) = 213.6$, $p < 0.001$; FVB: $F(2, 1281) = 93.82$, $p < 0.001$; C57BL/6: $F(2, 801) = 62.96$, $p < 0.001$

bias in seizure prevalence of the Arl mice population (Fig. 4b). To evaluate the degree of seizure activity, we used a modified Racine Scale to quantify seizure severity (Fig. 4c & Supplemental Video 1). We found that approximately all mice exhibiting seizures scored between 3 and 4 on a modified Racine Scale (Fig. 4c & Supplemental Video 1). We rarely found mild seizures occurring in this population and did not experience any seizure related deaths or disruptions of fertility. To verify that the spontaneously occurring spastic patterns in the Arl mice were caused by epileptic activity in the brain and not by skeletal muscle spasms, we performed EEG/EMG recordings on 8 Arl mice as well as C57BL/6 control mice. Of the 8 Arl mice used in this experiment, half were known to exhibit seizures and half had no known history of seizure activity. Mice were recorded with EEG/EMG equipment for 48 h. We evaluated EEG/EMG recordings with Sirenia Seizure Pro software and manual inspection of the EEG/EMG waves to detect epileptic events. 17 seizure events occurred during this 48-h period, distinguished by a high amplitude of EEG waves lasting for a time period no less than 5 s (Fig. 4d). Of the 17 seizures (11 from females and 6 from males) recorded, erratic epileptic activity lasted from a range of 16 to 126 s, with an average time of 52 s. In contrast, we did not observe any epileptic activity in C57BL6 mice.

Seizures are known to cause astrocyte reactivity, a condition commonly correlated with many neurological diseases [45, 46]. Next, we sought to determine if the naturally occurring seizures resulted in astrocyte reactivity. If so, brains of Arl seizure mice would maintain a high level of GFAP intensity and hypertrophied astrocytes with additional long processes. We chose to examine these characteristics, because GFAP is a commonly accepted astrocyte marker that increases expression under reactive conditions, and morphological changes in these cells are characteristic in the development of reactivity [47–50]. Figure 4e shows that Arl mice with a known history of seizures were found to display heightened intensity of GFAP and additional processes of GFAP positive astrocytes when compared to controls. These morphological changes and alterations in GFAP expression are consistent with the development of astrocyte reactivity in the brain [23, 48–50]. These data indicate that Arl mice exhibit spontaneous seizure activity, which could be used as a model to study the effect of seizure-induced astrocyte reactivity on primary cilia.

Naturally occurring seizures reduce the length of astrocyte and neuronal primary cilia in the hippocampus

AC3 is mostly enriched in neuronal primary cilia, while Arl13b is widely expressed in astrocytic primary cilia in the adult mouse brain [1, 17]. To date, it is not clear how spontaneous seizures affect Arl13b-positive astrocytic cilia and AC3-positive neuronal cilia. As Arl mice exhibiting seizures conferred an excellent model of excitotoxicity, we sought to examine if seizures cause any morphological changes in Arl13b- and AC3-positive primary cilia. We stained and analyzed brain tissue of Arl mice with a known history of seizures and Arl mice with no known history of seizure activity. Our immunostaining results showed that Arl seizure mice had shorter Arl13b-positive cilia in the DG than those of Arl mice with no known history of seizures (Fig. 5a-b). Quantification of cilia length showed significantly shorter cilia in the CA3 and the DG, but not in the CA1 (Fig. 5c-d). Moreover, analyses of AC3-positive cilia of Arl seizure mice showed a marked reduction of AC3-positive cilia length in the CA3 region and a moderate reduction in length in the CA1 and the DG compared to those of non-seizure mice (Fig. 5e-h). Nevertheless, the ciliation frequency of Arl13b- and AC3-positive cilia was not significantly changed in the DG region by seizure (Fig. 5i&j). Additionally, the presence of seizures did not alter Centrin2-GFP expression in the three regions of the hippocampus of Arl mice (Fig. 5k). Thus, spontaneous seizures reduce the length of both neuronal and astrocytic primary cilia in regions of the hippocampus.

Elevated Arl13b expression proximal to injured tissue

To further evaluate the changes of primary cilia under reactive conditions, we employed a model of traumatic

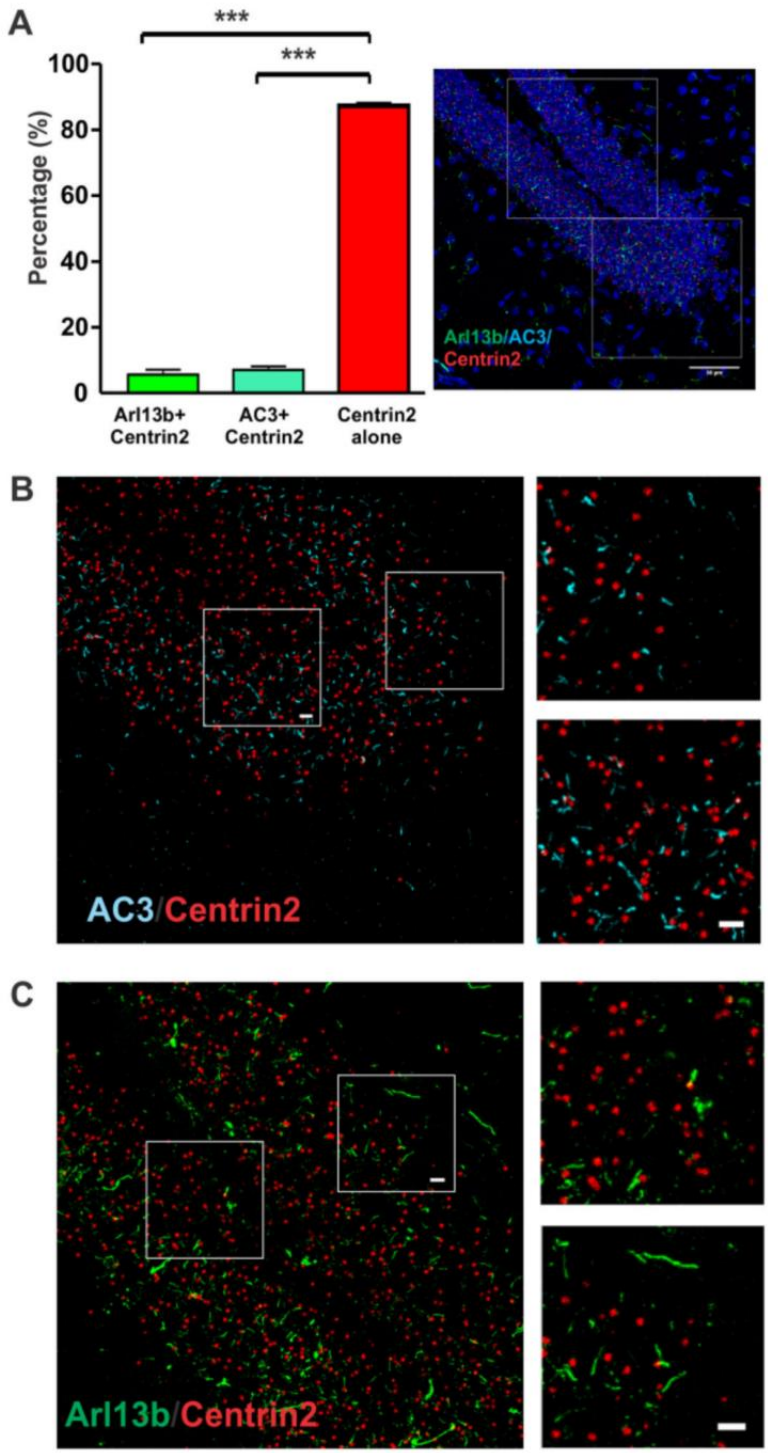

Fig. 3 Centrin2-GFP is not consistently localized at the base of primary cilia. **a** The percentage of co-expression of Centrin2 with known cilia markers (AC3 or Arl13b) had significant difference from Centrin2 alone (***, $p < 0.001$, unpaired Student's t-test). $N = 5$ Arl mice. Cilia number: Arl13b-positive, 48; AC3-positive: 46. Centrin2: 446. **b-c** Zoom-in images from the image of A. Centrin2 was not always present at the base of Arl13b-positive cilia or AC3-postive cilia. Centrin2 imaging density over 50 μm2 regions per mouse was calculated. Green: Arl13b, Cyan: AC3, Red: Centrin2. Scale bar: 5 μm

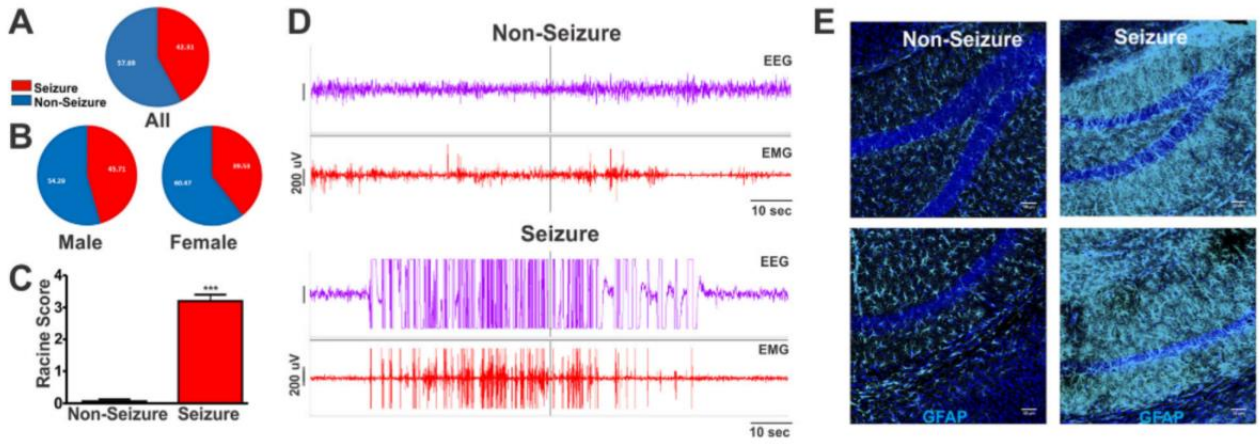

Fig. 4 Arl mice exhibit a high incidence of spontaneous seizure activity. **a** Naturally occurring seizures occur in a large proportion of Arl mice. Blue: non-seizure; red: seizure. $N = 78$. **b** Both male and female Arl mice had seizure activity. Males had 16 mice out of 33 total exhibiting seizures. Females had 17 seizure mice out of 43 total. **c** Arl seizure mice exhibit a high Racine score on average. 15 non-seizure mice were compared with 10 seizure mice. ***, $p < 0.001$, unpaired Student's t-test. **d** EEG/EMG recordings confirmed the occurrence of seizures among Arl mice. Epileptic waveform of EEG/EMG recording verified seizure activity in a mouse grading high on Racine score (bottom), compared to non-seizure Arl mice which lacked high-amplitude EEG/EMG waves (top). **e** Immunofluorescence staining of non-seizure and seizure brain tissue shows drastically elevated GFAP expression in tissues from seizure mice, indicative of astrocyte reactivity. Top, DG; bottom, CA1 region. Scale bar, 50 μm

brain injury, which causes the development of astrocyte reactivity, the generation of glial scarring [51], and is often used in brain injury research [52, 53]. We used a cortical injury model and assessed tissue around injury sites. Surprisingly, we failed to detect the presence of Arl13b-positive cilia proximal to the damaged tissue. Interestingly, although Arl13b-positive cilia were undetectable, Arl13b fluorescence intensity drastically increased in cell bodies in proximity to injured tissues (Fig. 6a-c). The percentage of Arl13b-positive cells proximal to the injury site was significantly higher than that in control tissue of the contralateral hemisphere of the same brain (Fig. 6c). To exclude the possibility that the increase of Arl13b is simply caused by an immunostaining background, we compared Arl mice with no known history of seizures with a cortical injury with C57BL/6 control mice with a cortical injury. Both mCherry signal and immunofluorescence staining using Arl13b antibody yielded similar results: Arl13b-positive cilia were undetectable, while the Arl13b expression shifted to the cell body and was strongly elevated near injury sites (Fig. 6d-e). We employed ImageJ to quantify Arl13b expression intensity over a range of 500 μm from the injury site. Arl13b expression intensity was found to be substantially higher close to the damaged tissue and decrease with distance from the injured site (Fig. 6f). In contrast, Arl13b intensity in control tissue (the opposite hemispheres of the same animals) remained consistent and at low levels (Fig. 6f). Similarly, GFAP exhibited increased expression near injured tissues, indicative of reactive astrogliosis in the glial scar (Fig. 6g). Interestingly, the relative expression density of Arl13b correlated with that of GFAP expression in the proximity of injured tissues (Fig. 6h). The relocation of Arl13b expression to the cell body suggests that Arl13b may regulate cell division or tissue repair in injured tissues.

Brain injury shortens AC3-positive primary cilia

Next, we examined AC3-positive primary cilia near injury sites to determine if effects were consistent with the shortening effect of seizures. We found that, unlike Arl13b-positive cilia, AC3-positive cilia were discernable among neurons close to the injury sites, excluding the immediate glial scarring (Fig. 7a). There was no obvious shift in the localization of AC3 to the cell body and all visible AC3-positive cilia maintained proper shape (Fig. 7a). The frequency of AC3-positive cilia in injured tissues was not significantly changed compared to non-injured tissues (Fig. 7b). However, the length of AC3-positive cilia was markedly shorter near damaged tissues than those in non-injured tissues (Fig. 7c). CDFs and density comparisons also confirmed the reduction of cilia length (Fig. 7d). These data suggest that although brain injury does not cause dismantling of neuronal cilia, it does decrease their length. These results, together with the seizure-induced shortening on neuronal cilia, suggest an adaptive morphological change under reactive conditions to reduce ciliary signals being sent to neurons.

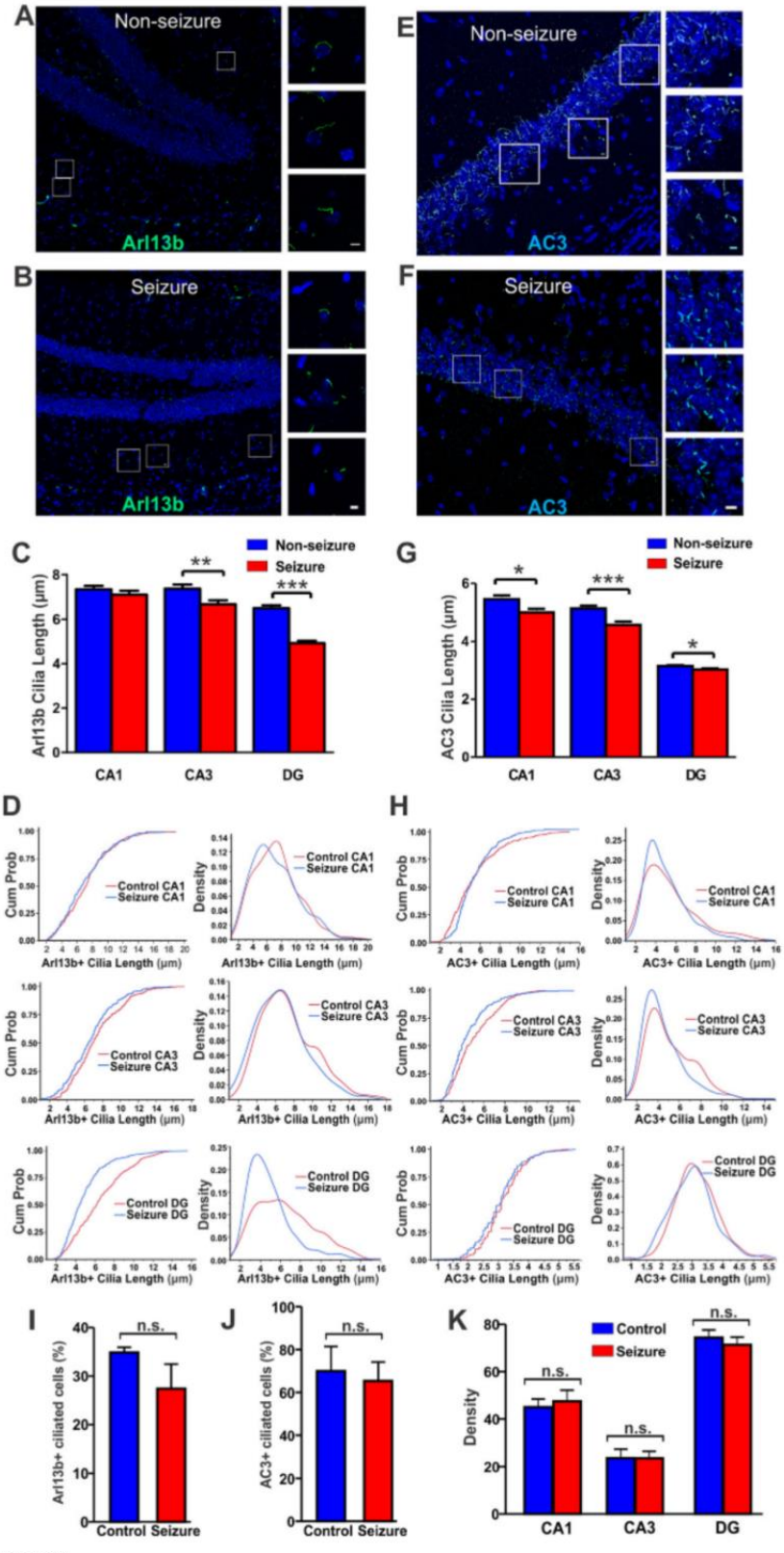

Fig. 5 (See legend on next page.)

(See figure on previous page.)
Fig. 5 Naturally occurring seizures reduce the length of AC3-positive and Arl13b-positive primary cilia in the hippocampus. **a-b** Arl13b-positive cilia in the hippocampal CA1 and DG regions of Arl seizure mice (**b**) were shorter than those of non-seizure Arl control mice (**a**). Scale bar: 5 μm. **c** The length of Arl13b-positive cilia in the CA1 and DG regions, but not in the CA3 region, was significantly shorter in Arl seizure mice than in Arl non-seizure mice (***, $p < 0.001$, unpaired Student's t-test). Arl non-seizure controls, $N = 4$; Arl seizure mice, $N = 5$. Cilia number: Non-seizure mice: 160, 130, and 253; Seizure mice: 180, 131, and 183. **d** CDFs and histogram density comparison present the length of Arl13b-positive cilia in the CA1, CA3, and DG regions. **e-f** AC3-positive cilia in the CA3 region of Arl non-seizure control mice (**e**) and Arl seizure mice (**f**). Scale: 5 μm. **g** Cilia length comparison revealed the shortening of AC3-positive cilia in three hippocampal regions of seizure mice (CA1: *, $p < 0.05$, CA3: ***, $p < 0.001$, DG: *, $p < 0.05$, unpaired Student's t-test). Non-seizure controls, $N = 4$; seizure mice, $N = 5$ animals. Cilia number: non-seizure mice: 403, 471, and 527; seizure mice: 374, 294, and 375. **h** CDFs and histogram density show AC3-positive cilia length in the hippocampal CA1, CA3, and DG regions. **i** Seizure does not significantly affect the percent of Arl13b-positive cilia in the DG. Data collected from 3 non-seizure and 3 seizure Arl mice. Cell number: control: 185; seizure: 196. Cilia number: control: 64; seizure: 51. n.s. not significant, with unpaired Student's t-test. **j** Seizure does not significantly affect the percent of AC3-positive cilia in the DG. Data collected from 3 non-seizure and 3 seizure Arl mice. Cell number: control: 292; seizure: 414. Cilia number: control: 221; seizure: 282. n.s. not significant, with unpaired Student's t-test. **k** Centrin2-GFP expression in hippocampal regions in Arl seizure mice had no significant difference with that in Arl non-seizure mice. Centrin2 imaging density over 50 μm^2 regions per mouse was calculated. Data were collected from 3 non-seizure and 3 seizure Arl mice. $p = 0.6$, 0.9, and 0.5 respectively with unpaired Student's t-test

Discussion

Arl mice contain fluorescent proteins that label Arl13b-positive primary cilia and Centrin2-positive centrosomes [33]. This strain has been used to investigate the roles of primary cilia in development [33–35]. We first found that overexpression of Arl13b significantly elongates both astrocyte and neuronal primary cilia in the hippocampus. The longer cilia suggest possible gain-of-function features, which may correlate with augmented function. We also show that a high percentage of Arl mice exhibit spontaneous seizures. This phenotype could be partly due to genetic background of the Arl strain, which contains a hybrid cross with the FVB/N strain. Populations of FVB/N mice are known have higher seizure incidence than other strains. Seizure activity in FVB/N mice has been associated with astrocyte reactivity and neuronal death [54]. Similar to our cohort of Arl mice, seizures are known to emerge in FVB/N mice at 2–16 months of age as a result of mild to moderate stimuli [55]. However, the seizure incidence in our population of Arl mice (42%) is much higher than what has been reported in FVB/N mice (17–20%) [56, 57], raising the possibility that this difference may be caused by the transgenic overexpression of Arl13b and increased length of neuronal primary cilia in the brain. Elongated neuronal primary cilia could potentially elevate basal neuronal activity, consequently increasing the incidence of seizures. Thus, we postulate that the epileptic activity among Arl mice is partly due to the partial FVB background and elongated neuronal primary cilia may increase the seizure frequency. However, long-term spontaneous seizure in mice may in turn lead to the shortening of neuronal primary cilia, which may result from ciliary adaptive change under excitotoxicity.

Neurons are terminally differentiated cells and lose the ability to divide at maturity. Hence, it is not surprising to observe that neuronal primary cilia are relatively stable and the ciliation frequency does not change under seizure (Fig. 5) and traumatic brain injury (Fig. 7). Nevertheless, neuronal primary cilia become shorter in all regions of the hippocampus in Arl mice under spontaneous seizures. The shortening of AC3-positive cilia perhaps reflects adaptive changes of neuronal primary cilia in response to excitotoxicity insults. It has been reported that a disruption of radial patterning of neuronal primary cilia, as well as the absence of change in glial cilia in the hippocampus accompany a pilocarpine-induced seizure model [58]. In our study, although neuronal primary cilia were found to become shorter, we cannot verify the disruption of radial patterning of neuronal primary cilia upon seizure. The different results may be due to the spontaneous and long-term seizure occurrence versus brief seizure occurrence induced by a convulsant. Additionally, the significantly longer Arl13b-positive primary cilia in the Arl mice may also affect the increased seizure occurrence, due to alterations in signaling or possibly variations in astrocyte function decreasing their ability to recycle synaptic neurotransmitters. It is possible that the ciliary shortening in AC3-positive primary cilia may be due to alterations in ciliary protein receptors. Yet, the exact function of neuronal primary cilia is not well appreciated, and further research is required to understand how neuronal ciliary signaling regulates neuronal excitability and epileptic conditions.

Astrocytes are the most abundant cells in the mammalian brain and fulfill a variety of physiological functions, including providing trophic support neurons, and recycling neurotransmitters, maintaining homeostasis, and remodeling synapses [59–62]. Unlike neurons, astrocytes maintain the capacity of cell division, and new astrocytes are continuously generated in many regions during postnatal development [63]. Astrocytes become reactive in response to reactive insults, including epilepsy [64, 65] and traumatic brain injury [66]. Under these neuropathological events, they proliferate upon the initiation of reactivity [62, 67–69]. In this study, we first examined

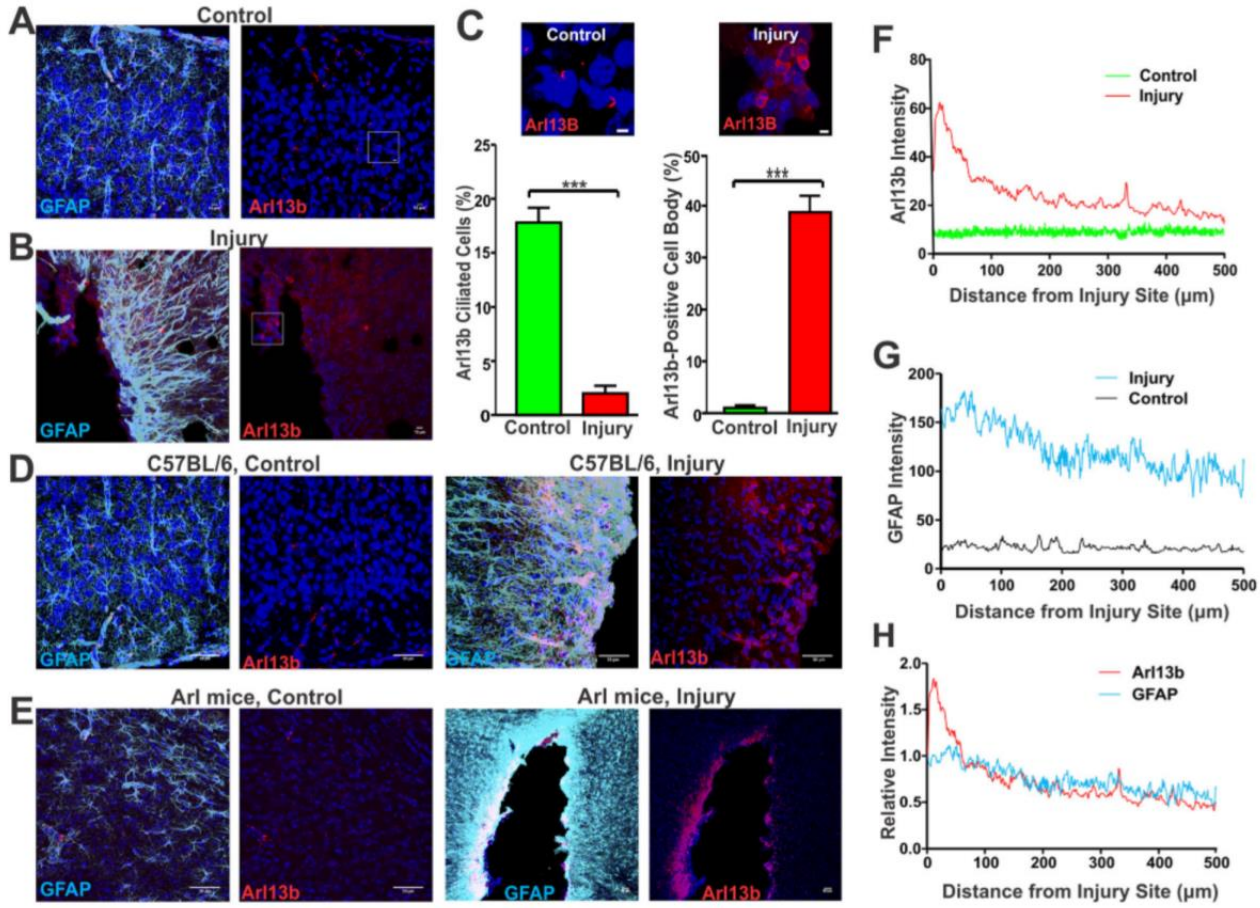

Fig. 6 Absence of Arl13b-positive astrocytic primary cilia but robust Arl13b expression in tissues proximal to injured sites. **a-b** Increased Arl13b expression proximal to an injury site (**b**) compared to a non-injury site (A). Scale: 5 μm. Note that Arl13b-positive primary cilia were detected in non-injured tissues (**a**), but undetectable in injured tissues (**b**). **c** The percentage of ciliated cells near injury sites decreased dramatically compared to control tissues (left). ***, $p < 0.001$, unpaired student's t-test. Injured tissues: total cell number: 665, ciliated cell N: 13; non-injured tissues: total cell number: 265, ciliated cell number: 47. Injured tissues had significantly increased percentage of Arl13b-positive cells compared to that of non-injury tissues (right). ***, $p < 0.001$, unpaired Student's t-test, $N = 3$. Injury site cell $N = 806$; non-injury site cell number 600. Two Arl13b images from injured and non-injured sites are shown in the left. Non-injury sites were from the opposite hemisphere of the injury site of same mouse. **d** Increased Arl13b expression near injured sites in the cortex of C57BL/6 mice. GFAP (cyan) and Arl13b (red) were stained with their antibodies, respectively. Left, non-injured site; right, injured site. **e** Increased Arl13b expression near injured sites in Arl mice. Red: Arl13b-mCherry; Cyan: immunofluorescence staining using anti-GFAP antibody. **f** Distinct Arl13b expression density in injured and non-injured tissues. Arl13b had the highest expression near to the injury site. $N = 5$. **g** GFAP expression was strongly increased near to injured tissues compared to non-injured tissues. **h** Correlation of relative expression density of GFAP and Arl13b over a range of 500 μm distance from the injured site. ***, $p < 0.001$ by correlation analysis

the effects of spontaneously occurring seizures on primary cilia. We found that there was a shortening of Arl13b-positive primary cilia in regions of the hippocampus. To further determine the morphological change of primary cilia during astrocyte reactivity, we employed a cortical injury model and examined primary cilia close to the injury sites. Arl13b-positive primary cilia were not detectable near injured tissues. Surprisingly, Arl13b relocated to the cell body and its protein expression is drastically intensified in the proximity of injured tissues (Fig. 6). Limited by available antibodies, we were unable to definitively prove if astrocytic cilia were ablated near the injury site or if the Arl13B expression merely shifted. The increased expression of Arl13b is correlated with elevated GFAP expression, suggesting a role of Arl13b in astrocyte proliferation and tissue repair.

Arl13b is a member of the Ras family of GTPases [27]. Mutations in Arl13b are known to result in defective cilia formation leading to Joubert syndrome, a ciliopathy characterized by neurological abnormalities and cognitive delay [70]. Arl13b associates with the ciliary membrane through palmitoylation and is required for

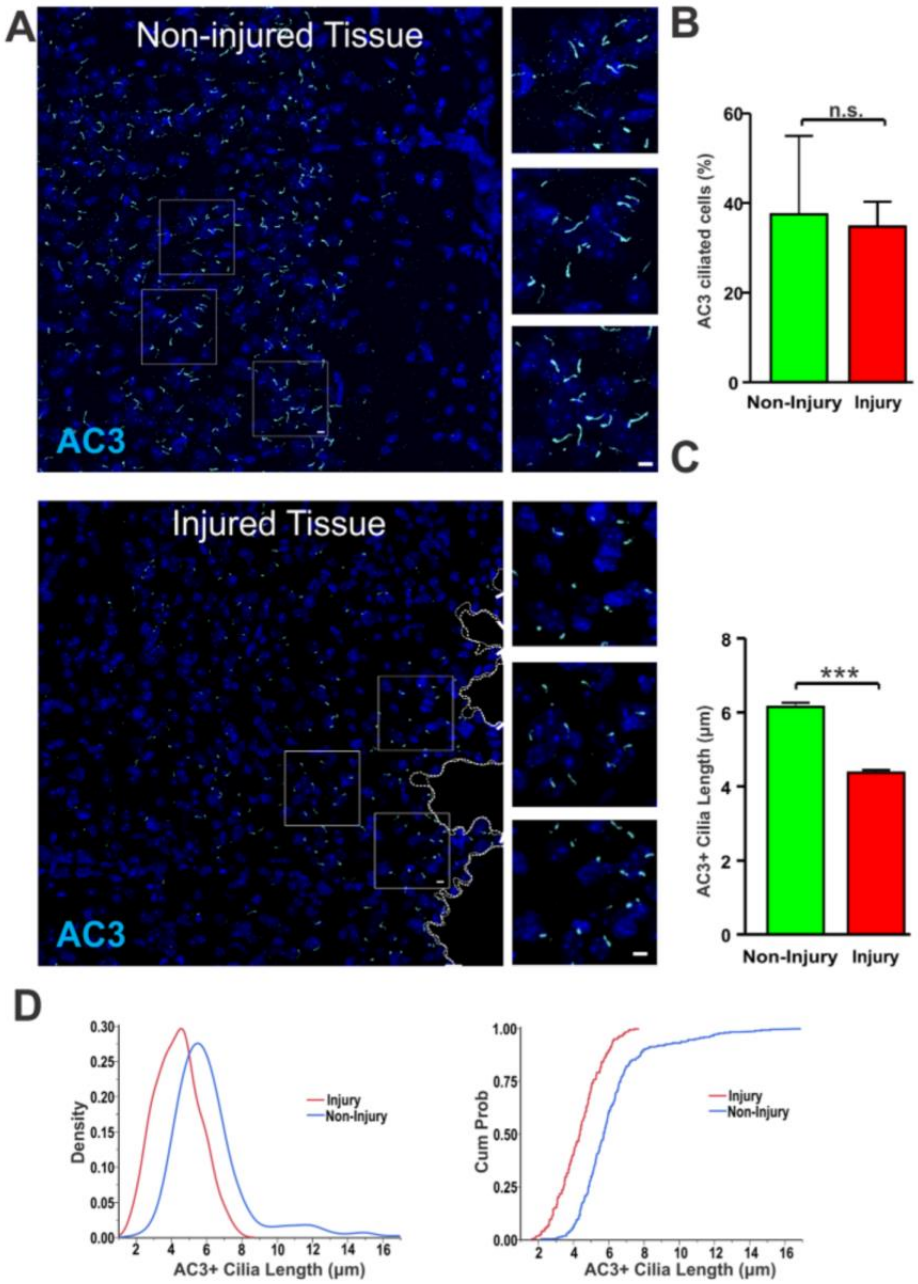

Fig. 7 Tissue injury decreases the length of AC3-positive primary cilia. **a** AC3-positive cilia were shortened close to injured tissues. Scale bar: 5 μm. Top, non-injured tissues; bottom, injured tissues. **b** The frequency of AC3-positive cilia was not changed between injured and non-injured tissues (n.s. not significant, unpaired Student's t-test). **c** Comparison of AC3-postive cilia lengths reveals significant decrease in cilia length proximal to injury sites compared to injured tissues (*** $p < 0.001$, unpaired Student's t-test). $N = 5$, C57BL/6 mice. Non-injured sites were from opposite hemisphere of the injury site of the same animals. Cilia number: non-injured sites: 271; injured sites: 326. **d** CDFs and density comparison indicate the shortening of AC3-positive cilia length near to injury sites

trafficking of proteins within primary cilia [71]. Moreover, Arl13b is also known to regulate the trafficking of Shh signaling components to primary cilia, elements known to have a role in reparations following brain injury [28]. Relevantly, disruption of Arl13b inhibits Shh signaling over-activation and suppresses medulloblastoma formation [72]. It is well recognized that the Shh pathway mediates a developmental signal pathway vital to proper neural tube formation and body patterning [73, 74]. Defects in Shh can result in severe physiological abnormalities [75–77]. Mutations of Arl13b correlate with deformed primary cilia and abrogated Shh modulation [27] Shh induction increases following the acute phase after brain injury, thereby enhancing the

proliferation of astrocytes under reactive conditions [78]. Given the strong association between Arl13b and Shh signaling, Arl13b translocation from the primary cilium to the cell body may regulate Shh signal transduction for tissue regeneration in the event of brain injury.

In summary, our findings validate the Arl strain as a useful mouse model to study primary cilia, which could be used as a gain-of-function tool to study the roles of both astrocytic and neuronal primary cilia. We also present the evidence of spontaneous seizure occurrence among Arl mice and unravel the effects of spontaneous seizures on astrocyte and neuronal primary cilia. Both types of primary cilia in the hippocampus are found to be shortened in reactivity induced by spontaneous seizure conditions. We further reveal that traumatic brain injury not only shortens neuronal primary cilia, but also highly elevates Arl13b expression proximal to the injury sites, implicating Arl13b in the regulation of astrocyte reactivity and tissue regeneration. This work suggests that the Arl13b-mediated signaling may represent potential therapeutic targets for tissue repair [8]. However, further studies are warranted to elucidate the molecular mechanisms of astrocytic primary cilia and Arl13b-mediated signaling in tissue regeneration following brain injury.

Acknowledgements
We are very grateful to Dr. Linnea Morley and Nicole Abate for informing us of the onset of spontaneous seizure occurrences among Arl13b-mCherry; Centrin2-GFP mice.

Authors' contributions
A.S. and X. C. designed research; A.S., J.Y., M.S., Y.Z. and C.P. performed research; A.S., J.Y., M.S., Y.Z., C.P. and X. C. analyzed data; A. S. and X. C. wrote the paper. The author(s) read andapproved the final manuscript.

Funding
This study was supported by National Institutes of Health Grants R21MH105746, K01AG054729, and P20GM113131–7006 to X.C.; Cole Neuroscience and Behavioral Faculty Research Awards to X.C.; and UNH Summer TA Research Fellowships to A.S., J.Y., M.S., and Y.Z.

Availability of data and materials
The data generated by this work will be made accessible to the public.

Ethics approval and consent to participate
All animal procedures were approved by the Institutional Animal Care and Use Committee of the University of New Hampshire and conducted in accordance with their guidelines. This project does not involve human subjects.

Consent for publication
All authors have consented to publishing this manuscript.

Competing interests
The authors declare that the research was conducted in the absence of any commercial or financial conflict of interest.

Received: 6 December 2019 Accepted: 24 February 2020
Published online: 02 March 2020

References
1. Sterpka A, Chen X. Neuronal and astrocytic primary cilia in the mature brain. Pharmacol Res. 2018;137:114–21..
2. Singla V, Reiter JF. The primary cilium as the cell's antenna: signaling at a sensory organelle. Science. 2006;313(5787):629–33.
3. Pan J, Snell W. The primary cilium: keeper of the key to cell division. Cell. 2007;129(7):1255–7.
4. Qiu L, et al. Type 3 adenylyl cyclase: a key enzyme mediating the cAMP signaling in neuronal cilia. Int J Physiol Pathophysiol Pharmacol. 2016;8(3):95–108.
5. Koemeter-Cox AI, et al. Primary cilia enhance kisspeptin receptor signaling on gonadotropin-releasing hormone neurons. Proc Natl Acad Sci U S A. 2014;111(28):10335–40.
6. Phua SC, et al. Dynamic remodeling of membrane composition drives cell cycle through primary cilia excision. Cell. 2019;178(1):261.
7. Malicki JJ, Johnson CA. The cilium: cellular antenna and central processing unit. Trends Cell Biol. 2017;27(2):126–40.
8. Veland IR, Lindbaek L, Christensen ST. Linking the primary cilium to cell migration in tissue repair and brain development. Bioscience. 2014;64(12):1115–25.
9. Anvarian Z, et al. Cellular signalling by primary cilia in development, organ function and disease. Nat Rev Nephrol. 2019;15(4):199–219.
10. Babu D, Roy S. Left-right asymmetry: cilia stir up new surprises in the node. Open Biol. 2013;3(5):130052.
11. Pazour GJ, Witman GB. The vertebrate primary cilium is a sensory organelle. Curr Opin Cell Biol. 2003;15(1):105–10.
12. Guemez-Gamboa A, Coufal NG, Gleeson JG. Primary cilia in the developing and mature brain. Neuron. 2014;82(3):511–21.
13. Vaisse C, Reiter JF, Berbari NF. Cilia and Obesity. Cold Spring Harb Perspect Biol. 2017;9(7).
14. Valente EM, et al. Primary cilia in neurodevelopmental disorders. Nat Rev Neurol. 2014;10(1):27–36.
15. Loskutov YV, et al. LPA signaling is regulated through the primary cilium: a novel target in glioblastoma. Oncogene. 2018;37(11):1457–71.
16. Alvarez-Satta M, Matheu A. Primary cilium and glioblastoma. Ther Adv Med Oncol. 2018;10:1758835918801169.
17. Kasahara K, et al. Visualization of astrocytic primary cilia in the mouse brain by immunofluorescent analysis using the cilia marker Arl13b. Acta Med Okayama. 2014;68(6):317–22.
18. Bishop GA, et al. Type III adenylyl cyclase localizes to primary cilia throughout the adult mouse brain. J Comp Neurol. 2007;505(5):562–71.
19. Myster DL, Duronio RJ. To differentiate or not to differentiate? Curr Biol. 2000;10(8):R302–4.
20. Schou KB, Pedersen LB, Christensen ST. Ins and outs of GPCR signaling in primary cilia. EMBO Rep. 2015;16(9):1099–113.
21. Chen X, Xia Z, Storm DR. Stimulation of electro-olfactogram responses in the main olfactory epithelia by airflow depends on the type 3 adenylyl cyclase. J Neurosci. 2012;32(45):15769–78.
22. Chen X, et al. Ablation of type III adenylyl Cyclase in mice causes reduced neuronal activity, altered sleep pattern, and depression-like phenotypes. Biol Psychiatry. 2016;80(11):836–48.
23. Sofroniew MV, Vinters HV. Astrocytes: biology and pathology. Acta Neuropathol. 2010;119(1):7–35.
24. Schiweck J, Eickholt BJ, Murk K. Important Shapeshifter: mechanisms allowing astrocytes to respond to the changing nervous system during development, Injury and Disease. Front Cell Neurosci. 2018;12:261.
25. Perea G, Navarrete M, Araque A. Tripartite synapses: astrocytes process and control synaptic information. Trends Neurosci. 2009;32(8):421–31.
26. Higginbotham H, et al. Arl13b in primary cilia regulates the migration and placement of interneurons in the developing cerebral cortex. Dev Cell. 2012;23(5):925–38.
27. Larkins CE, et al. Arl13b regulates ciliogenesis and the dynamic localization of Shh signaling proteins. Mol Biol Cell. 2011;22(23):4694–703.
28. Mariani LE, et al. Arl13b regulates Shh signaling from both inside and outside the cilium. Mol Biol Cell. 2016.
29. Nozaki S, et al. Regulation of ciliary retrograde protein trafficking by the Joubert syndrome proteins ARL13B and INPP5E. J Cell Sci. 2017;130(3):563–76.
30. Jakel S, Dimou L. Glial cells and their function in the adult brain: a journey through the history of their ablation. Front Cell Neurosci. 2017;11:24.

31. Mangia S, et al. The in vivo neuron-to-astrocyte lactate shuttle in human brain: evidence from modeling of measured lactate levels during visual stimulation. J Neurochem. 2009;109(Suppl 1):55–62.
32. Wang H, et al. Portrait of glial scar in neurological diseases. Int J Immunopathol Pharmacol. 2018;31:2058738418801406.
33. Bangs FK, et al. Lineage specificity of primary cilia in the mouse embryo. Nat Cell Biol. 2015;17(2):113–22.
34. Bernet A, et al. Cell-lineage specificity of primary cilia during postnatal epididymal development. Hum Reprod. 2018;33(10):1829–38.
35. Kim YK, et al. Localization of primary cilia in mouse retina. Acta Histochem. 2013;115(8):789–94.
36. Van Erum J, Van Dam D, De Deyn PP. PTZ-induced seizures in mice require a revised Racine scale. Epilepsy Behav. 2019;95:51–5.
37. Phelan KD, et al. Pilocarpine-induced status epilepticus in mice: a comparison of spectral analysis of electroencephalogram and behavioral grading using the Racine scale. Epilepsy Res. 2015;117:90–6.
38. Chen X, et al. Diarylamidines: high potency inhibitors of acid-sensing ion channels. Neuropharmacology. 2010;58(7):1045–53.
39. Guadiana SM, et al. Type 3 adenylyl Cyclase and Somatostatin receptor 3 expression persists in aged rat neocortical and hippocampal neuronal cilia. Front Aging Neurosci. 2016;8:127.
40. Wang WJ, et al. The conversion of centrioles to centrosomes: essential coupling of duplication with segregation. J Cell Biol. 2011;193(4):727–39.
41. Delaval B, et al. Centrin depletion causes cyst formation and other ciliopathy-related phenotypes in zebrafish. Cell Cycle. 2011;10(22):3964–72.
42. Ying G, et al. Centrin 2 is required for mouse olfactory ciliary trafficking and development of ependymal cilia planar polarity. J Neurosci. 2014;34(18):6377–88.
43. Mullee LI, Morrison CG. Centrosomes in the DNA damage response--the hub outside the Centre. Chromosom Res. 2016;24(1):35–51.
44. Bose A, Dalal SN. 14–3-3 proteins mediate the localization of Centrin2 to centrosome. J Biosci. 2019;44(2).
45. Farrell JS, Wolff MD, Teskey GC. Neurodegeneration and pathology in epilepsy: clinical and basic perspectives. Adv Neurobiol. 2017;15:317–34.
46. Rossi AR, et al. Gabapentin administration reduces reactive gliosis and neurodegeneration after pilocarpine-induced status epilepticus. PLoS One. 2013;8(11):e78516.
47. Eng LF, Ghirnikar RS. GFAP and astrogliosis. Brain Pathol. 1994;4(3):229–37.
48. Li K, et al. Reactive astrocytes in neurodegenerative diseases. Aging Dis. 2019;10(3):664–75.
49. Liddelow SA, Barres BA. Reactive astrocytes: production, function, and therapeutic potential. Immunity. 2017;46(6):957–67.
50. Zhang S, et al. GFAP expression in injured astrocytes in rats. Exp Ther Med. 2017;14(3):1905–8.
51. Chen Y, Swanson RA. Astrocytes and brain injury. J Cereb Blood Flow Metab. 2003;23(2):137–49.
52. Balasingam V, et al. Reactive astrogliosis in the neonatal mouse brain and its modulation by cytokines. J Neurosci. 1994;14(2):846–56.
53. Miyake T, et al. Quantitative studies on proliferative changes of reactive astrocytes in mouse cerebral cortex. Brain Res. 1988;451(1–2):133–8.
54. Goelz MF, et al. Neuropathologic findings associated with seizures in FVB mice. Lab Anim Sci. 1998;48(1):34–7.
55. Wetherington J, Serrano G, Dingledine R. Astrocytes in the epileptic brain. Neuron. 2008;58(2):168–78.
56. Kohnken RA, Schwahn DJ. Lack of chronic histologic lesions supportive of sublethal spontaneous seizures in FVB/N mice. Comp Med. 2016;66(2):105–11.
57. Silva-Fernandes A, Pedro O, Nuno S, Patricia M. Motor and Behavioural Abnormalities Associated with Persistent Spontaneous Epilepsy in the fvb/n Mouse Strain. Scand J Lab Anim Sci. 2010;37:213–22.
58. Kirschen GW, et al. The radial organization of neuronal primary cilia is acutely disrupted by seizure and ischemic brain injury. Front Biol (Beijing). 2017;12(2):124–38.
59. Verkhratsky A, et al. Neurological diseases as primary gliopathies: a reassessment of neurocentrism. ASN Neuro. 2012;4(3).
60. Sofroniew MV. Astrogliosis. Cold Spring Harb Perspect Biol. 2015;7(2):a020420.
61. Sofroniew MV. Astrocyte barriers to neurotoxic inflammation. Nat Rev Neurosci. 2015;16(5):249–63.
62. Pekny M, Pekna M. Astrocyte reactivity and reactive astrogliosis: costs and benefits. Physiol Rev. 2014;94(4):1077–98.
63. Ge WP, Jia JM. Local production of astrocytes in the cerebral cortex. Neuroscience. 2016;323:3–9.
64. Tian GF, et al. An astrocytic basis of epilepsy. Nat Med. 2005;11(9):973–81.
65. Oberheim NA, et al. Loss of astrocytic domain organization in the epileptic brain. J Neurosci. 2008;28(13):3264–76.
66. Burda JE, Bernstein AM, Sofroniew MV. Astrocyte roles in traumatic brain injury. Exp Neurol. 2016;275(Pt 3):305–15.
67. Burda JE, Sofroniew MV. Reactive gliosis and the multicellular response to CNS damage and disease. Neuron. 2014;81(2):229–48.
68. Pekny M, et al. Astrocytes: a central element in neurological diseases. Acta Neuropathol. 2016;131(3):323–45.
69. Pekny M, Nilsson M. Astrocyte activation and reactive gliosis. Glia. 2005;50(4):427–34.
70. Cantagrel V, et al. Mutations in the cilia gene ARL13B lead to the classical form of Joubert syndrome. Am J Hum Genet. 2008;83(2):170–9.
71. Roy K, et al. Palmitoylation of the ciliary GTPase ARL13b is necessary for its stability and its role in cilia formation. J Biol Chem. 2017;292(43):17703–17.
72. Bay SN, Long AB, Caspary T. Disruption of the ciliary GTPase Arl13b suppresses sonic hedgehog overactivation and inhibits medulloblastoma formation. Proc Natl Acad Sci U S A. 2018;115(7):1570–5.
73. Ribes V, Briscoe J. Establishing and interpreting graded sonic hedgehog signaling during vertebrate neural tube patterning: the role of negative feedback. Cold Spring Harb Perspect Biol. 2009;1(2):a002014.
74. Pal K, Mukhopadhyay S. Primary cilium and sonic hedgehog signaling during neural tube patterning: role of GPCRs and second messengers. Dev Neurobiol. 2015;75(4):337–48.
75. Heussler HS, et al. Extreme variability of expression of a sonic hedgehog mutation: attention difficulties and holoprosencephaly. Arch Dis Child. 2002;86(4):293–6.
76. Tsukui T, et al. Multiple left-right asymmetry defects in Shh(−/−) mutant mice unveil a convergence of the shh and retinoic acid pathways in the control of Lefty-1. Proc Natl Acad Sci U S A. 1999;96(20):11376–81.
77. Roessler E, et al. Mutations in the human sonic hedgehog gene cause holoprosencephaly. Nat Genet. 1996;14(3):357–60.
78. Amankulor NM, et al. Sonic hedgehog pathway activation is induced by acute brain injury and regulated by injury-related inflammation. J Neurosci. 2009;29(33):10299–308.

Publisher's Note